TECHNICAL UNIVERSITY OF CRETE

SCHOOL OF ELECTRONIC AND COMPUTER
ENGINEERING

Spectral Cube Construction From Hyper Spectral Scanning Imaging

Chantzi Efthymia

efichantzi@gmail.com

Diploma Thesis

for the award of the degree of

Polytechnical Diploma

in Electronic and Computer Engineering, ECE

Thesis Committee

Balas Constantinos, Associate Professor, Supervisor
Kalaitzakis Constantinos, Professor
Bucher Matthias, Assistant Professor

October 16, 2013

Acknowledgments

It is a great opportunity to bestow my heartful regards to all people who have been either directly or indirectly involved in the fulfillment of this diploma dissertation.

First and foremost, i would like to thank my beloved family, especially my mother, and dedicate to them this work. If it had not been for their understanding, encouragement and endless love, the implementation of my studies would not have been possible.

I would also like to show my greatest appreciation to my professor and supervisor, Constantinos Balas, for giving me the opportunity to do this wonderful dissertation. Not only did he help me completing my studies, but also motivated me to work more efficiently and professionally by conducting a lot of extra research, being familiar with experimental devices and gaining valuable knowledge.

Finally, yet importantly, i would like to express my gratitude towards the whole team of the "Optoelectronics Lab", whose contribution and support have been instrumental. I am really grateful to Tsapras Thanasis(PhD candidate), Kavvadias Vassilis(MSc student) and Epitropou George(MSc student) for their numerous brainstorming discussions, help with the construction of the experimental set up, and selfless advice.

Abstract

This diploma thesis deals with a new method in acquiring and reconstructing the spectral cube in hyper spectral imaging. The method employs a spatial variable band-pass optical filter, which is translated over a two dimensional sensor's area. That way the sensor's pixel columns acquire optical information captured at different wavelengths at a time. By translating the variable filter, all the spectral bands are captured by the sensor's pixels in time sequence. After completing the acquisition process, the spectral and spatial information are stored in a multiplexed fusion. The next step is to disentangle the multiplexed information, so that the spectral cube to contain a stack of images each one captured at a different wavelength. The specially developed method relies on the re-sampling of the stored data with the aid of geometrical transformations. This results in a straightforward and fast de-multiplexing of the dataset and the reconstruction of spectral cube consisted of hundreds of narrow band spectral images, spanning both the visible and near infrared part of the spectrum. Technical evaluation of the method showed a series of distincted advantages over prior art included but not limited to unparallel light throughput and high, user defined spectral resolution. Moreover, the measurement of Modulation Transfer Function(MTF) of the system with the contribution of a specially developed method showed that the spatial resolution of the spectral images, in terms of lp/mm, is high and wavelength dependent. The above features make our approach suitable in demanding spectral imaging applications, such as microscopic images and non-destructive analysis.

Contents

List of Figures

List of Algorithms

List of Tables

Chapter 1

Introduction

It is important to outline the bedrocks of this work in order to render readers familiar with the basic concepts and developed methods and interested throughout the progress of the presentation. However, followers who feel confident, as far as their knowledge is concerned on these scientific domains, may sidestep this section of introduction and continue with the following chapters.

1.1 Spectroscopy

If it had been for a single scientific term that could thoroughly describe the topic of this project, that would be ***spectroscopy*** [1] [2]. Spectroscopy responds to the field of study including the interaction between matter and radiated energy. Historically, it is originated from the dispersion of visible light according to its wavelength. Later on, the concept was greatly expanded to comprise any interaction with radiative energy as a function of its wavelength(λ) or frequency(ν). As a result, the definition of spectroscopy was expanded to an alternative field, that one of frequency ν. A further extension added energy(E) as a variable, due to the equation $E = h \cdot \nu$. Spectroscopic data is often represented by a spectrum, meaning the plot of the response in proportion of wavelength or frequency.

As it has been mentioned above, **spectroscopy** is strictly associated with the measurement of radiation intensity with reference to the wavelength or frequency. This sort of measurements can be conducted by experimental spectroscopic devices such as spectrometers, spectrophotometers, spectrographs or spectral analyzers.

1.2 Spectrometry

Spectrometry [3] constitutes the technique that is being used so as to assess the concentration or amount of a specific chemical compound. It is a com-

---

[1] http://en.wikipedia.org/wiki/Spectroscopy
[2] http://loke.as.arizona.edu/~ckulesa/camp/spectroscopy_intro.html
[3] http://en.wikipedia.org/wiki/Spectrometry

mon practice to combine spectrometry along with spectroscopy, mentioned above, in physical and analytical chemistry for the identification of substances through the spectrum either emitted from or absorbed by them.In addition, they do contribute to the field of astronomy and remote sensing as well. The majority of large telescopes is equipped with spectrometers, since the last ones have been instrumental to measurements, as far as chemical compositions and natural properties of astronomical objects are concerned.

1.3   Spectral Imaging (SI)

Spectral imaging is a branch of spectroscopy and photography in which a complete spectrum or partial spectral information (such as the Doppler shift or Zeeman splitting of a spectral line) is acquired at each position of an image plane. Spectral imaging does allow extraction of additional information the human eye fails to capture with its receptors for red, green and blue. Applications related to astronomy, solar physics, analysis of plasmas in nuclear fusion experiments, planetology, and Earth remote sensing are sparked by the benefits of spectral imaging.

Various distinctions among techniques are applied, based on criteria including spectral range, spectral resolution, number of bands, width and contiguousness of bands, and application. The terms include **Multi Spectral Imaging** 1.3.3, **Hyper Spectral Imaging** 1.3.4, full spectral imaging, imaging spectroscopy or chemical imaging. These terms are seldom applied to the use of only four or five bands that are all within the visible light range.

Important new developments in the field of biomedical optical imaging (OI) allow for unprecedented visualization of tissue microstructure and enable quantitative mapping of disease-specific endogenous and exogenous substances [1]. Spectral imaging (SI) is one of the most promising OI modalities, belonging to this general field, and it will be reviewed in more detail in this section of Chapter 1.

SI combines **spectroscopy with imaging**. A spectral imager provides spectral information at each pixel of a two-dimensional (2D) detector array. The SI systems acquire a three-dimensional (3D) data set of spectral and spatial information, known as spectral cube. The spectral cube can be considered as a stack of images, each of them acquired at a different wavelength. Combined spatial and spectral information offers great potential for the non-destructive/invasive investigation of a variety of studied samples.

Spectroscopy finds applications in analytical chemistry since a long time.

Different spectroscopy types and modalities exist, depending on the optical property that it is intended to be measured, namely, absorption, spontaneous emission (fluorescence, phosphorescence), scattering (Rayleigh elastic, Raman inelastic) spectroscopy, etc. As the light travels into the sample, photons are experiencing absorption, which may result in fluorescence emission and multiple scattering due to the local variation of the index of refraction. Spectrometers measure the intensity of the light emerging from the sample as a function of the wavelength. The collected light passes through a light-dispersing element (grating), which spatially splits the light wavelengths onto the surface of an optical sensor array, interfaced with a computer for recording and processing the spectrum. Sample illumination can be provided by either a broadband (e.g., white light) or a narrowband light source. In the first case, the measured spectra provide information for the absorption and scattering characteristics of the tissue. In the second case, the measured spectra probe the fluorescence characteristics of the sample. Particularly, in steady-state fluorescence spectroscopy, a narrowband light source is used for fluorescence excitation, such as lasers, LEDs, or filtered light sources, emitting typically in the blue-ultraviolet band. A sensitive optical sensor is used for collecting the emission spectra. [2]

The collected emission spectra can provide diagnostic information for the compositional status of the sample. This makes spectroscopy an indispensable tool for nondestructive analysis and for the development of novel, noninvasive diagnostic approaches. Particularly, in biomedical sciences, *the diagnostic potential of tissue spectroscopy is based on the assumption that the absorption, fluorescence, and scattering characteristics of the tissue change during the progress of the disease.*

Over the last 20 years, spectroscopy has been extensively investigated as a tool for identifying various pathologic conditions on the basis of their spectral signatures. It has been demonstrated that spectroscopy can successfully probe intrinsic or extrinsic chromophores and fluorophores, the concentration of which changes during the development of the disease. In its conventional configuration, spectroscopy uses single-point probes that cannot easily sample large areas or small areas at high spatial resolution (SR). It is obvious that this configuration is clearly suboptimal when solid and highly heterogeneous materials, such as the biological tissues, are examined. In these cases, the collected spectrum is the result of the integration of the light emitted from a great number of area points. This has the effect of mixing together signals originating from both pathologic and healthy areas, which makes the spectral signature-based identification problematic. Looking at the same problem from another perspective, **point spectroscopies** are considered as inefficient in cases where the mapping of some characteristic, spectrally identifiable property, is of the utmost importance.

Spectroscopy probes optical signals with **high spectral resolution** but with **poor spatial resolution (SR)**. The vastly improved computational power together with the recent technological developments in tunable optical filter and imaging sensor technologies have become the catalysts for merging together imaging and spectroscopy. Both areas, imaging and spectroscopy, continue to be affected by technological innovations that enable faster acquisition of superior-quality data. **SI has the unique feature of combining the advantages of both imaging and spectroscopy (high spatial and spectral resolution) in a single instrument**. In SI, light intensity is recorded as a function of both wavelength and location. In the image domain, the data set includes a full image at each individual wavelength. In the spectroscopy domain, a fully resolved spectrum at each individual pixel can be recorded. These devices can measure the spectral content of light energy at every point in an image. Multiple images of the same scene at different wavelengths are acquired for obtaining the spectra. As an example, an SI device integrating an imaging sensor with 1000×1000 pixels provides 1 million individual spectra. A spectrum containing 100 data points results from an equal number of spectral images. Assuming that the intensity in each pixel is sampled at 8 bits, then the size of the resulting spectral cube equals to 100 Mbytes. Due to the huge size of the collected data sets, SI data processing, analysis, and storage require fast computers and huge mass memory devices. Several mathematical approaches are used for spectral classification and image segmentation on the basis of the acquired spectral characteristics. The spectra are classified using spectral similarity measures, and the resulting different spectral classes are recognized as color-coded image clusters. SI can be easily adapted to a variety of OI instruments such as camera lenses, telescopes, microscopes, endoscopes, etc. For this reason, applications of SI span from planet and earth inspection (remote sensing) to internal medicine and molecular biology. [1]

1.3.1   Spectral Cubes

The information that is primarily collected by spectral imagers and then appropriately processed based on the kind of application running, is stored in 3D data structures for further analysis. This sort of data structures are known as **Spectral Cubes (SC)** [4]. A spectral cube consists the three dimensional projection of a great number of consecutive and registered sets of hyper spectral or multi spectral images. Being more specific, the first two dimensions respond to spatial dimensions, for account of pixel coordinates and the third one refers to spectral dimension, meaning a specific wavelength of the electromagnetic spectrum. A glance at figures 1.1a and 1.1b offer

---

[4] http://en.wikipedia.org/wiki/Hyperspectral_imaging

profound perception of how a spectral cube does look like.

<table>
<tr><td>(a) 3-D projection</td><td>(b) 3-D coordinates</td></tr>
</table>
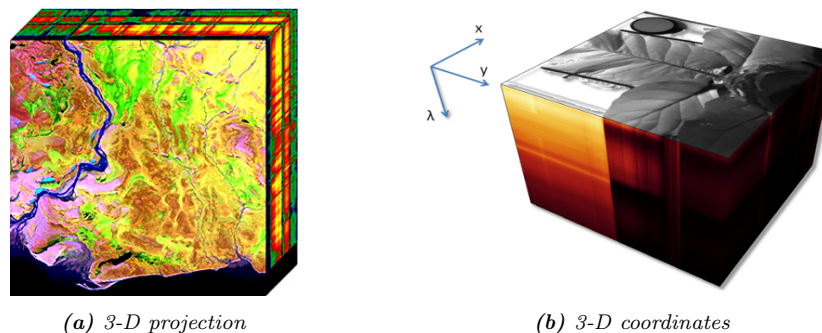
Figure 1.1: *Hyper Spectral Cubes*

1.3.2 Color vs. Spectral Imaging

Photons encountering the pixels of an imaging sensor create electrons in pixel cells **(photoelectric effect); thereby, the number of photons is proportional to the number of electrons**. The photon's wavelength information, however, is not "transferred" to the electrons. Hence, unfiltered imaging chips are color blind. Color or SI devices employ optical filters placed in front of the imaging chip. Color imagers use either Si charge coupled devices (CCD) or C-MOS sensors, which are sensitive in the visible and in the near-infrared (NIR) part of the spectrum (400-1000 nm). A band-pass filter is used for rejecting the NIR band (700-1000 nm). In 3-chip configurations, three photon channels are created with the aid of a trichroic prism assembly, which directs the appropriate wavelength ranges of light to their respective sensors. Camera electronics combine the red, green, and blue (R, G, B) imaging channels composing a high-quality color image, which is delivered to external devices through an analog or digital interface. An alternative, cheaper, and more popular color camera configuration employs a single chip, where the color filters are spread, similar to a mosaic, across all pixels of the sensor. Due to the fact that each pixel "sees" only one primary color, three pixels are required to record the color of the corresponding area of the object. This reduces significantly the SR of the imager. This unwanted effect is partially compensated with a method called **"spatial color interpolation"** carried out by the camera electronics. The interpolation algorithm estimates the two missing primary color values for a certain pixel by analyzing the values of its adjacent pixels. In practice, even the most excellent color space interpolation methods cause a low-pass effect. Thus, single chip cameras yield images that are more blurred than those of 3-chip or of monochrome cameras. This is especially evident in cases of subtle, fiber-shaped image structures. Color cameras emulate the human vision for

color reproduction and are real-time devices since they record three spectral bands simultaneously at very high frame rates. Human vision-emulating color imaging devices usually describe color with three parameters (RGB values), which are easy to interpret since they model familiar color perception processes. They share, however, the limitations of human color vision. Color cameras and human color vision allocate the incoming light to three color coordinates, thus missing significant spectral information. Due to this fact, objects emitting or remitting light with completely different spectral components can have precisely the same RGB coordinates, a phenomenon known as **metamerism**. The direct impact of the metamerism is the inability of the color imaging systems to distinguish between materials having the same color appearance but different chemical composition. This sets serious limitations to their analytical power and consequently, to their diagnostic capabilities. [1]

Unlike images taken with standard color (RGB) cameras, SI information is not discernible to the human eye. In SI, a series of images is acquired at many wavelengths, producing a spectral cube. Each pixel in the spectral cube, therefore, represents the spectrum of the scene at that point. The nature of imagery data is typically multidimensional, spanning spatial and spectral dimensions (x, y, λ).

A color camera captures typically three images corresponding to the band-pass characteristics of the RGB primary color filters. Color image pixels miss significant spectral information as it is integrated into three, broad spectral bands. The color of a pixel can be represented as vector in a three-dimensional "color space" having the RGB values as coordinates. SI systems collect a stack of pictures, where each image is acquired at a narrow spectral band and all together compose the spectral cube. A complete spectrum can be calculated for every image pixel, which can be otherwise represented as a vector in a "multidimensional spectral space".

1.3.3 Multi Spectral Imaging

Multi Spectral Imaging (MI) [5] is responsible for capturing image data at specific frequencies across the electromagnetic spectrum. The wavelengths may be separated by filters or by the use of instruments that are sensitive to particular wavelengths, including light from frequencies beyond the visible light range, such as infrared. **MI** images are the main type of images acquired by remote sensing (RS) radiometers. Dividing the spectrum into many bands, **MI** is the opposite of panchromatic, which records only the total intensity of radiation falling on each pixel. Spectral imaging with more

---

[5] http://en.wikipedia.org/wiki/Hyperspectral_imaging

numerous bands, finer spectral resolution or wider spectral coverage may be called **Hyper Spectral** or **Ultra Spectral** (1.3.4).

1.3.4   Hyper Spectral Imaging

Hyper Spectral Imaging (HI) [6] is a technology widely used for remote imaging, in an effort to extract a maximum of information out of images captured under strongly varying imaging conditions. It provides options for three-dimensional data generation with high spectral resolution across the full electromagnetic spectrum of frequencies, beyond the visible. This visual extension beyond the scope of human eye renders **HI** a powerful analytical tool, which has been extensively used in a wide variety of fields including *agriculture, medicine, artistics [3] [4], satellite imaging [5], astronomy, surveillance [6], [7], chemical imaging, physics and environment [5].*

1.3.5   Hyper Spectral vs Multi Spectral Imaging

The distinction between **Hyper Spectral** and **Multi Spectral** pertains to the number of narrow bands or the type of measurement. **Multi Spectral** deals with several images at discrete and somewhat narrow bands. Being "discrete and somewhat narrow" is what distinguishes **MI** in the visible from color photography. A **MI** sensor may have many bands covering the spectrum from the visible to the long wave infrared. **MI** images do not produce the "spectrum" of an object. On the other hand, **Hyper Spectral** deals with imaging narrow spectral bands over a continuous spectral range, and produce the spectra of all pixels

Figure 1.2: *Multi Spectral vs. Hyper Spectral Imaging*

in the scene. So, a sensor with only 20 bands can also be **HI** when it covers the range from 500 to 700 nm with 20 bands each 10 nm wide. Figure 1.2 helps us looking at the differences pinpointed above more closely.

---

[6]http://en.wikipedia.org/wiki/Hyperspectral_imaging

1.4 Hyper Spectral Analysis

Spectral analysis [7] when combined with spatial data adds a significant amount of information that can be used to improve image exploitation and interpretation. To combine spectral information with spatial imagery, the sensor or camera has to be able to create images within the user defined narrow spectral bands rather than the wide-band imagery that the conventional cameras produce. Compared to conventional filter based imaging systems, spectral cameras provide higher spectral and spatial resolution, flexible wavelength selections in software, broader spectral coverage and shorter acquisition times.

1.5 Hyper Spectral Cameras

Hyper Spectral Analysis can be achieved by an hyper spectral camera system that includes optics, an imaging spectrograph, a camera displaying the spectral information and a software package to display and calculate the results. Hyper spectral cameras are used to acquire the hyper spectral target image at tens or hundreds of wavelengths simultaneously. Such developed softwares create new possibilities for imaging applications where spectroscopy methods can be totally attuned to standard and efficient image processing methods. The recorded full spectrum for each pixel of the image can be leveraged to a wide variety of purposes, such as classification, material detection, accurate colour calculations or chemometrics over the full range. [1]

1.5.1 Hardware Configuration and Calibration

SI camera systems, either HSI or MSI, consist of a monochrome sensor, an electronically controlled spatial or spectral scanning mechanism, imaging optics, and a computer platform for storage, display analysis, and processing of imaging data. Control electronics synchronize the scanning and the data capturing processes, so that a set of spectral images are collected as members of the spectral cube. [1]

The number of the spectral bands that an SI system is capable of acquiring determines the distinction between multi spectral imaging (MSI) and hyper spectral imaging (HSI). MSI devices typically acquire 5-20 spectral bands, while HSI systems acquire up to a few hundreds of spectral bands (see 1.3.5).

---

[7] http://en.wikipedia.org/wiki/Hyperspectral_imaging

Ultra spectral imaging (USI) devices are currently under development with the capacity of acquiring thousands of very narrow spectral bands.

SI systems use monochrome sensors or sensor arrays, which can capture only two of the three spectral dimensions of the spectral cube at a time. To capture the third dimension, spatial or spectral scanning is required. Depending on the method employed for building the spectral cube, SI devices are classified in different categories. The categorization is as follows:

1. *whiskbroom* SI devices, where a linear sensor array is used to collect the spectrum (λ dimension) from a single point at a time; the other two spatial coordinates are collected with (x, y) spatial scanning.

2. *pushbroom* SI devices in which a 2D sensor array is used, the one dimension of which captures the first spatial (x) coordinate and the other the spectral coordinate in each camera frame; the second spatial coordinate (y) is captured with line (slit) scanning.

3. *staring* SI devices, where a 2D sensor array is coupled with an imaging monochromator, which is tuned to scan the spectral domain and in each scanning step, a full spectral image frame is recorded.

Whiskbroom and pushbroom imagers utilizing spatial scanning for building the spectral cube do not provide live display of spectral images, since they are calculated from the spectra after the completion of the spatial scanning of the corresponding area. Staring imagers, on the other hand, are based on the tuning of the imaging wavelength and the spectra are calculated from the spectral cube composed by the spectral images that are captured in time sequence. Compared to the other approaches, staring imagers have the advantage of displaying live spectral images, which is essential for aiming and focusing.

Selecting the SI camera optimal configuration and components requires a "systems" approach. The intended application determines the SI system's spectral range and resolution. Si CCD detectors can be used to cover the spectral range ultraviolet(UV), visible and NIR up to 1 µm. InGaAs detectors are suitable for the up to 1.7 µm NIR range. For longer infrared wavelengths, HgCdTe or InSb cameras must be used. Ideally, the wavelength range of the monochromators should match at least a significant part of the spectral range within which the selected detector is sensitive. Narrowband imaging and monochromator optics reduce the overall light throughput of an SI system. Moreover, the light throughput of the monochromator depends on the wavelength. Furthermore, the quantum efficiency (QE) of the detector also changes with the wavelength.

SI system's calibration is very essential in order to achieve "device-independent" spectral measurements. Calibration can be performed with the aid

of a reference sample displaying a known or a flat spectrum over the entire operating wavelength range. A calibration curve or a lookup table can be obtained by comparing the known spectral characteristics of the calibration sample with that measured by the SI system spectra. Image brightness can be corrected on the basis of the calibration data, after spectral image acquisition. The calibration curve or the lookup table can also be integrated into the system's software for controlling the detector's exposure time during image acquisition, in all tuning steps of the filter. By changing the detector's exposure or gain settings, the wavelength dependence of the SI system's response is compensated and the spectral images that are acquired and captured are calibrated. [1]

1.6   Hyper Spectral Imaging Applications

As it has already been mentioned, there exist numerous applications emerging from the spectral analysis that is being provided by Hyper Spectral imaging. For nearly a decade, this technology was primarily used for purposes like surveillance, reconnaissance, environmental and geological studies. However, the application of hyper spectral imaging in the biomedical arena has been negligible due to high-instrumentation costs and problems arising from the clinical use of hyper spectral sensors. With recent achievements in sensor technology and increasing affordability of high performance spectral imagers, hyper spectral systems constitute one of the most important key areas in medical imaging. The early diagnosis of cancer, one of the thorniest medical problems, is now possible, since the evolution of hyper spectral sensors allows the scanning of a patient's body to identify precancerous lesions or to provide critical spectral data through endoscopic procedures. The extension and improvement of hyper spectral imaging in biomedical and clinical diagnosis is within the grasp of researchers. [8] [9]

The advantages of this technology regarding diagnostic health care applications include a high-resolution imaging of tissues either at macroscopic or cellular levels and the capability to generate highly accurate spectral information related to the patient, tissue sample, or any other disease condition. In particular, the vast investment of hyper spectral imaging in medicine lies on the generation of wavelength-specific criteria for disease conditions on spectral features. As a consequence, an ideal technology for high-throughput patient screening and non-invasive diagnosis is begotten.

Due to their unparalleled ability to reveal abnormal spectral signatures, hyper spectral medical instruments hold great potential for non-invasive diagnosis of cancer, retinal abnormalities and assessment of wound conditions, for instance diabetes. A portable hyper spectral imager could also aid the

analysis of human body fluids, such as blood, urine, saliva, semen and determine blood oxygenation levels of tissues, which could be of prime importance during surgeries. Yet importantly, it could perform diagnosis for dental diseases. It is a great advantage for a patient the fact that not only does an early diagnosis of an ailment take place, but an appropriate treatment may also be applied at the same time. [1]

Hyper spectral signatures when combined with targeting algorithms would in essence offer unique diagnostic information. There is an increasing level of interest on the part of health care providers to investigate possible ways of reducing health care costs by providing timely treatments for many types of disease conditions. **Hyper Spectral scanning imaging** is expected to contribute a lot in this pursuit. [2]

1.7 Measures of Spectral Similarity

Considering the spectral nature of the project, it is essential to be able to compare the estimated spectra with the reference spectra, in order to probe the efficiency of the system. The spatial information is perceived as a group of n-dimensional vectors in the processing procedure, where n responds to the total number of different spectra being measured. As a consequence, a wide variety of statistic measures can be applied in order to measure the degree of similarity between the achieved and expected results. The metrics, which has been used for the needs of this implementation, are following. [10] [11]

1.7.1 Euclidean Distance/Euclidean Norm

In mathematics, the **Euclidean Distance** or **Euclidean Norm** is the ordinary distance between two points that one would measure with a ruler. In Cartesian coordinates if $\mathbf{p} = (p_1, p_2, ..., p_n)$ and $\mathbf{q} = (q_1, q_2, ..., q_n)$ are two points in Euclidean n-space, then the distance from $\mathbf{p}$ to $\mathbf{q}$ or from $\mathbf{q}$ to $\mathbf{p}$ is given by the formula:

$$
\begin{aligned}
d(p,q) = d(q,p) &= \sqrt{(q_1 - p_1)^2 + (q_2 - p_2)^2 + \cdots + (q_n - p_n)^2} \\
&= \sqrt{\sum_{i=1}^{n}(q_i - p_i)^2} \\
&= \parallel q - p \parallel
\end{aligned} \tag{1.7.1.1}
$$

1.7.2   Root Mean Square Error (RMSE)

Mean Square Error (MSE) is one of many ways to quantify the difference between values implied by an estimator and the true values of the quantity being estimated. MSE measures the average of the squares of errors. The error is the amount by which the value implied by the estimator differs from the quantity that is being estimated. Taking the square root of MSE yields the **Root Mean Square Error (RMSE)** or **Root Mean Square Deviation (RMSD)**, which has the same units as the quantity being estimated. If $\mathbf{p} = (p_1, p_2, ..., p_n)$ and $\mathbf{q} = (q_1, q_2, ..., q_n)$ are two vectors, then the 1.7.2 between them is given by the formula 1.7.2.1:

$$RMSE(p, q) = \sqrt{\frac{\sum_{i=1}^{n}(p_i - q_i)^2}{n}} \qquad (1.7.2.1)$$

1.7.3   Spectral Angle Mapper (SAM)

The **Spectral Angle Mapper** is a physically based spectral classifier that determines the spectral similarity between the vectors of measured and reference spectra. This kind of similarity is estimated based on the angle between the two aforementioned vectors. The smaller the angle is, the greater approach to the reference spectra is achieved. In other words, smaller angles reflect increased similarity. This angle metric between vectors $\mathbf{p}$ and $\mathbf{q}$ is estimated by the formula 1.7.3.1:

$$SAM(p, q) = \hat{\theta} = \arccos\left(\frac{p * q}{\| p \| \| q \|}\right) \qquad (1.7.3.1)$$

Chapter 2

Hyper Spectral Imager

2.1 Problem Definition And Description

The task assigned to this thesis does require an innovative reconstruction of the three dimensional data structure, known to us, as spectral cube (1.3.1). This kind of spectral cube is going to result from the spectral distinction in the images provided by a hyper spectral scanning procedure. This form of distinction aims at creating a set of images, where each one responds to a specific rather than multiple spectral bands. Although it may seem to be a simple task to deal with, there is a wide variety of aspects to be implemented and factors that must be taken into consideration, in order to provide an efficient solution. The diversity of activities that has to be covered gives a multilateral potential to the nature of the required work.

First of all, a spectral cube is consisted of a great number of images captured in very close narrow bands. These images are gained by a **hyper spectral camera**, which needs to be constructed as well [9], for the purposes of this project. As long as this type of hyper spectral camera has been available, the second step of the procedure is to capture the consecutive images **manually** *step by step* and later **automatically**.

After having successfully acquired the images, which must be noiseless and well focused, from the experimental set up, the aforementioned reconstruction leads the implementation [12]. Being more specific, this reconstruction refers to the acquisition of a new set of images, in which a single one wavelength is represented by each one of the new reconstructed images. In particular, we manage to provide a series of registered images that are algorithmically reconstructed and each one responds to a single band every few nanometers across the electromagnetic spectrum. As a result, our spectral cube is created by the hyper spectral scanning of a "target-scene". Last but not least, the spectral response is being estimated at different pixel positions, in order to demonstrate the efficiency and accuracy of the implementation, before the head start of new phases [13].

High light throughput, not real-time reconstruction and protection from photobleaching phenomena are expected to be the main characteristics of our HSI.

2.2 Set Ups

2.2.1 Manual-Step Set Up

The initial concept of the experimental set up includes the construction of a system that is going to perform **manual** hyper spectral scanning by the contribution of a user. The different parts required along with all the necessary technical information, are included in the following tables and figures.
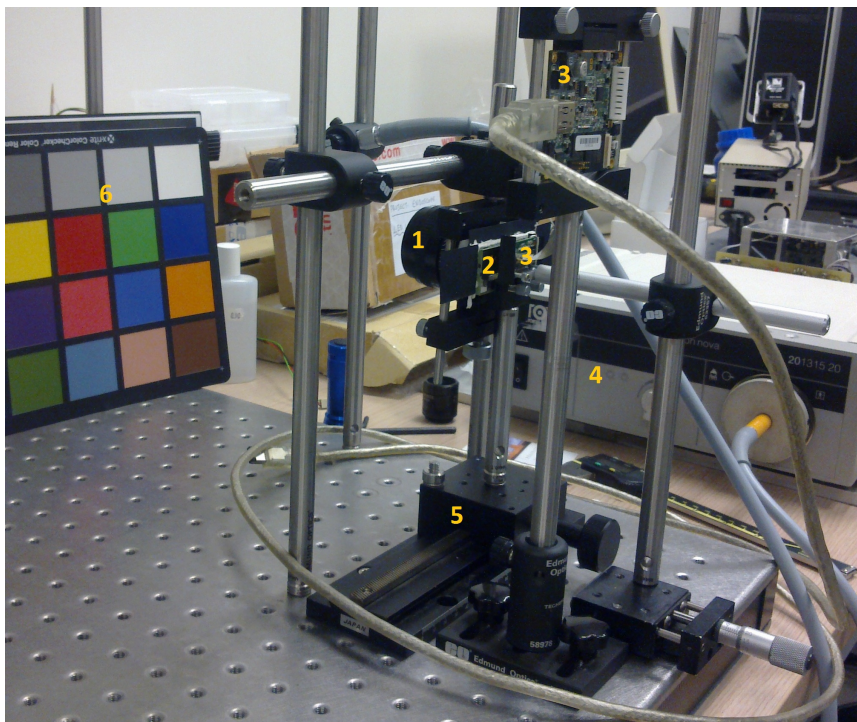
Figure 2.1: *Manual-Step HSI Set Up*

The marked different components are listed right above:

1. Sofradir-EC(Electrophysics) L25F1.4 25mm f/1.4 C-Mount Objective Lens with Iris (*figure 2.4, table 2.1*)

2. Linear Variable Short-Wave Pass Filter($330 - 745$ nm, $\#83 - 983$, Edmund Optics) (*figure 2.5, table 2.2*)

3. PointGrey Dragonfly®2 1/3" Sony® CCDs BW or Color (IEEE-1394a FireWire digital camera) (*figure 2.7, tables 2.3, 2.4*)

4. Halogen/Xenon Light Source (*figure 2.8, table 2.5, figure 2.11*)

5. Filter Holder, Stepper Stage

6. X-Rite ColorChecker$^{\circledR}$ (*figure 2.13*)
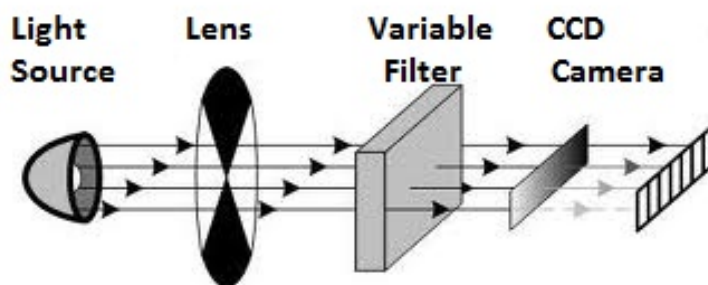
Figure 2.2: *Optical Elements*

It should be also mentioned that the **FlyCap Point Grey Research** program has been used for calibration, viewing and capturing purposes of the hyper spectral scanned images. Calibration and focus of lens are performed once, before the beginning of the hyper spectral scanning.

2.2.2   Auto-Step Set Up

The final experimental set up has been upgraded to a new imaging system that performs the hyper spectral scanning procedure automatically. This task includes automatic and thus, accurate movement of a stepper motor that holds the variable filter. Apart from this, the auto-step HSI provides calibration automatically, as well. In this point, it should be mentioned that the calibration of camera and the focus of lens take place once, before the beginning of the hyper spectral scanning, right as in the manual-step set up. The only difference is that all these procedures are implemented by the contribution of an appropriately designed matlab GUI. The **single intervention** along with the **abolishment of the "slit-scan" technique** are the two innovations we introduce in such a HSI. The used components and materials are the same with those of the manual-step set up and are going to be presented analytically in the following section of this Chapter.
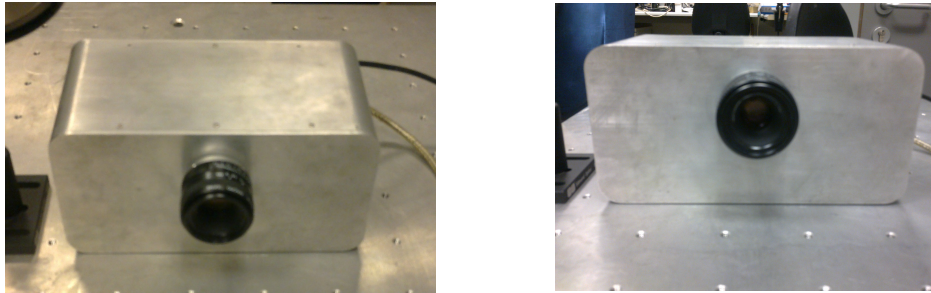
Figure 2.3: *Auto-step HSI*

2.2.3 Technical Specifications And Features

Sofradir-EC(Electrophysics) L25F1.4 25mm f/1.4 C-Mount Objective Lens with Iris

The Sofra L25F1.4 25mm F1.4 C-Mount Objective Lens features manual focus and an integrated adjustable iris diaphragm. These lenses also feature broadband lens coatings making them ideal low cost solutions for imaging in the near-infrared spectral range with reduced flare and ghosting. A C-Mount Extension Tube kit is also available for those applications requiring close focus and higher magnification.

Figure 2.4: *Sofradir-EC*

FEATURES	universal C-Mount for cameras and viewers, manual focus, integral adjustable iris diaphragm, broadband lens coatings for near-infrared imaging.
TECH SPECS	Objective Lens $\longmapsto$ 25mm

Table 2.1: *Sofradir-EC Specifications*

Linear Variable Band-Pass Filter$(330 - 745$ **nm,** $\#83 - 983$**, Edmund Optics)**

Designed for both individual and combined use, short, long-wave and band-pass Variable Edge Filters allow for blocking and passing of targeted wave-

lengths. Used independently, the short-wave linear variable filter has a wavelength range of $330 - 750$ nm with an average transmission of 97% from $400 - 750$ nm. The long-wave linear variable filter has a wavelength range of $300 - 845$ nm and an average transmission of 97% across the entire range. Bandpass filters only transmit a certain wavelength band, and block others. When combined, Linear Variable Filters can operate as a laser-line filter or a variable bandpass filter with tunable center wavelength and bandwidth.

A linear variable filter has an interference coating intentionally wedged in one direction to create a linear shift of the center wavelength across the length of the substrate. This shift allows for the broad filtering capabilities demonstrated by the short and long-wave variable filters. Short and long-wave variable filters work inversely of one another; the short-wave variable filter passes light throughout the filter's length until a blocking band is reached, whereas

Figure 2.5: *Linear Variable Filter*

the long-wave variable filter blocks light until a transmission band is reached. Blocking and transmission bands are adjustable by reorienting the filter to the light source.

With its broad blocking and transmission range, a single linear variable filter can replace an entire filter set. When synchronized with a single moving grading spectrometer, combined long and short-wave linear variable filters reduce scattered light and harmonics. In addition, combined linear variable filters can be used as a single variable excitation filter for various fluorescence applications using white light sources.

Dimensions (mm)	15×60
Slope Factor (%)	1.6
Linear Dispersion (%)	0.57
Transmission (%)	
400-750 nm	97
Optical Density OD	> 4.0
Wavelength (nm)	$330 - 750$
RoHS	compliant

Table 2.2: *Specs of Linear Band-pass Filter.*
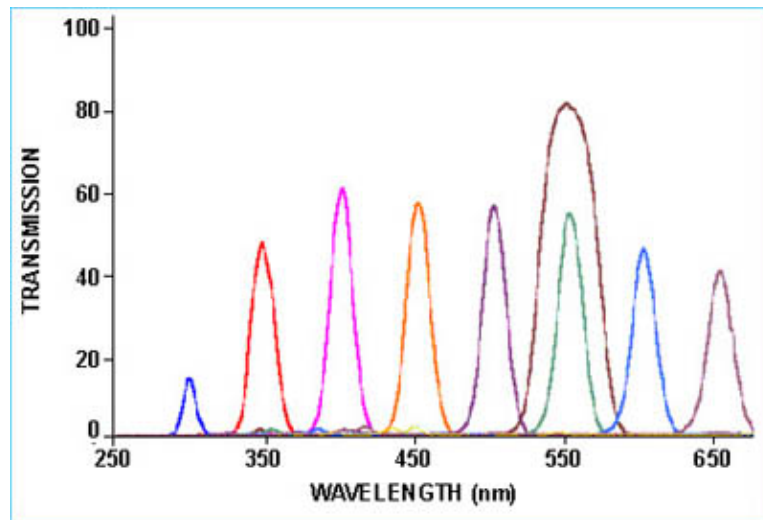
Figure 2.6: *Transmission of Band-Pass Filter.*

PointGrey Dragonfly®2 1/3" Sony® CCDs BW or Color

The Dragonfly®2 is a flexible, full-featured IEEE-1394a (FireWire) camera designed for imaging product development. The Dragonfly®2 has an 8-pin GPIO connector located on the back of the camera and case. Inputs can be configured to accept an external trigger signal. Outputs can be configured to send an output signal, strobe or PWM signal and can drive most TTL devices at approximately 10mA. The Dragonfly2 has a logic level serial port with a bandwidth capacity of up to 115.2 Kbps.

The Dragonfly®2 is also equipped with the ability to save and restore camera settings and imaging parameters via on-board memory channels. This is useful for saving default power-up settings, such as gain, shutter, video format and frame rate, etc., that are different from the factory defaults. The field-programmable gate array (FPGA) chip controls all camera functionality, including exposure, resolution and frame rate, pixel binning, user memory channels and more. It can also be updated with new functionality in the field.

Figure 2.7: *PointGrey Dragonfly®2 CCD Camera*

The two different models of the Dragonfly2 CCDs Camera that were used for the measurements of this project and their specifications are included in tables 2.3 and 2.4, respectively.

Models	Lens Specification
DR2-BW/COL-XX	Sony 1/3" CCD, BW/COLOR, 640×480
DR2-HIBW/HICOL-XX	Sony 1/3" CCD, BW/COLOR, 1024×768

Table 2.3: *Dragonfly® 2 CCD Camera Models.*

Specification	BW/COL	HIBW/HICOL
Image Sensor Type		Sony 1/3" progressive scan CCDs
Image Sensor Model	1CX424	1CX204
Sensor pixel size	$7.4\mu m$ square pixels	$4.65\mu m$ square pixels
Maximum Resolution	640×480	1024×768
Maximum Frame Rate	60 FPS	30 FPS
Lens Mount		C/CS-Mount, M12 microlens
A/D Converter		Analog Devices 12-bit analog-to-digital converter
Video Data Output		8, 16 and 24-bit digital data
Partial Image Modes		Pixel binning and region of interest modes via Format_7
Interfaces		6-pin IEEE-1394 for camera control and video data transmission 8
Power Requirements		8-30V, max 2W at 12V
Gain		Automatic/Manual/One Push Gain modes 0dB to 24dB
Shutter		Automatic/Manual/One Push/Extended Shutter modes 0.01ms to 66.63ms at 15 FPS, greater than 5s in extended mode
Gamma		0.50 to 4.00
Trigger Modes		DCAM v1.31 Modes 0, 1, 3, 4, 5 and 14
Signal To Noise Ratio		Greater than 60dB at 0dB gain
Dimensions		$64mm \times 51mm$ (bare board w/o case or lens)
Mass		45 grams (bare board w/ lens holder and C-mount adapter)
Camera Specification		IIDC 1394-based Digital Camera Specification v1.31
Emissions Compliance		Complies with CE rules and Part 15 Class A of FCC Rules
Operating Temp.		Commercial grade electronics rated from 0° to 45°C
Storage Temperature		-30° to 60°C
Remote Head Option		Available with 6-inch shielded ribbon cable
Case Enclosed Option		Available (except with remote head option)

Table 2.4: *Dragonfly® 2 CCD Camera Specifications.*

Light Source

The experimental procedure of the hyper spectral scanning has been held with the contribution of a light source. The **Halogen OSL 1 -EC Fiber Illuminator** was the first light source to be included in the setup. This unit is a high intensity fiber coupled light source that contains a 150 W halogen lamp with a 1000:1 exponentially variable control. It is designed to deliver strong, cool light for *microscopy and lab applications.*

Figure 2.8: *Halogen Fiber Illuminator*

Specifications	
Input Voltage	110-120 VAC, 220-240 VAC, 180W MAX
Light Input	40.000 foot-candles
Lamp Adjustment Range	1000:1(0 to 100%)
Color Temperature	3200K with standard EKE Lamp at Max Intensity
Lamp Life	250-10.000 hours
Humidity Range	0-80% Non considering
Weight(Light Source w/o Fiber bundle)	7.5lbs(3.4kg)

Table 2.5: *OSL 1-EC Fiber Illuminator specifications*

A careful look at the emission diagram (figure 2.9) provides useful information about the ability of the lamp to maintain the emitted spectra information inalterable and noiseless. It is obvious that the dynamic range of the OSL 1-EC Fiber Illuminator is extremely low at the wavelength range from 300 to 500 nm.
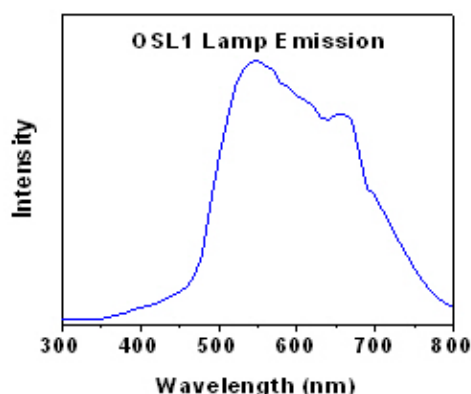
Figure 2.9: *OSL 1-EC emission diagram*

This fact indicates that the acquired spectra information under these conditions of illumination in the hyper spectral scanning procedure will be distorted in the aforementioned electromagnetic area. This is the reason for inserting an other kind of light source that is more sensitive in the ultra violet and violet region, so as to be able to improve the performance of the hyper spectral imager and get satisfactory results across the whole range of the variable filter. The light source that is going to sidestep this blue band insufficiency is the **Xenon Nova 201315-20, Storz**.

(a) *product*

Specifications	
Low-Intensity Illumination	yes
High-Intensity Illumination	yes
Watts(generator)	175
# of lamps	1
Lamp Duration	500 hours
Light Temperature	6000 K
Power Needed	100-240 VAC
Hz(operating)	50/60
Weight	8.8lbs (4kg)
Illumination Level Setting	continuous
Mode (imaging system)	manual

(b) *specifications*

Figure 2.11: *Xenon Nova 201315-20, Storz*

X-Rite ColorChecker®

The X-Rite ColorChecker® is a unique test pattern,which is scientifically designed to help determine the true color balance or optical density of any color rendition system. It is an industry standard that provides a non-subjective comparison with a "test pattern" of 24 scientifically prepared colored squares. Each color square(or patch) represents a natural object-human skin, foliage, blue sky, etc, providing a qualitative reference to quantifiable values. Each color will reflect light in the same way in all parts of the visible spectrum, thus maintaining color consistency over different illumination options. Some applications include *spectroscopy*, machine vision, photography, graphic arts, electronic publishing, and television. It is ideal for testing and standardizing color inspection and analysis systems.

The component of our hyper spectral imager, which is used as the target-image, is the **Large X-Rite ColorChecker® #37-756, Edmund**.
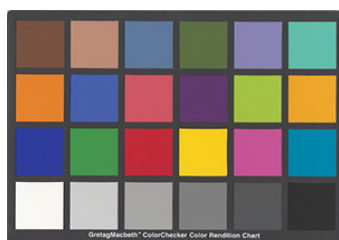
(a) *product*

Specifications	
Length (inches)	8
Width (inches)	11.5
Number of Patches	24
RoHS	Compliant

(b) *specifications*

Figure 2.13: *X-Rite ColorChecker®*

2.3 Scanning Procedure and Experimental Conditions

The experimental hyper spectral scanning procedure is conducted under darkness conditions, with the only light contribution that one of the selected light source. The four patches of the X-Rite ColorChecker® shown in figure 2.14, are chosen to be the target of scanning. The variable linear filter is being moved manually in front of the CCD camera by the user. The step of the filter movement does respond to 0.5 mm in the stepper stage. It needs to be mentioned that the procedure starts when the filter covers an initial small part of the CCD camera and ends up when the whole filter has passed through it. In this way, a complete hyper spectral cube of images is obtained. The images are handled by specific settings as far as gain, shutter and frame rate are concerned. These parameters are set to values that best serve the calibration conditions of experiment and camera equipment and at the same time prevent measurements from being obscured and saturated. Furthermore, it should be stated that a lot of attention is poured in the focusing of lens, so as to assure focused and clear images that will lead to an *efficient reconstruction*. All of these procedures are taking place only **once** and **before** the beginning of scanning in both set ups.
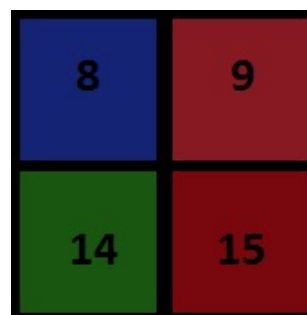
Figure 2.14: *Purplish Blue(patch no.8), Moderate Red(patch no.9), Green(patch no.14), Red(patch no.15)*

2.4 Reconstruction Algorithm

The main purpose of the reconstruction is to provide images that correspond to a single specific wavelength across the whole region of the scanned area of the filter. The images, captured by the aforementioned hyper spectral scanning procedure, except for the first and the last one, contain a great many of bands on account of the serial movement of filter. In other words, the algorithm that is going to be developed, needs to be able to pinpoint and separate the different spectral bands in the consecutive images. After having successfully completed the separating section, the founded same bands in the hyper spectral images must be processed [14] [15], and appropriately connected in order to result in the reconstruction of the initial target-image and thus, the acquisition of the reconstructed spectral cube.

In this point, it is important to state the criterion upon which the separation of different spectral bands takes place and the kind of connection that is required. The step of the filter movement is initially corresponded to 50 columns of each new scanned image. Being more specific, a step of **0.5 mm** of the filter movement through the CCD camera is algorithmically translated to a shift of 50 columns between two consecutive scanned images. However, this shift is parameterized in the respective code (algorithm 1) and assigned to a lot of other values, whose behavior must be and is examined extensively in the section **"Results" (2.5)**.

The construction of the final spectral cube is based on the diagonal connection of the spectral bands. This kind of connection refers to three different phases of scanning, that one till the total covering of image-target by the filter, that of total covering and that of uncovering. As far as the **till-covering** part is concerned, each image adds a fixed number of columns to the reconstruction till the maximum number of columns, provided by the type of CCD camera used, is reached, whereas, the same number of columns are subtracted during the **till-uncovering** process.

Figure 2.15 lends valuable insight to the conceptualization of the algorithmic concept mentioned above [16] [17]. In particular, it demonstrates the consecutive steps of filter *leftwise* or *rightwise* through the CCD camera that should be pinpointed in the scanned images. Then, the following diagonal incorporation of all covering phases results in the reconstructed cube.

(a) *rightwise(scanning from left to right)*   **(b)** *leftwise(scanning from right to left)*
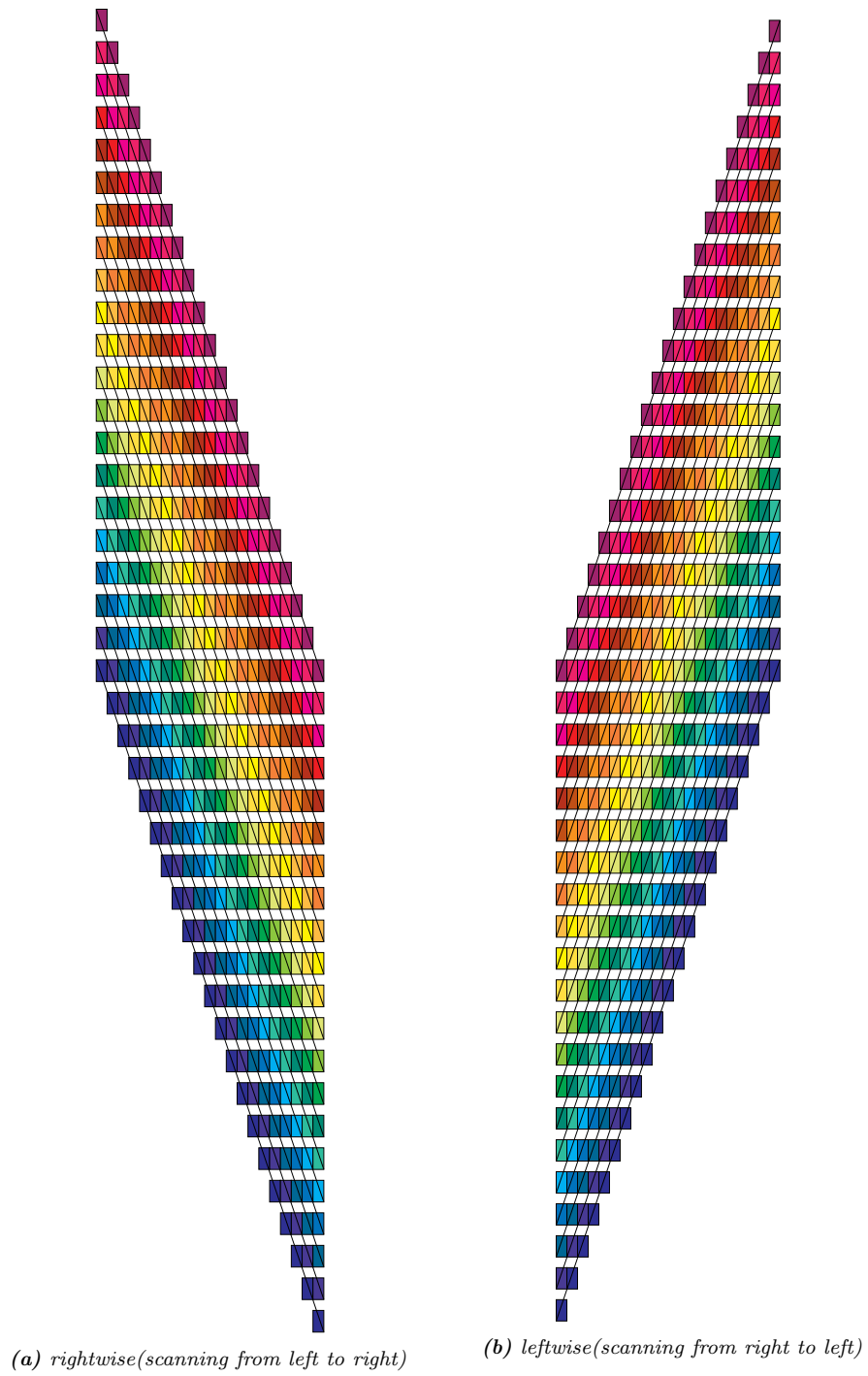
Figure 2.15: *Schematic Diagonal Reconstruction Of Spectral Cube*

2.5 Results

2.5.1 Spectral Cube Images & Spectra

It is expected that the patches would behave differently while the filter is scanning the target-image. This can be justified by the fact that blue bands cause illumination of blue patch, green bands of green patch, red bands of red and moderate red patch, respectively. Thus, illumination of a specific patch is accompanied with a sense of darkness for the rest of the three others. The aforementioned alternation in illumination constitutes a good way to confirm the efficient function of the reconstruction algorithm at a first stage. Reconstructed spectral images consisted of different fixed number of columns representing the step of the filter, are following. Estimated and reference spectra are also included, so as to examine quantitatively the effectiveness of our reconstruction.

(a) 430 nm (b) 460 nm (c) 490 nm (d) 510 nm

(e) 520 nm (f) 540 nm (g) 555 nm (h) 575 nm

(i) 595 nm (j) 630 nm (k) 665 nm (l) 695 nm
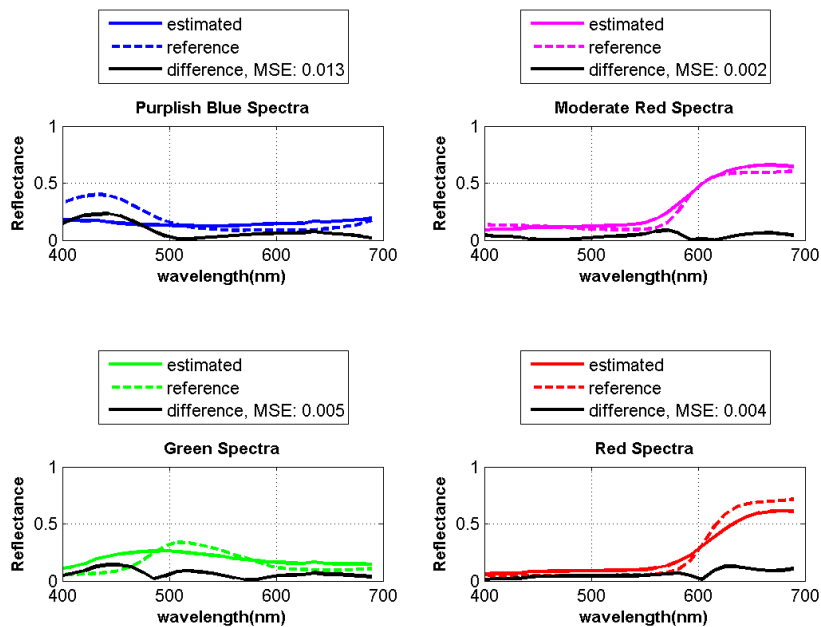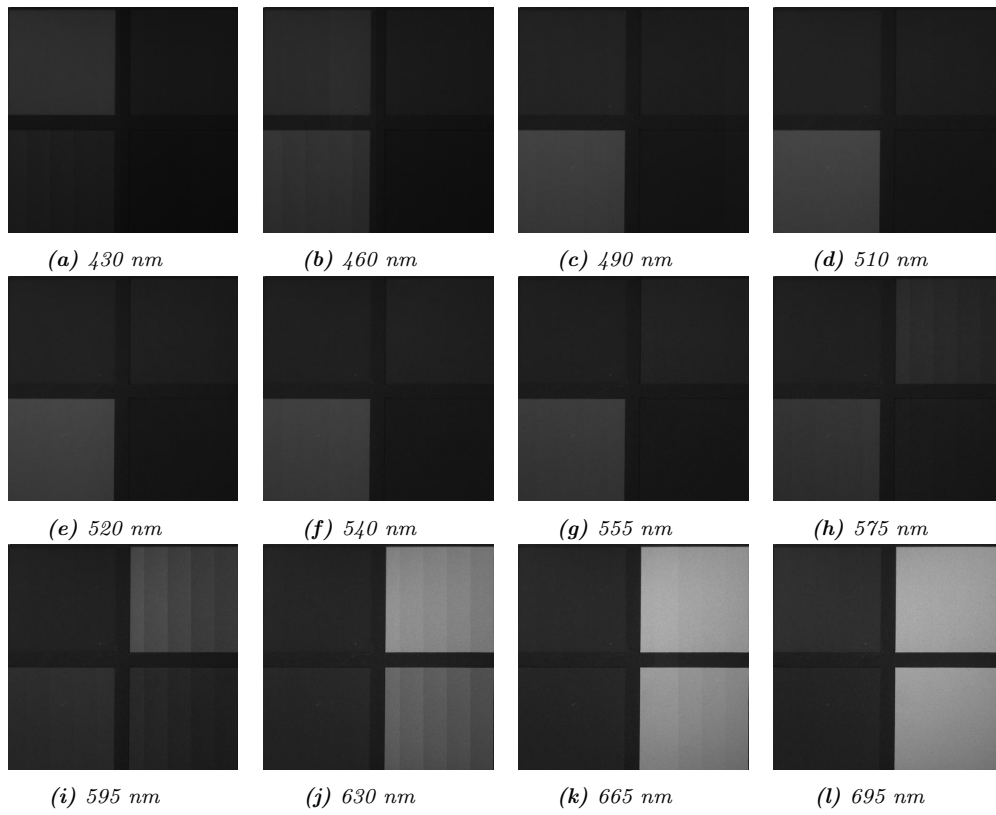
(m) reference and estimated spectra

Figure 2.16: step of reconstruction ⟼ 50 columns

(a) 430 nm (b) 460 nm (c) 490 nm (d) 510 nm

(e) 520 nm (f) 540 nm (g) 555 nm (h) 575 nm

(i) 595 nm (j) 630 nm (k) 665 nm (l) 695 nm
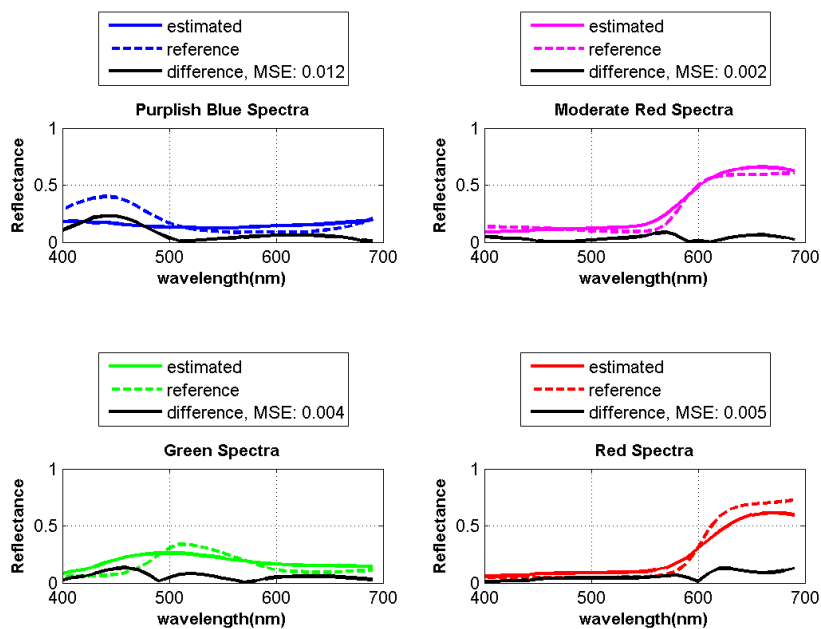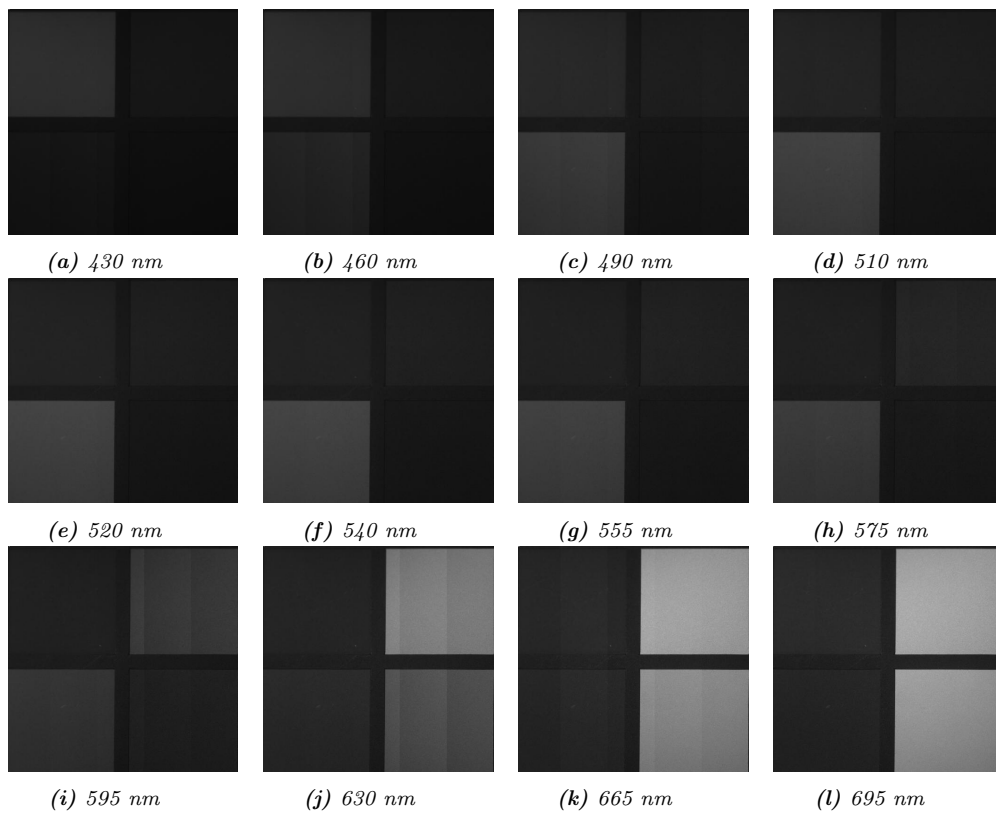
(m) reference and estimated spectra

Figure 2.17: step of reconstruction ⟼ 100 columns

(a) 430 nm   (b) 460 nm   (c) 490 nm   (d) 510 nm

(e) 520 nm   (f) 540 nm   (g) 555 nm   (h) 575 nm

(i) 595 nm   (j) 630 nm   (k) 665 nm   (l) 695 nm
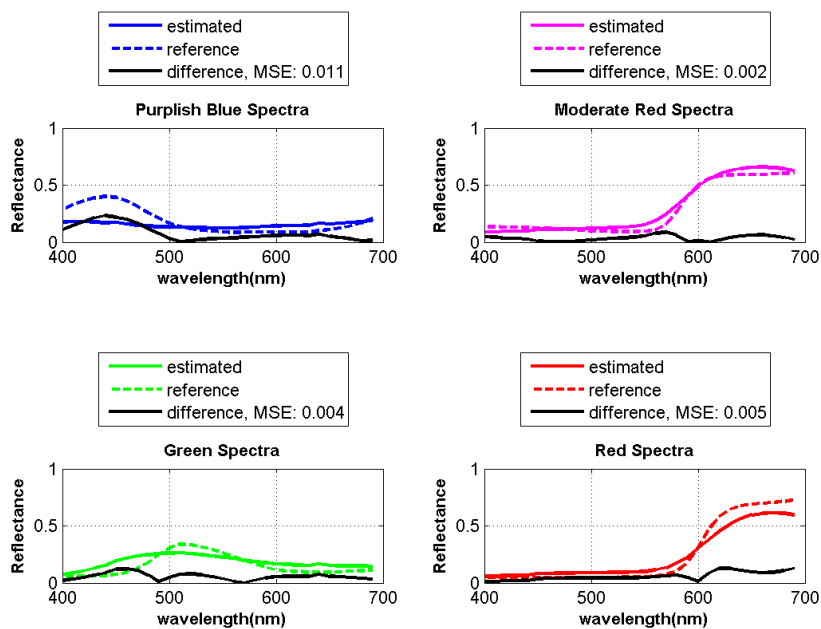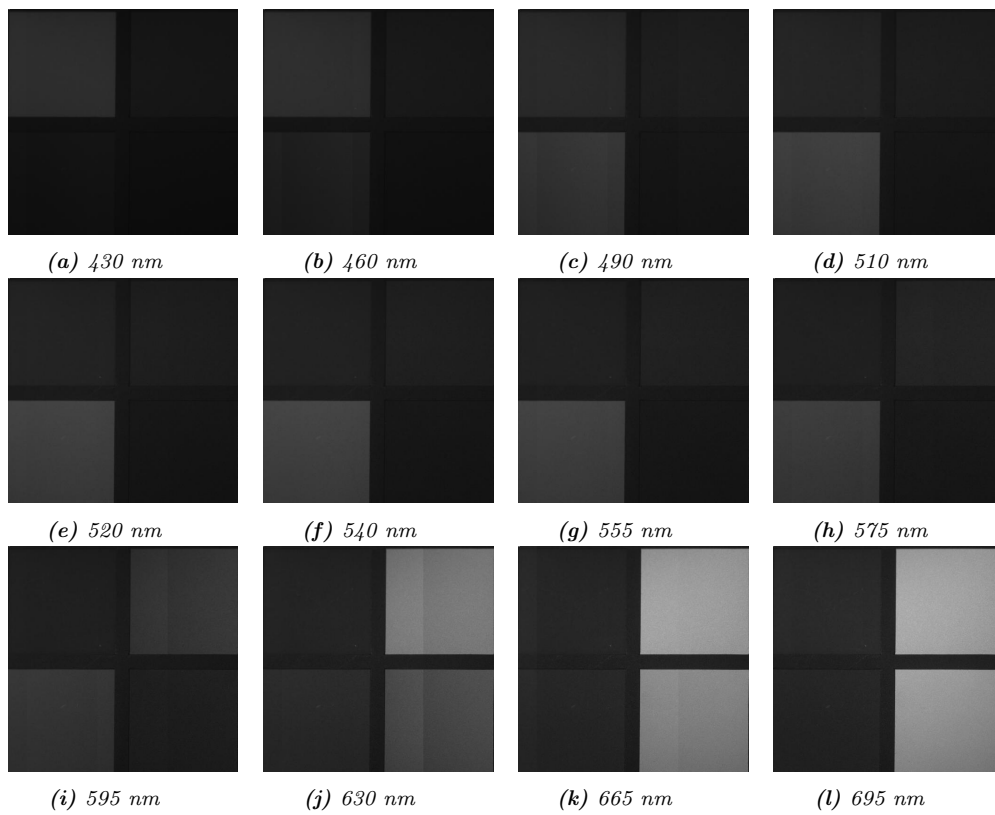
(m) reference and estimated spectra

Figure 2.18: step of reconstruction ⟼ 150 columns

(a) 430 nm   (b) 460 nm   (c) 490 nm   (d) 510 nm

(e) 520 nm   (f) 540 nm   (g) 555 nm   (h) 575 nm

(i) 595 nm   (j) 630 nm   (k) 665 nm   (l) 695 nm
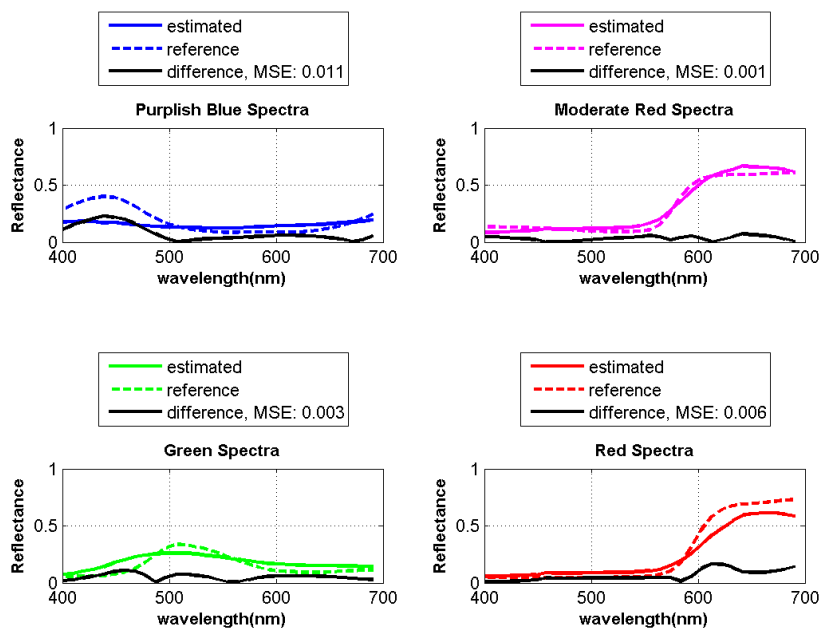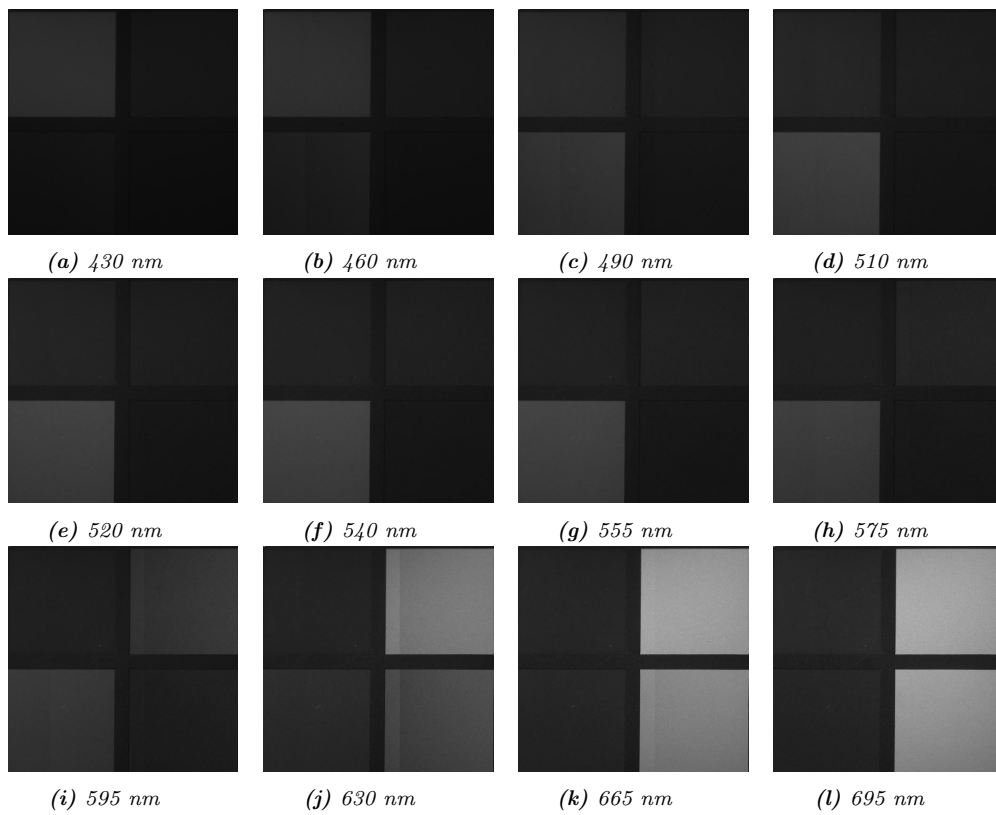
(m) reference and estimated spectra

Figure 2.19: *step of reconstruction ⟼ 200 columns*

(a) 430 nm   (b) 460 nm   (c) 490 nm   (d) 510 nm

(e) 520 nm   (f) 540 nm   (g) 555 nm   (h) 575 nm

(i) 595 nm   (j) 630 nm   (k) 665 nm   (l) 695 nm
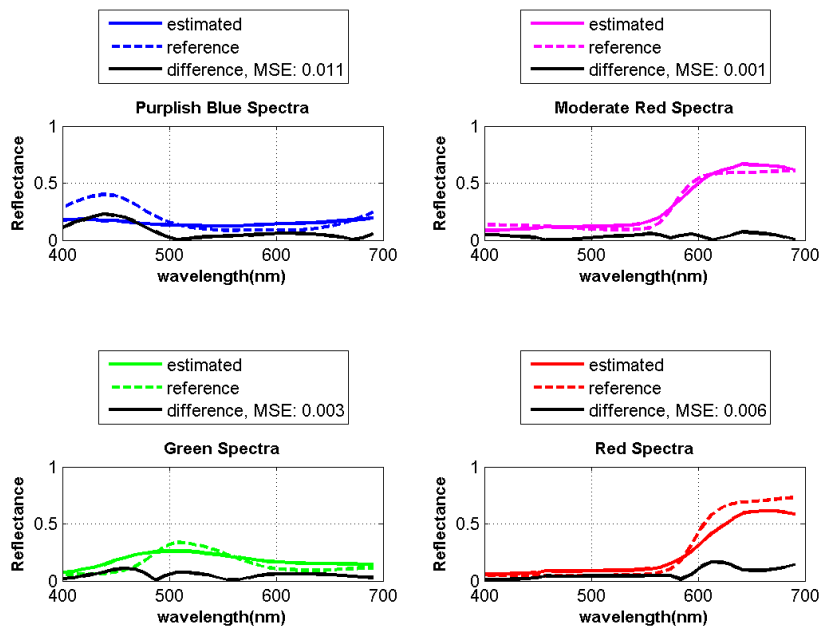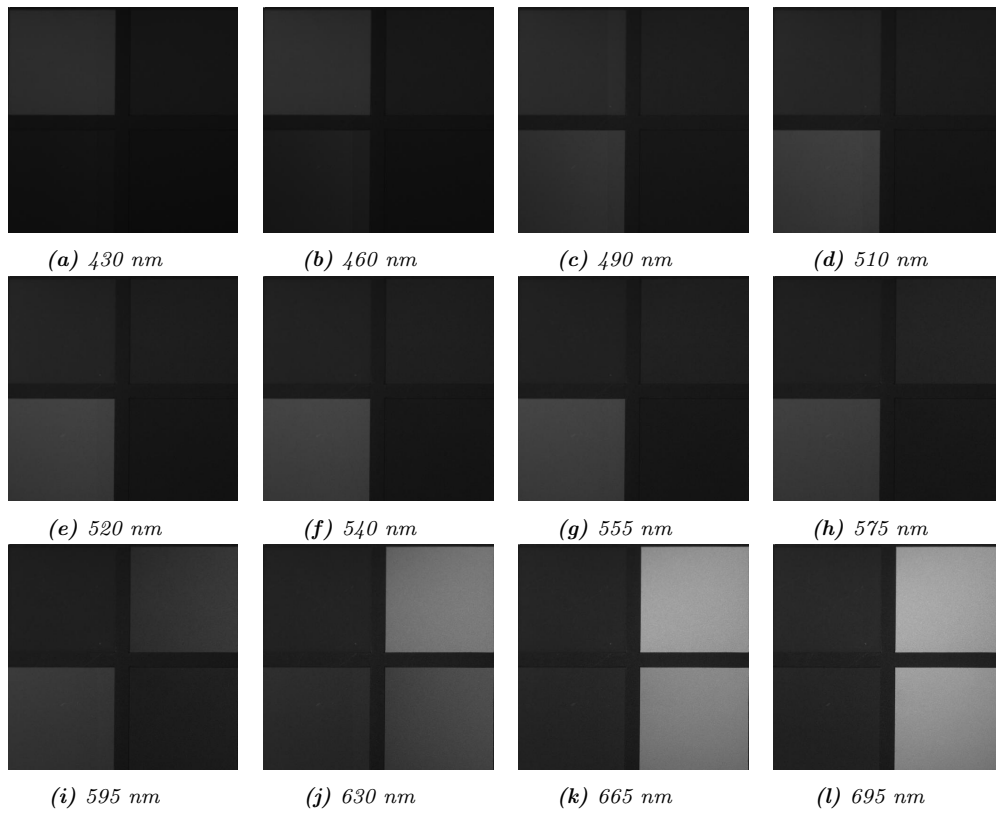
(m) reference and estimated spectra

Figure 2.20: step of reconstruction ⟼ 300 columns

Judging by figures 2.16, 2.17, 2.18, 2.19 and 2.20, the required alternation in illumination of patches is achieved at all different selections of the columns-step. However, a problem is derived, as far as the appearance and quality of images are concerned. This does refer to the observation of stripes of different intensity across the same spectral bands. Chances are that this malfunction regards to the improper separation of the spectral bands. Although, larger steps eliminate this phenomenon, they do not obliterate it. As a result, there must be other approaches to the reconstruction rather than corresponding a fixed number of columns-step to each step of the filter, which may lead to a more efficient solution.

Despite the fact that the reconstructed images leave a lot to be desired, a great tendency of similarity is observed between the estimated and reference spectra, as the comparisons suggest, except for the Purplish Blue patch. It is necessary to mention that larger steps respond to lower values of mean square error(mse) between the two curves and thus, to more efficient reconstruction [13] [10]. The difference is not actually important, but this does not mean that these stripes do not affect the estimation of spectra. So, undistorted reconstructed images indicate efficiency and efficacy.

An other important issue that needs to be discussed is the difference of spectra concerning the Purplish Blue patch. The low dynamic range of the Halogen light source is responsible for this misalignment, which is solved by replacing it with the Xenon light source, as it is analytically explained in subsection 2.2.3 of this Chapter. Re-conducting the same experiments under these circumstances, improves the aforementioned spectra estimation, as expected (see figure 2.21).
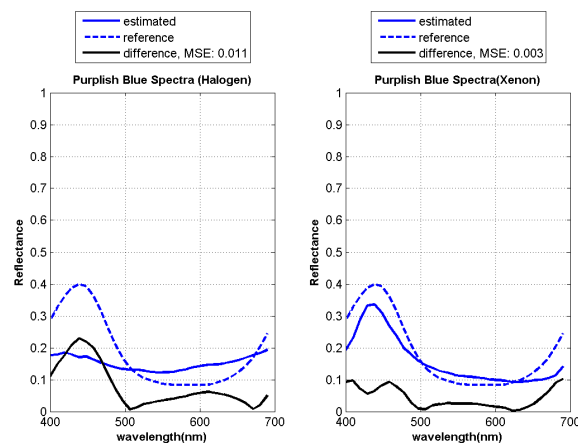
Figure 2.21: *Halogen vs. Xenon light source* $\longmapsto$ *reflectance of Purplish Blue patch*

2.6   Brief Summary

Figure 2.22 provides a *flow-diagram* of all the procedures developed and presented in Chapter 2. Each part is represented by a rounded-corner rectangle and constitutes a different phase of the total implementation.
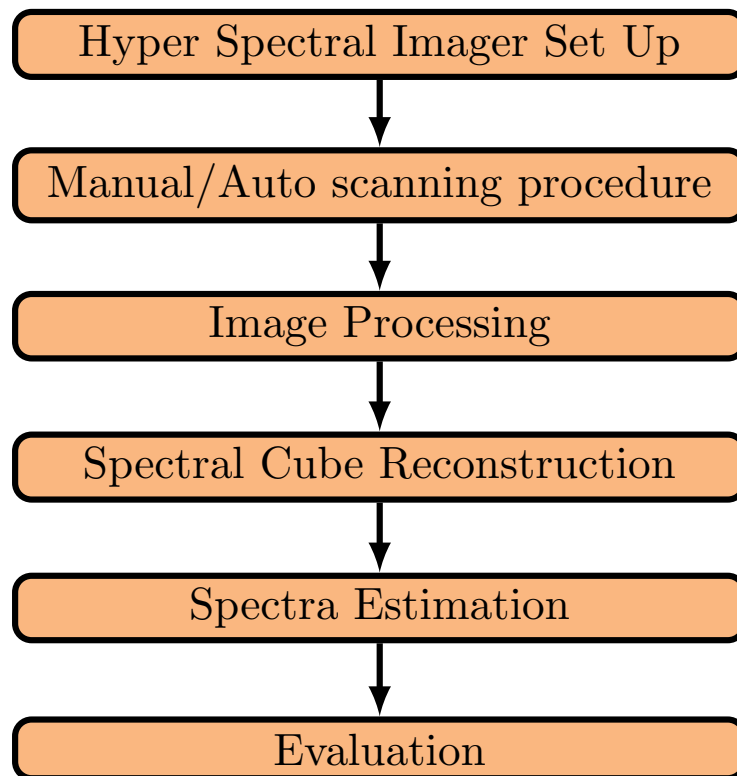
Figure 2.22: *Flow-Diagram of the HSI implementation*

Chapter 3

Algorithmic Prediction of Steps

3.1   Problem Definition

Although the estimation of spectra has been quite accurate and satisfying (Chapter 2), the reconstructed images are **"stripe-distorted"**. This distortion does vary across the different spectral bands. Regardless the number or the extent of stripes, the problem calls for solution, since these images are far from being functional.

It should be reminded that the step of filter in front of the CCD responds to 0.5 mm, while capturing the images from the experimental scanning set up. In addition, it should be mentioned that this step has been algorithmically translated to a fixed number(e.g 50, 100, 150, etc.) of columns for each one of the hyper spectral scanned images, so far.

The distorted appearance of the reconstructed cube images is likely to be sparked by this initial **fixed correspondence** of steps. Being more specific, the aforementioned step of the filter should be assigned to a number of columns that is not fixed, but repeatedly predicted by an appropriate optimized algorithm [18] [11]. This does make sense since the step of the filter can be steady and known in advance, whereas the number of columns that belongs to a specific spectral band of a hyper spectral image cannot.

3.2   Software

The exact number of columns that must be leveraged to the reconstruction of images as the filter is moving and scanning the "target-image", is going to be induced by an algorithm. This algorithmic approach is likely to pinpoint the step interpreted in columns, between two consecutive scans. So, the suggested algorithmic process works on two consecutive images each time and ends up covering the whole set and thus, offering all the necessary steps for the reconstruction.

After having successfully predicted the steps, an axis that incorporates them is created for each spectral band. The connection of the axis' points yields the spectral cube images. The **prediction of steps** and **diagonal incorporation of the columns-points** render an innovative perspective to the

implementation of the project and may be giving a head start to the proper, non-distorted or at least improved reconstruction of images. A thorough presentation of the developed algorithms is going to offer insight to the points mentioned above.
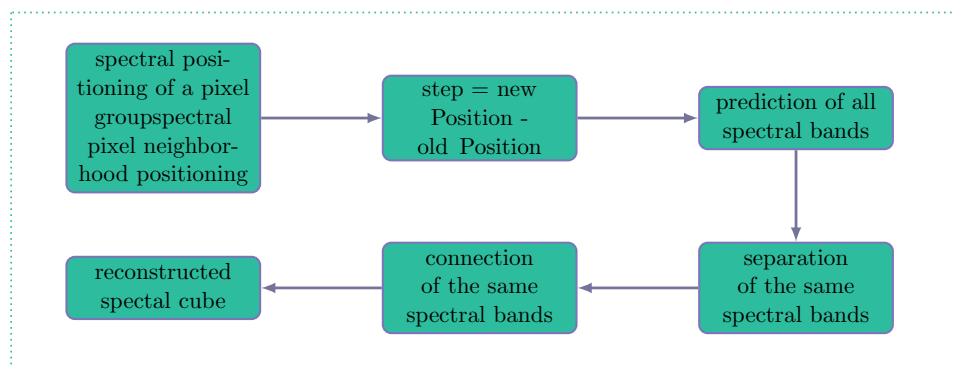
Figure 3.1: *Flow-chart of Dynamic Reconstruction presented in Chapter 3.*

3.3   Preconception

The main idea of the algorithm that predicts the number of columns for each step of the filter, is based on locating the number of columns of the last band of the previous scan to the current one. At its essence, this change of position in the oriented set of columns would result in the desirable shift. However, the aforementioned algorithmic procedure is complicated and seeks further explanation for complete conceptualization. On account of this complexity, the presentation is going to be rather extensive and notably detailed.

As it has already been stated, the used "target-image" is consisted of four different colored patches. Each patch is characterized by a unique spectrum. This means that a region of a spectral curve may be flat in some consecutive bands, while the same region of an other patch's spectral curve may reflect fluctuations. As a consequence, each image cannot be featured by a single one step. On the contrary, the algorithm should be implemented in each patch separately and exclude 4 different "step-results".

The final choice of a single one step of each quartet has not been decided yet. It is under trial phase and will be confirmed by the **auto-step** camera. In this stage, the maximum of all 4 steps is chosen, due to the fact that a

smaller step does not contain regions of a larger step and is more likely to cause distorted images, earlier.

It is essential to underline that the algorithmic concept described above, responds specifically to the current target. Chances are that if a different target was used, the proper prediction of steps would not have been possible. However, the elimination of stripes will be firstly examined in these four patches of the color checker, and then, if applicable, the algorithmic procedure will be expanded, in order to provide some kind of calibration for any kind of target-images.

3.4   Algorithmic Prediction

The algorithmic function, which predicts the step between two consecutive hyper spectral images, scans the bounds of each patch and tries to locate the columns where the current spectrum and the spectrum of the previous subelement have the minimum difference. The term **spectrum** indicates the median value of a small neighborhood of pixels (algorithm 2). This quantity constitutes the criterion that accounts for the comparison between the two images.

In this way, we will be able to pinpoint the change of columns-position of filter at every new scan. Figure 3.2 depicts the bounds of each patch, as well as how pixel-neighborhoods(or pixel-subelements) do look like and are oriented. Subelements are chosen in the middle of the picture in order to assure uniform illumination conditions, which are essential for an efficient post processing.

Figure 3.2:   subelements for comparison

Using algorithm 3 for each one of the four different patches, yields four different steps of columns and their corresponding spectral difference between the new and old position. As it has already been mentioned, the criterion for the comparison is the **minimum spectral difference**. Table 3.1 contains the aforementioned steps along with spectral differences for all four patches that are estimated for 10 consecutive scanned images, as an example.

45

Table 3.1: *Steps and Spectral Difference of 4 Patches*

	Steps				Spectral Difference		
				Patches			
Green	Red	Purplish Blue	Moderate Red	Green	Red	Purplish Blue	Moderate Red
218	157	110	80	0	0	0	0
156	150	155	86	0	0	0	0
178	96	118	95	0	0	0	0
151	85	139	82	0	0	0	0
152	106	154	82	0	0	0	0
137	158	158	89	0	0	0	0
151	108	155	96	0	0	0	0
112	158	137	95	0	0	0	0
151	128	178	287	0	0	0	0
99	157	153	352	0	0	0	0

As it is outlined, the largest step along with the minimum spectral difference is chosen for the reconstruction. However, if the largest step is not accompanied with the minimum difference of spectra, a smaller one with the second minimum difference is selected. The aforementioned procedure is applied by algorithms 4 and 5, across the whole set of the scanned hyper spectral images. After their successful execution, a column-axis is created, where the columns correspond to the steps, which are included in table 3.2.

Table 3.2: *Selected Step*

218	156	178	151	154	158	155	158	287	352

Table 3.2 describes the last step between the previous and the current image of hyper spectral scanning. However, apart from the first image, which only contains one band and thus one step, the rest do contain more bands, which demonstrate more steps. For example, the second image includes the second and first band-step of the filter, the third image includes the third, second and first band-step of the filter and so on, until the total bands-steps of filter match the second dimension of scanned images, meaning the number of *columns*. This task is being implemented by algorithm 6.

Giving table 3.2 as input into algorithm 6 yields table 3.3.

1	218	0	0	0	0	0	0
1	156	156+218=**374**	0	0	0	0	0
1	178	178+156=**334**	334+218=**552**	0	0	0	0
1	151	151+178=**329**	329+156=**485**	485+218=**703**	0	0	0
1	154	154+151=**305**	305+178=**483**	483+156=**639**	639+218=**857**	0	0
1	158	158+154=**312**	312+151=**463**	463+178=**641**	641+156=**797**	797+218=**1015**	0
1	155	155+158=**313**	313+154=**467**	467+151=**618**	618+178=**796**	796+156=**952**	952+218=1170=**1024**
1	158	158+155=**313**	313+158=**471**	471+154=**625**	625+151=**776**	776+178=**954**	954+156=1110=**1024**
1	287	287+158=**445**	445+155=**600**	600+158=**758**	758+154=**912**	912+151=1063=**1024**	0
1	352	352+287=**639**	639+158=**797**	797+155=**952**	952+158=1110=**1024**	0	0

Table 3.3: *Axis of all Spectral Steps*

Algorithm 7 is being executed right after algorithm 6. Taking the output

of the latter as input into the first one, produces the new columns-bounds for each one of the spectral cube images. The concept shown in figure 2.15, which is associated with the diagonal connection of spectral bands, is fundamental for the appropriate reconstruction that we adopt.

The execution of the aforementioned algorithm results in the construction of table 3.4. Being more specific, each row of the table indicates a spectral band. In other words, the number of total rows equals to the total number of the reconstructed spectral bands. For each spectral band, pairs of columns that are algorithmically pinpointed through the consecutive hyper spectral images, respond to separate sections of a spectral band.

1	218	156	374	334	552	485	703	639	857	797	1015	952	1024
1	156	178	334	329	485	483	639	641	797	796	952	954	1024
1	178	151	329	305	483	463	641	618	796	776	954	0	0
1	151	154	305	312	463	467	618	625	776	912	1024	0	0
1	154	158	312	313	467	471	625	758	912	0	0	0	0
1	158	155	313	313	471	600	758	952	1024	0	0	0	0
1	155	158	313	445	600	797	952	0	0	0	0	0	0
1	158	287	445	639	797	0	0	0	0	0	0	0	0
1	287	352	639	0	0	0	0	0	0	0	0	0	0

Table 3.4: *Pre-Completed Axis Table*

Columns across each row of table 3.4 correspond to the spectral bounds of a specific wavelength that is being reconstructed. These bounds derive from the consecutive scanned images and are expressed in pairs. The first number of a pair illustrates the beginning and the second one the end of the specific spectral section of the same spectral band. For example, if we elaborate on the first row of the aforementioned table, we realize that there is a total of 14 columns, which indicates 7 pairs of columns (first pair: 1-218, last pair: 952-1024).

One last issue has been left in order to come up with the final axis of steps that will lead to the functional reconstruction of images. This is exactly where algorithm 8 lies. It is responsible for the proper behavior between the pairs of columns. In other words, it checks the last bound of the current pair and the first of the next one. Three different relations, which are going to be explained through an example, are likely to arise. The appropriate modifications are made, as well.

Consider that the pre-completed axis is the table 3.5.

Table 3.5: *Example for conception of Algorithm 8*

a	b	c	d

Then, the possible cases and their respective modifications may be:

   i. if $b = c$, then $c = c + 1$

   ii. if $c < b$, then $c = b + 1$

   iii. if $c > b$, then $c = c$ ▷ loss of information in the reconstructed image

Inserting table 3.4 as input into algorithm 8, produces the results, which are depicted in table 3.6. This table constitutes the final axis of steps, whose appropriate connection gives the desirable reconstructed cube images.

1	218	219	374	375	552	553	703	704	857	858	1015	1016	1024
1	156	178	334	335	485	486	639	641	797	798	952	954	1024
1	178	179	329	330	483	484	641	642	796	797	1024	0	0
1	151	154	305	312	463	467	618	625	776	912	1024	0	0
1	154	158	312	313	467	471	625	758	912	0	0	0	0
1	158	159	313	314	471	600	758	952	1024	0	0	0	0
1	155	158	313	445	600	797	952	0	0	0	0	0	0
1	158	287	445	639	797	0	0	0	0	0	0	0	0
1	287	352	639	0	0	0	0	0	0	0	0	0	0

Table 3.6: *zero-green values indicate the end of pairs of bounds for a specific spectral band, light red non-zero values indicate uncompleted functional pairs of bounds due to inadequate number of images that are used for this example, since the execution of algorithms is being presented only in a subset of 10 images.*

Algorithm 9 offers proper connection of the pairs-columns that are depicted in table 3.6. Each row corresponds to a different reconstructed spectral cube image. Repetitive automatic connection of bounds for all rows of table yields the **whole reconstructed spectral cube**.

3.5 Results

3.5.1 Spectral Cube Images

The spectral cube images that are derived from the aforementioned algorithmic prediction of steps are shown in figure 3.3.
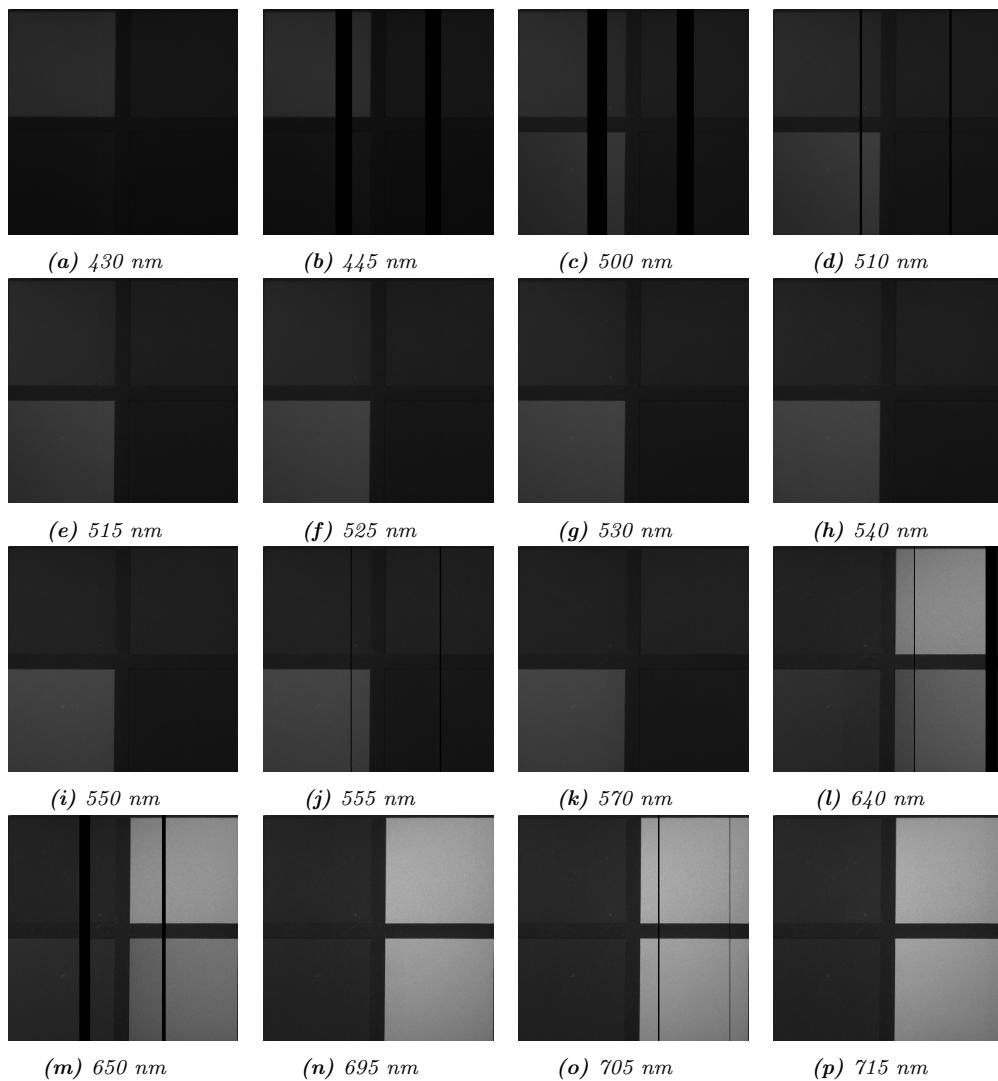
Figure 3.3: *Spectral Cube Images of dynamically predicted steps*

It is obvious that although the stripes have been eliminated significantly, the reconstruction is not functional due to the loss of information that is linked to larger steps. There are images with empty columns, which means that the algorithmic procedure leaks and thus, cannot be adopted. Furthermore, it cannot be applied to other target-images as it should, in order to provide some sort of calibration to the reconstruction that our HSI performs. As a result, all these algorithmic procedures that have been presented in Chapter 3, contributed a lot to the elimination of abnormalities in the intensity of reconstructed images and helped us verify that the step of columns **is not fixed**, as it was proposed in the beginning. However, as long as the expected results have not been reached, the research should be expanded.

Chapter 4

An Alternative Algorithmic Prediction

Since the algorithmic procedures of fixed and dynamically predicted step that have been implemented so far (Chapter 2 and 3), are far from providing an efficient reconstructed spectral cube, it is necessary to struggle to come up with an other algorithm that may yields better results, as far as the prediction of steps is concerned. A well known post processing imaging technique is the execution of mathematical operations between the images [19], because they can offer valuable information about the intensity of pixel values without having an impact on the content [13]. The images we use in order to reconstruct the cube, derive from the consecutive scanning of a target-scene with the contribution of the variable filter. As a result, each new image contains a new spectral band from the current scanning. This means that if we subtract two consecutive images, we are supposed to find the new inserted band, as the pixel values in this area will be differentiated. So, previous bands will give differences very close to zero (not zero as we are taking into consideration the existent noise) and the new inserted band will yield differences far from zero. This **discrimination** from a specific threshold is going to be the criterion of selecting the steps between two consecutive hyper spectral scanned images.

For the time being, we are going to analyze thoroughly how is the aforementioned threshold selected. Firstly, we are subtracting the scanned images in groups of two. Being more specific, this subtraction responds to the previous and current image of scanning. In this way, a matrix with the differences of pixel values is provided. The dimensions are the same with those of the scanned images. The second step is to find the mean value of differences across all columns of the matrix. This means that we have as many mean values as the columns of the image. The next action concerns the estimation of the **median** value [11] of all the mean values of the previous task. This median value minus the very small number of 10^{-6}, is the threshold that is used for the discrimination between the previous and new spectral band. The number of columns that are equal or smaller than this threshold constitute the previous bands, at odds with the rest of columns that indicate the new spectral band and thus, the step we are interested in. It is important to mention that the aforementioned discrimination is implemented under strict algorithmic conditions due to the existent noise. It is crucial

for the algorithm to find positions that conform to the criterion but they are accompanied with a sense of continuity. For instance, we may find that column 12 abides by the criterion and the next column that does so is the 100th. In this case, we choose 101 as the step and not 13.

The algorithmic approach of this Chapter is a kind of dynamic prediction like the one presented in Chapter 3. As a result, a great many of algorithmic functions remain the same. These correspond to the creation and connection of the separate spectral bands. The only thing that is differentiated, is the way the prediction of steps is being held. The functions that are responsible for this differentiation are going to be analyzed in the next sections of this Chapter.

4.1 Block Diagram of Implementation
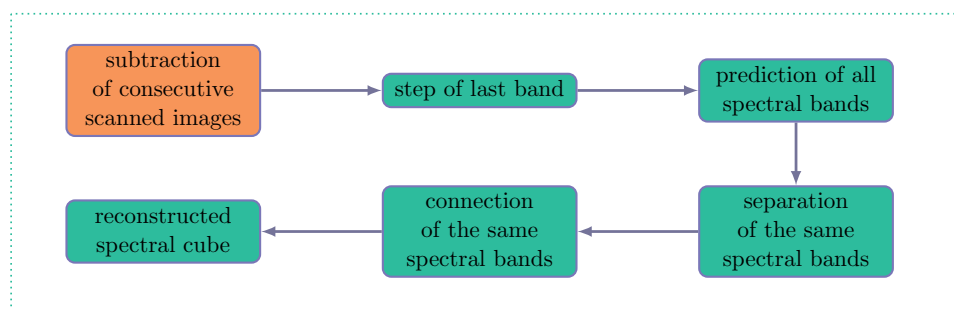
Figure 4.1: *Flow-chart of the Alternative Dynamic Reconstruction*

4.2 Developed Algorithms

After having successfully predicted the steps by subtraction of raw images between two consecutive scans through algorithms 10, 11, 12, the previously developed algorithms (6, 7, 8, 9) are being used for proper separation and connection of all separate bands that yield the reconstructed images. Detailed description and execution of these algorithms are presented in Chapter 3 and specifically in section 3.4.

4.3 Results

410 nm   415 nm   420 nm   425 nm

440 nm   445 nm   450 nm   455 nm

470 nm   475 nm   480 nm   485 nm

500 nm   505 nm   510 nm   515 nm

530 nm

535 nm

540 nm

545 nm

560 nm

565 nm

570 nm

575 nm

590 nm

595 nm

600 nm

605 nm

620 nm

625 nm

630 nm

635 nm
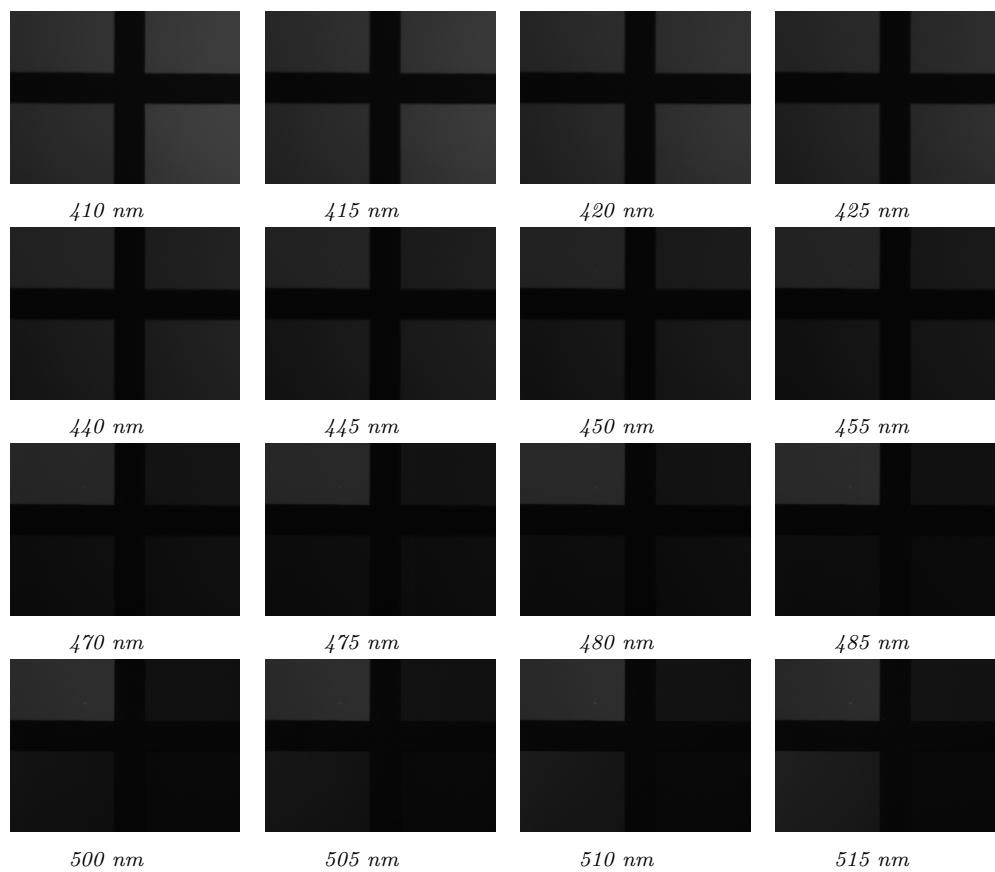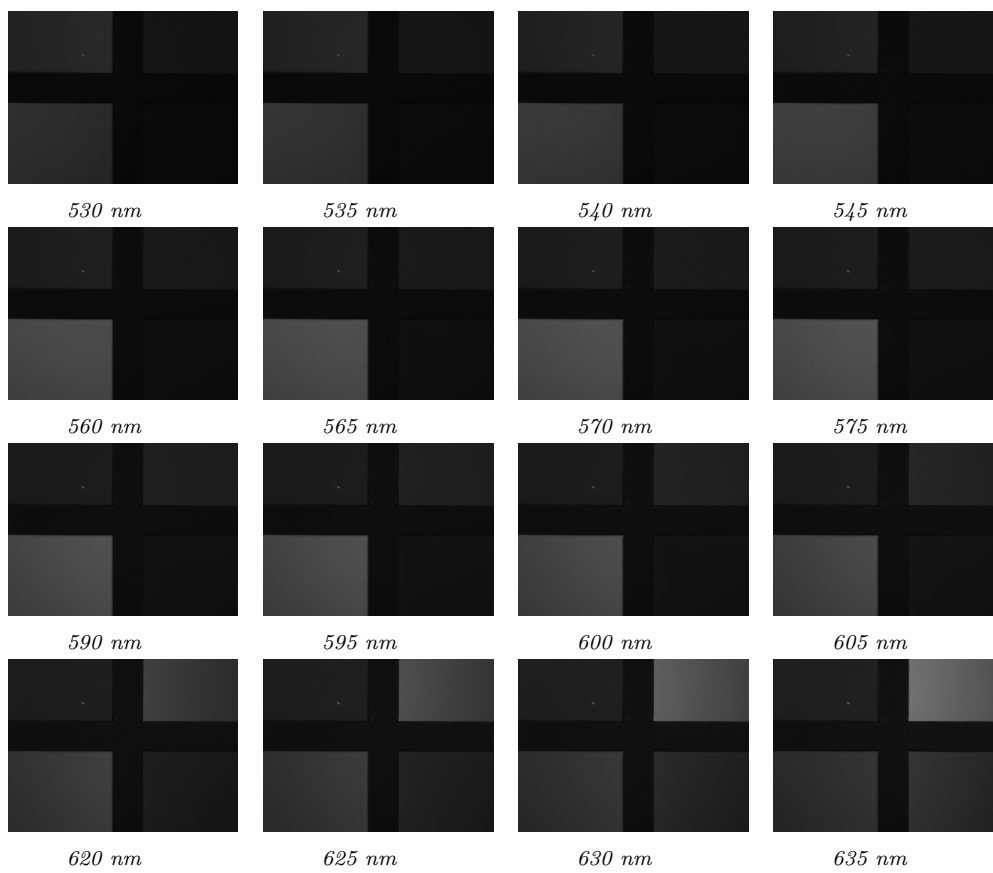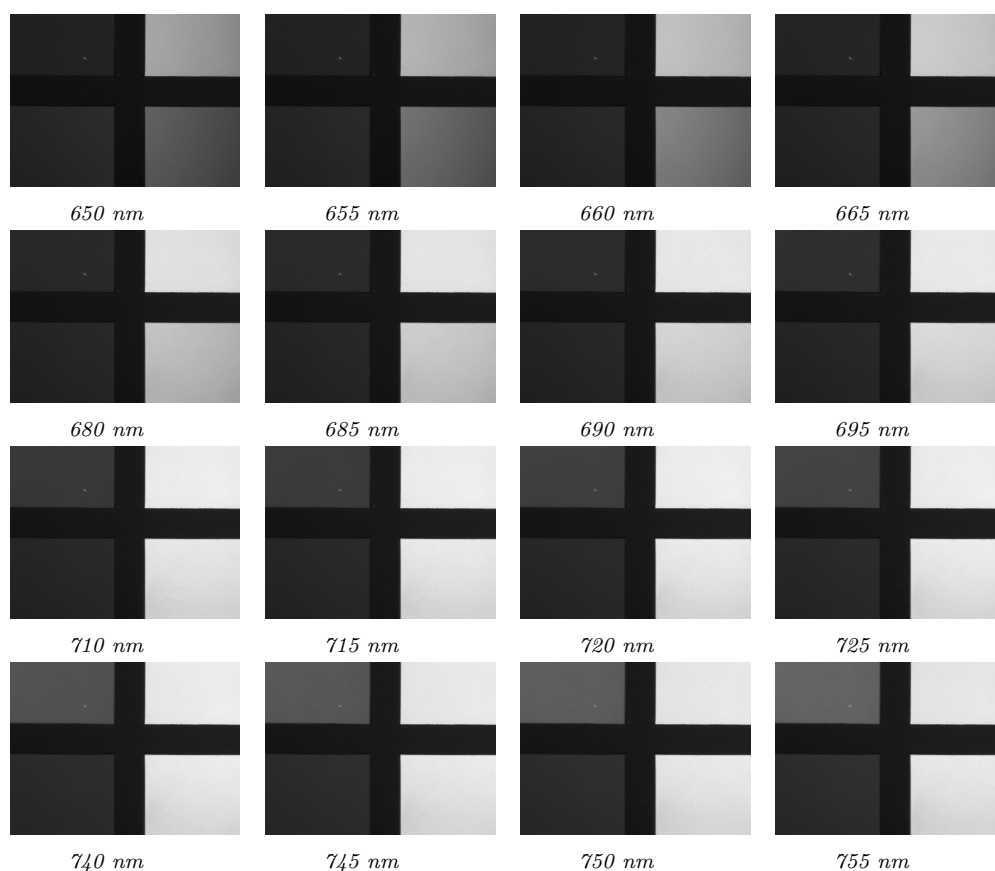
Figure 4.4: *Reconstructed Cube Images with dynamically predicted steps by subtraction of Raw Hyper Spectral Images*

4.4 Efficiency

The efficiency of such an algorithmic procedure does cling to a uniform and satisfactory performance for all kinds of target-images being used. This fact demonstrates that the step of the filter should be responded to the same columns-steps for each spectral band, no matter what is the content or texture of the target-scene. In other words, some sort of calibration should be applied and offer a clear reconstruction for all cases. That makes sense since the movement of the filter in each spectral band remains the same at every hyper spectral scanning procedure of our HSI. As a consequence, the step of columns that responds to the movement of filter should be the same, as well.

Taking all these into consideration, it is obvious that an effective algorithmic approach for the reconstruction we present, should hardly be affected by the

type of target-image being used. Letting alone the target-image, the developed algorithmic function must produce the **same** columns-steps for every performed reconstruction. Arguably, this is an apparent way to check the efficiency of the alternative algorithmic approach that is being described in this Chapter. Performing a great many of dynamic predictions at different targets, we realize that not only are the columns-steps across the same spectral bands differentiated, but also the reconstruction is getting distorted by stripes. This result holds important evidence that although this algorithmic approach is effective for the initial target-image we used, it is not able to provide our HSI with a **globally** efficient reconstruction. To sum up, this alternative algorithmic approach is **inappropriate**.

Chapter 5

Further Investigation

The implementations developed in Chapters 2 and 3 aimed at the Black and White(BW) reconstruction of Hyper Spectral Cubes. The inefficient results led us to the decision of further investigating the problem we encounter. It seems to be prevalent and we should cope with this situation, even if it is unlikely to find a solution. Outlining the factors that contribute to this malfunction of our imaging system would be evenly important. Elaborating on the behavior of the scanned hyper spectral images and performing color reconstruction [15] are going to be the two main subjects of this Chapter.

5.1   Raw Hyper Spectral Images

The Hyper Spectral Images provided by the scanning procedure need to be probed in detail, since the reconstructed images result from parts of them. Diagrams of spectra and histograms are going to be plotted in different pixel positions of the same patches across the whole scanned cube, so as to outline the shifts in spectra and the number of pixel counts, as far as the intensity values are concerned. Such information would be valuable and useful in order to specify the answer to our problem. The raw images used for the estimations come from both HSIs, manual-step and auto-step.

5.1.1 Manual HSI

(a) *Purplish Blue*

(b) *Moderate Red*

(c) *Green*

(d) *Red*
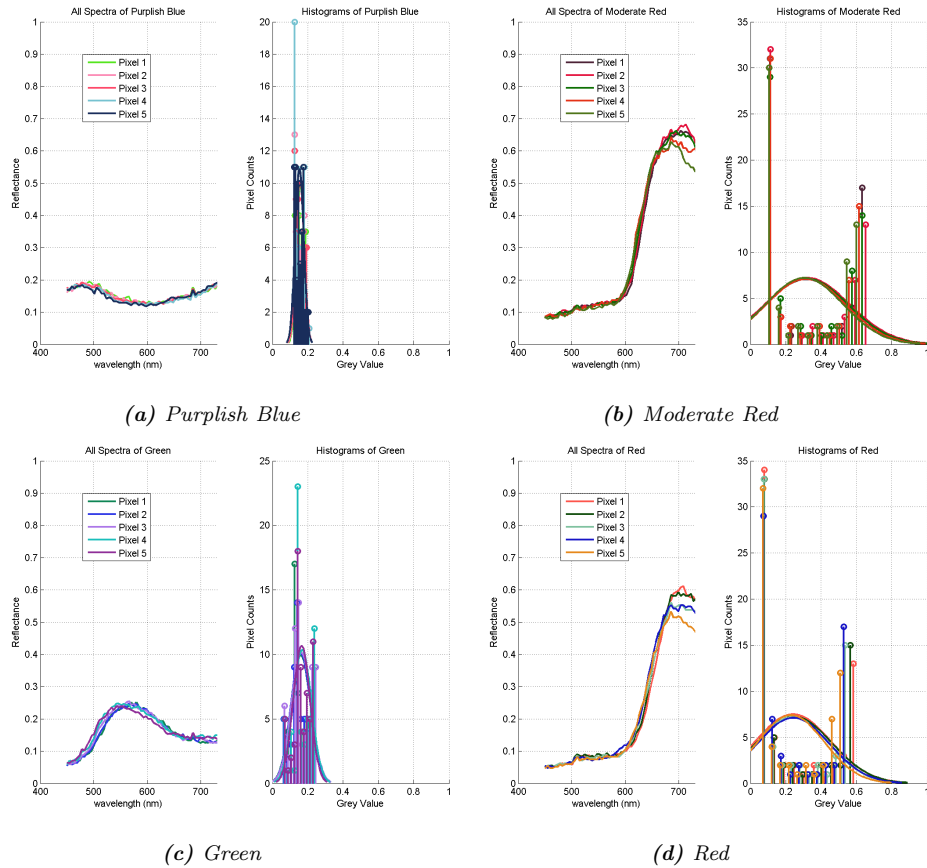
Figure 5.1: *Manual HSI*

Looking at figure 5.1, we observe that all patches, except for the Purplish Blue one that is too noisy to extract any conclusions, there are shifts across the different positions inside the same patches, but they are extremely narrow and not wide, as expected. It seems that the inserted bands resulting from the movement of the filter, are very close. As a result, very small spectral differences are indicated in consecutive pixel positions. Histograms [11] comprise similar intensities and some unremarkable but expected shifts, as well. Letting alone the spectral shifts, the distribution of pixel values [13] should remain unaffected, as it is indicated by the diagrams. However, chances are that noise and reflections of light in the set up account for some small deviations.

5.1.2   Auto HSI

(a) *Purplish Blue*

(b) *Moderate Red*

(c) *Green*

(d) *Red*
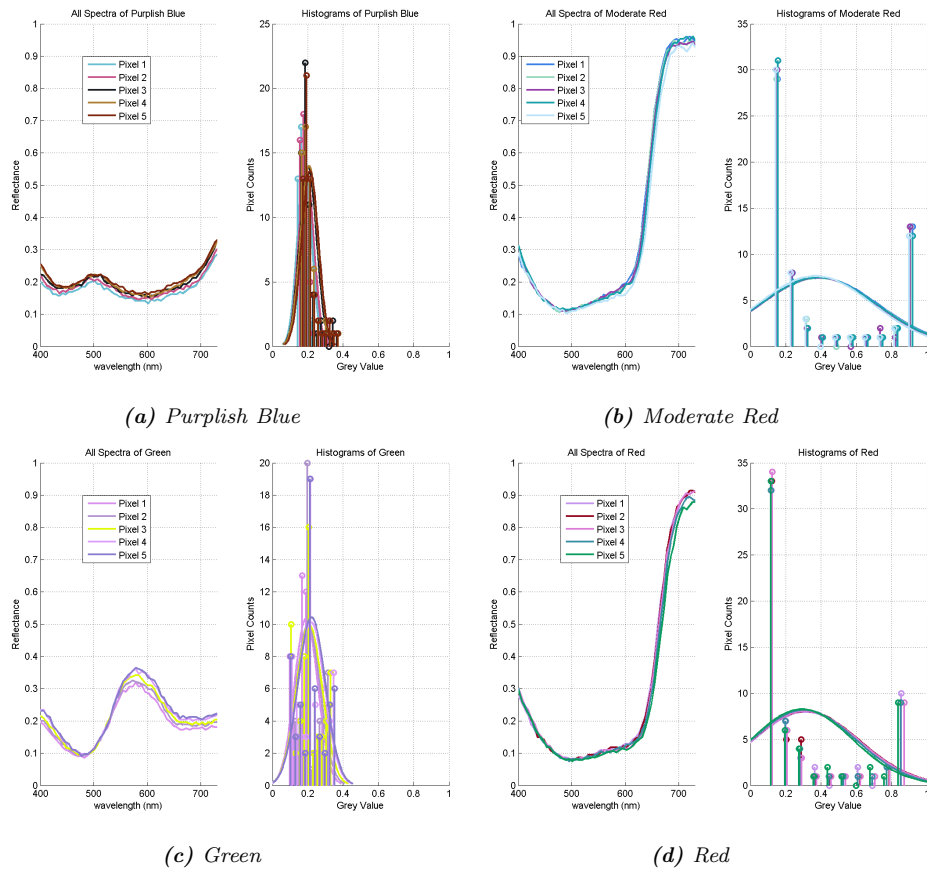
Figure 5.2: *Auto HSI*

Figure 5.2 does absolutely confirm the results from the previous figure,
which pinpoints convergence between the manual-step and auto-step HSI.
It should be stated that accuracy in the movement of the filter is provided
and this is why the shifts of spectra are even more narrow than the previous
diagrams of the manual-step set up. We see evidence that the movement of
the filter in front of the CCD camera is accompanied with the insertion of
bands that cover a big part of the sensor and thus, a big part of the new
scanned image. As a consequence, there is enough distance between the
pixels of the previous and the current scan. This is exactly where the wide
steps of columns that are introduced by our algorithmic implementation so
far, lie.

5.2   Color Reconstruction

Color Reconstruction consists the second landmark in our attempt to cue a response towards the problematic reconstruction. We are replacing the BW CCD camera with a **color**(COL) one and re-conducting the hyper spectral scanning experiments. The reconstruction is implemented with the **fixed and dynamically predicted steps**, so as to examine whether or not the spectral bands are separated correctly from the hyper spectral scanned images and then are connected properly. This task is within the gasp of our investigation and is expected to demystify an explanation, if not a solution, to our problem.

5.2.1   Fixed-Step

(a) *430 nm*   **(b)** *435 nm*   **(c)** *455 nm*   **(d)** *480 nm*

(e) *500 nm*   **(f)** *510 nm*   **(g)** *520 nm*   **(h)** *525 nm*

(i) *530 nm*   **(j)** *545 nm*   **(k)** *560 nm*   **(l)** *575 nm*

(m) *585 nm*   **(n)** *600 nm*   **(o)** *620 nm*   **(p)** *625 nm*
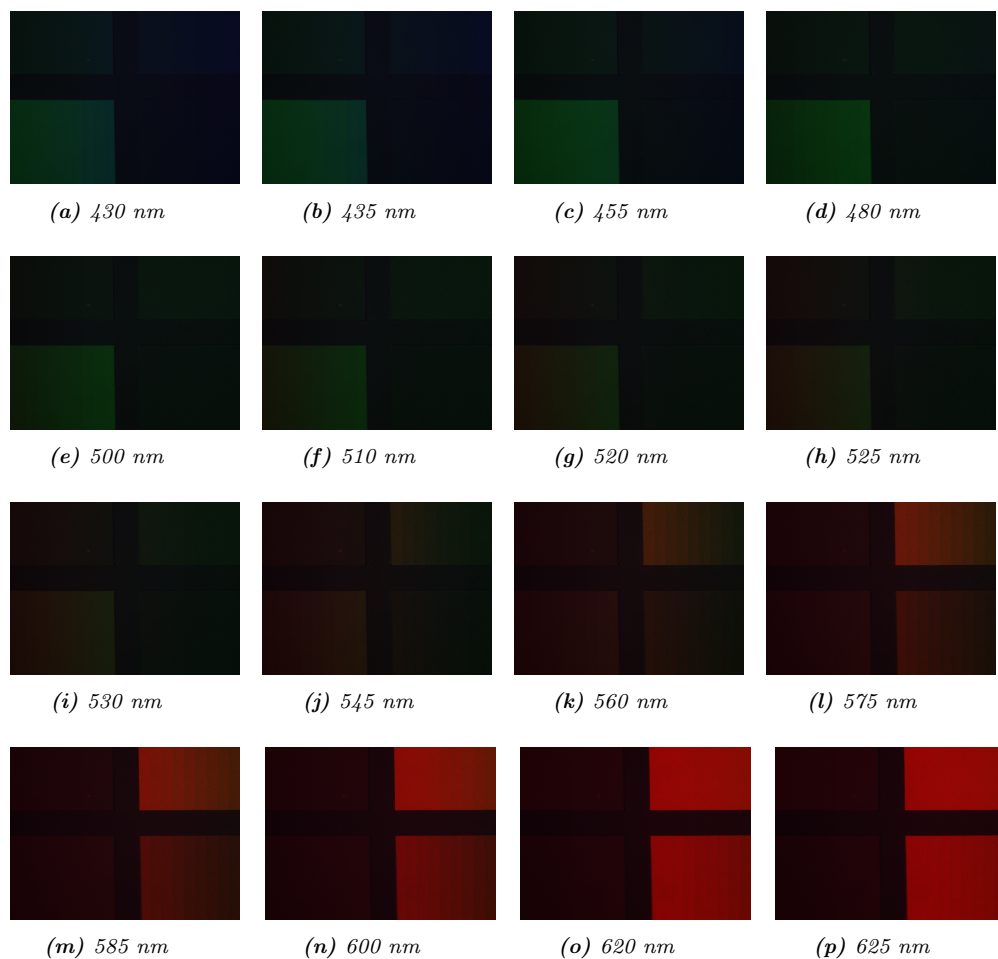
Figure 5.3: *step of color reconstruction $\longmapsto$ 50 columns*

(a) *430 nm* **(b)** *445 nm* **(c)** *455 nm* **(d)** *465 nm*

(e) *480 nm* **(f)** *510 nm* **(g)** *530 nm* **(h)** *550 nm*

(i) *560 nm* **(j)** *570 nm* **(k)** *580 nm* **(l)** *590 nm*

(m) *600 nm* **(n)** *610 nm* **(o)** *620 nm* **(p)** *655 nm*
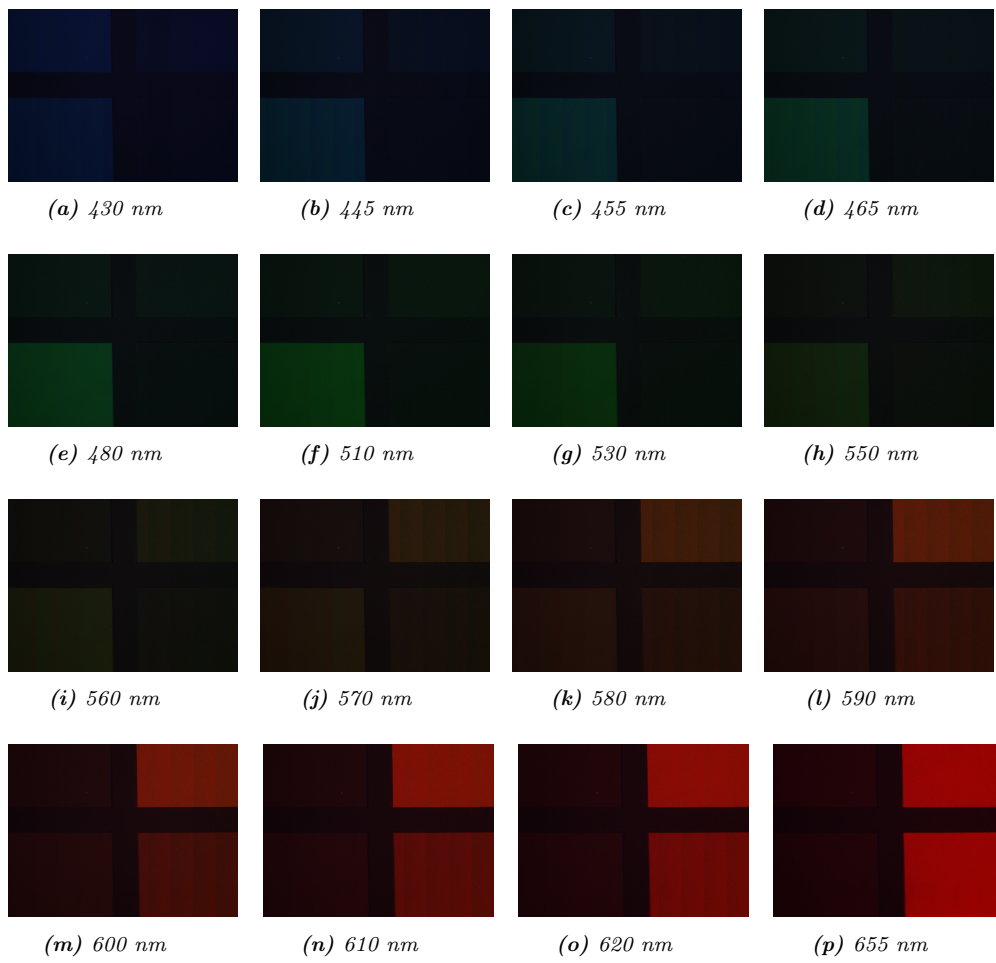
Figure 5.4: *step of color reconstruction ⟼ 100 columns*

(a) *430 nm* **(b)** *445 nm* **(c)** *455 nm* **(d)** *465 nm*

(e) *480 nm* **(f)** *510 nm* **(g)** *530 nm* **(h)** *550 nm*

(i) *560 nm* **(j)** *570 nm* **(k)** *580 nm* **(l)** *590 nm*

(m) *600 nm* **(n)** *610 nm* **(o)** *620 nm* **(p)** *655 nm*
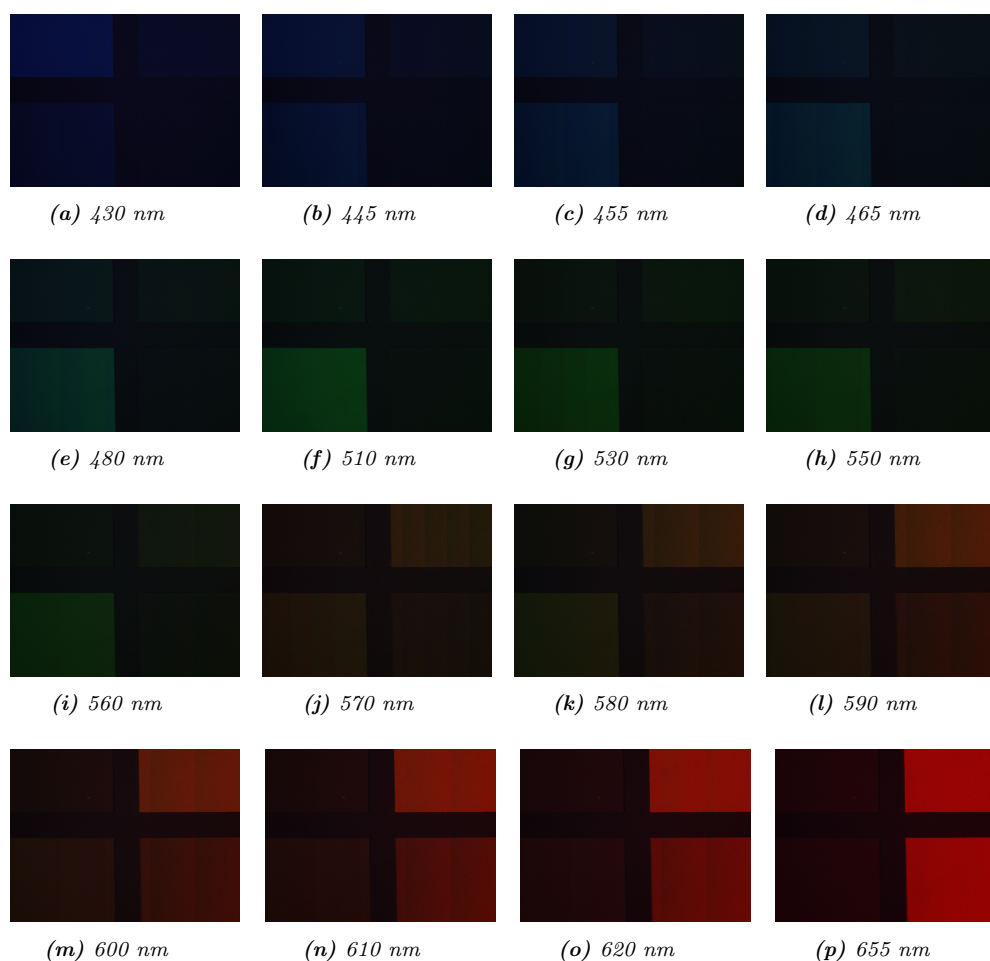
Figure 5.5: *step of color reconstruction ⟼ 200 columns*

Looking carefully at figures 5.3 , 5.4 and 5.5 , we realize that smaller fixed steps are accompanied with improper separation of spectral bands. Being more specific, small steps require a large number of scanned images in order to form a reconstructed band and this fact allows the insertion of next bands of the variable filter that should be corresponded to other spectral images. For instance, a blue image ends up containing green bands, if the step is assigned to 50 columns. Increasing the number of columns improves the reconstruction, but still yields stripes.

An other important issue that should be mentioned is that these stripes are not uniformly distributed in all spectral bands. This is sparked by the fact that although the filter is characterized as being **linear**, it contains some deviations across the wavelength range. They are not important but still can have great impact on the processing. As a consequence, different wavelengths respond to different shifts. This not absolutely linear corre-

spondence accounts for the fact that a fixed number of columns-steps may be sufficient for some spectral bands but insufficient for some others. As a conclusion, it is possible to find a large fixed step that would perform a satisfactory reconstruction for the majority of images, but it is unlikely to achieve a reconstruction totally free of stripes.

5.2.2 Dynamically Predicted-Step

(a) *430 nm*   **(b)** *445 nm*   **(c)** *455 nm*   **(d)** *465 nm*

(e) *480 nm*   **(f)** *510 nm*   **(g)** *530 nm*   **(h)** *550 nm*

(i) *560 nm*   **(j)** *570 nm*   **(k)** *580 nm*   **(l)** *590 nm*

(m) *600 nm*   **(n)** *610 nm*   **(o)** *620 nm*   **(p)** *655 nm*
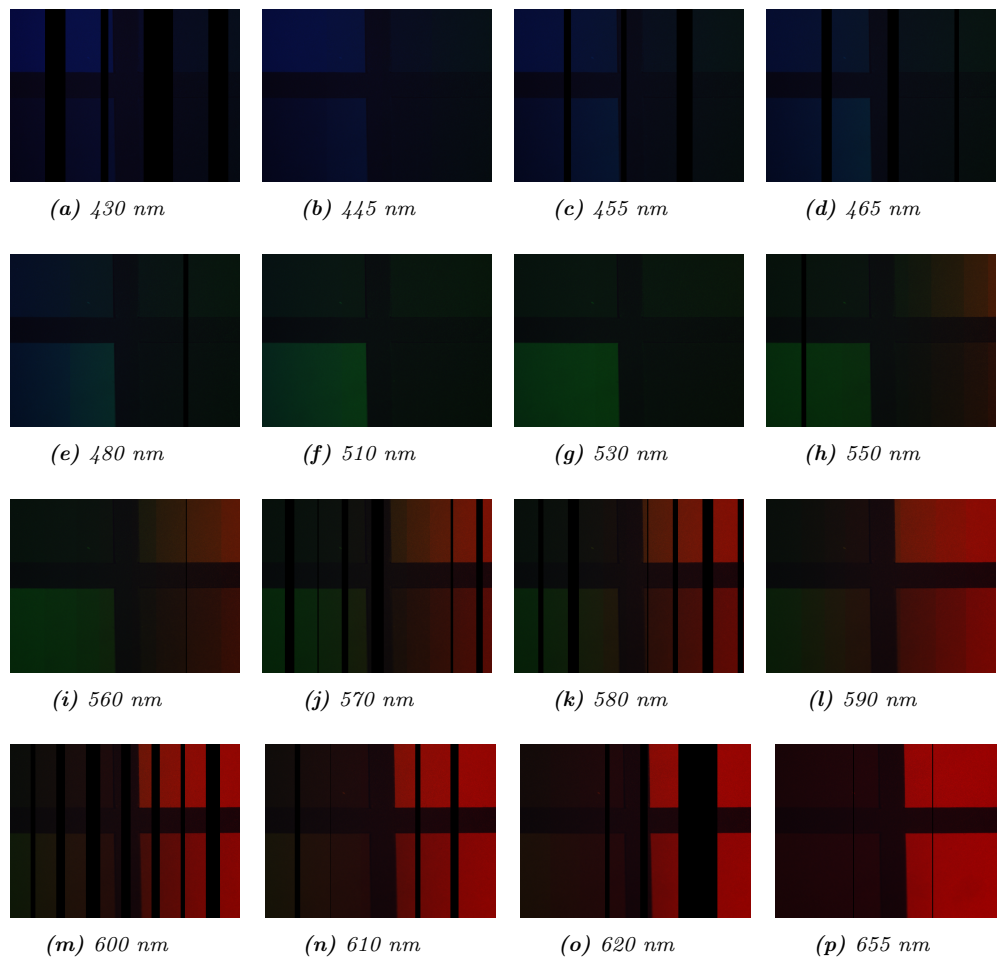
Figure 5.6: *dynamically predicted color reconstruction*

Judging by figures 5.3, 5.4, 5.5 and 5.6, it is obvious that neither fixed-step nor dynamically predicted-step algorithm does render the color reconstruction effective. However, color reconstruction shed light on the reason why is the distortion of images more intense with smaller steps. So, we end up to the conclusion that large column-steps are generally needed for each step

of the filter, in order to avoid spectral contamination. Although such an improvement is crucial for the quality of the reconstructed cube, it does not guarantee the total attenuation of stripes. There are still images, which are distorted, but the number of them has been markedly reduced. The problem is pretty deeply ingrained and may pertain to reasons that go beyond the scope of our approach.

Chapter 6

Final Implementation

The algorithmic techniques that have been followed so far and pertain to the reconstruction of hyper spectral cubes, have not been able to come up with reconstructed images of **high quality**, as required. The reasons for this malfunction vary and depend on the developed algorithmic concept. We have dealt with reconstructed images marked by stripes (Chapter 2, Chapter 5), reconstructed images that miss spectral information (Chapter 3, Chapter 5) and clear reconstructed images but only with specific target-images (Chapter 4). All these methods have been consecutively developed in order to sidestep all of the aforementioned problems. However, none of them have led to successful results.

Chances are that the reason for this malfunction may be deeply ingrained in issues, such as **the incorporation of the hardware of our HSI, the distance between the CCD camera and the variable edge filter, the consecutive and physically inevitable reflections of light inside the filter due to its thickness, the leak of some bands that concerns the "no slit-scan" technique we have adopted and the single-time calibration before the beginning of the hyper spectral scanning**. All these factors render our HSI extremely sensitive to intrinsic and external phenomena, which are not easily retreated.

In this Chapter, we are going to apply a method to measure exactly the columns of each new inserted spectral band, as strictly as it is possible. Assuring that the columns-steps in each step of the filter is not erroneous will give our investigation a head start. Not only is our research going to be limited in the domains mentioned above, but it is also likely to realize that the functionality of the introduced reconstruction cannot be completed with perfection.

6.1 Measuring the Step of Filter

Our auto-step HSI is programmable to take shots by doing equal movements of the motor step across the wavelength range. It should be mentioned that the amount of movement is changeable by having parameterized the respective code. Being more specific, it is possible to reduce or increase the distance of the filter's movement inside the CCD camera during the hyper

spectral scanning procedure. This refers to the alternation of a parameter in the *arduino* file that controls the movement of the filter. Smaller movement of the filter step indicates a total number of more scanned images than larger movement does. Despite the distance of filter's movement, it is crucial to measure exactly the step of columns. This is implemented by processing a small number of the first scanned images. In the very beginning of the hyper spectral scanning, the CCD camera is not totally covered by the filter. In this way, the end of the filter is visible as "no-content" information in the scanned image. This "no-content" information is moved in the next scan. Marking and pinpointing the exact position of these two consecutive "no-content" regions in scanned images result in estimating the step of columns that responds to the step of the filter. Subtracting the two column-positions gives us the desired step. We are going to perform a lot of experiments with different parameters in order to test and characterize the performance of the HSI.

6.2   Experiments

Our first attempt has been held by reducing the movement of the motor step. Although the reconstructed images have been improved, the stripes have not been totally attenuated. The same experiments have then been conducted by augmenting the movement of the motor step of the filter. ***The bigger the step of the filter, the more distortion in the reconstructed images***.

6.2.1   Calibration

Since the distortion still remains, we are going to perform calibration in each individual spectral band, as far as the values of shutter and gain are concerned. It is important to mention that the scanning procedure of the previous implementations was not individually calibrated at each step. This may significantly contributed to the creation of these stripes of different shadings.

6.3   Algorithmic Procedure

The exact measurement of the step of filter indicates that it is fixed with an unremarkable deviation approximately up to 5 columns. This fact spurs the application of the **fixed-step algorithmic reconstruction** (algorithm

1), which is notably developed in Chapter 2 and specifically in section 2.4.

6.4 Results

6.4.1 Step of 30 columns

The hyper spectral scanning procedure yields a total of 350 images. The reconstructed images are algorithmically created by incorporating 30 columns of each new scanned spectral band. Figures 6.1, 6.2, 6.3, 6.4, 6.5, 6.6, 6.7 depict instances of the reconstructed cube at all different spectral regions of the variable filter.
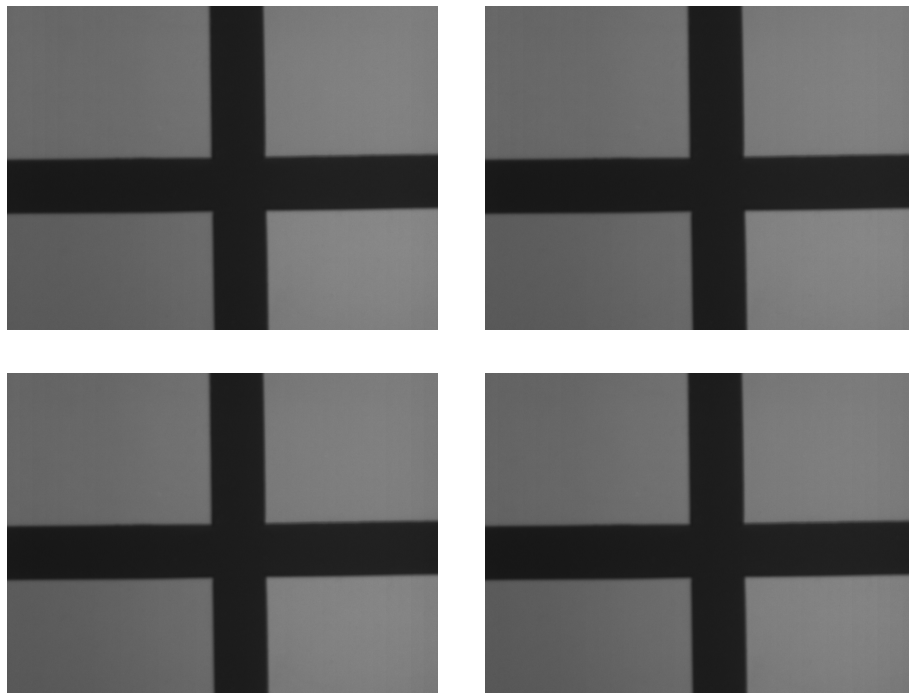
Figure 6.1: *Ultra Violet Region*
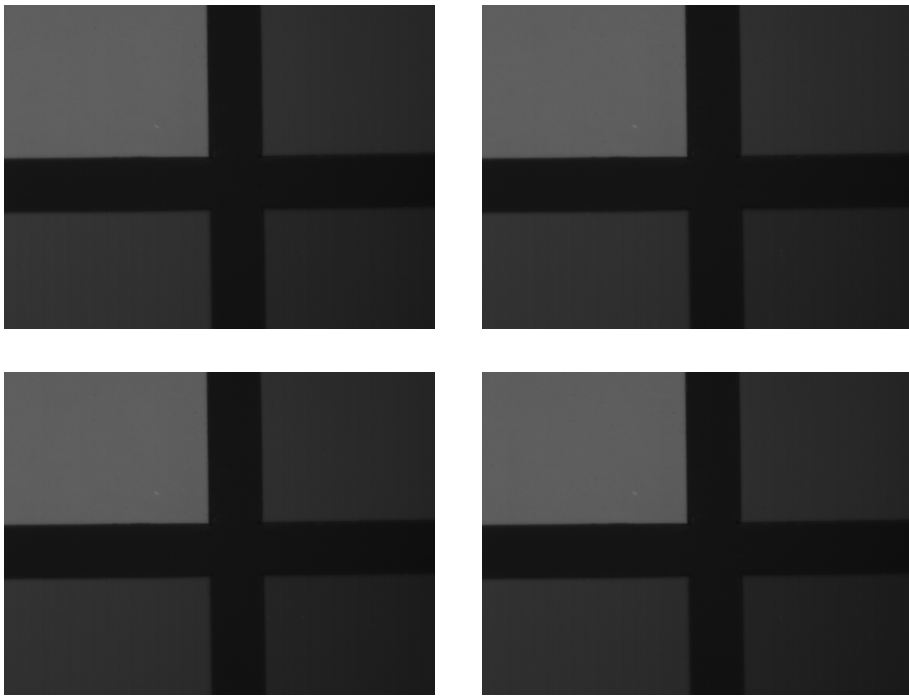
Figure 6.2: *Violet Region*
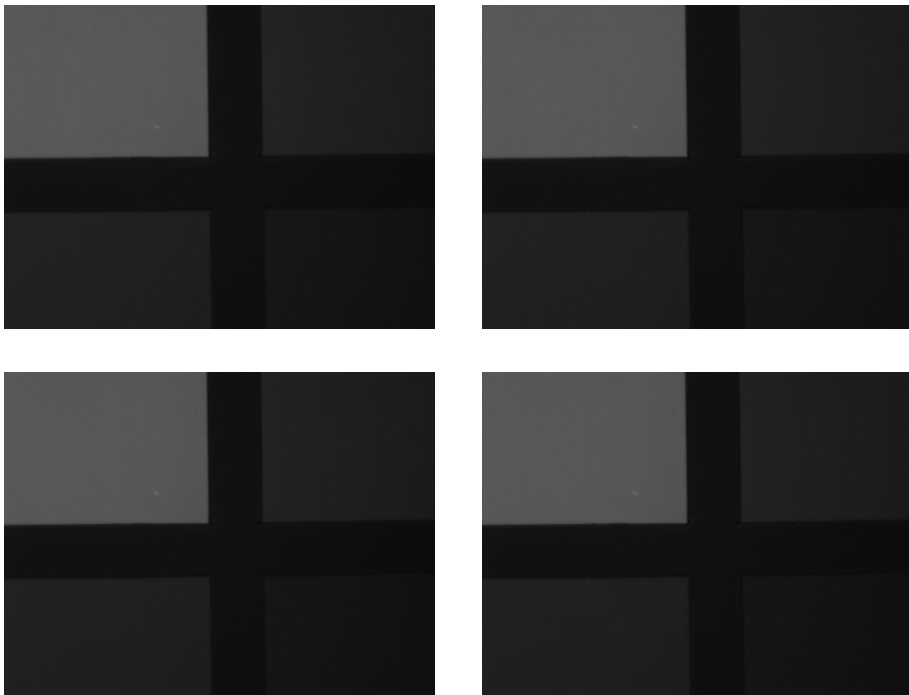
Figure 6.3: *Cyan Region*
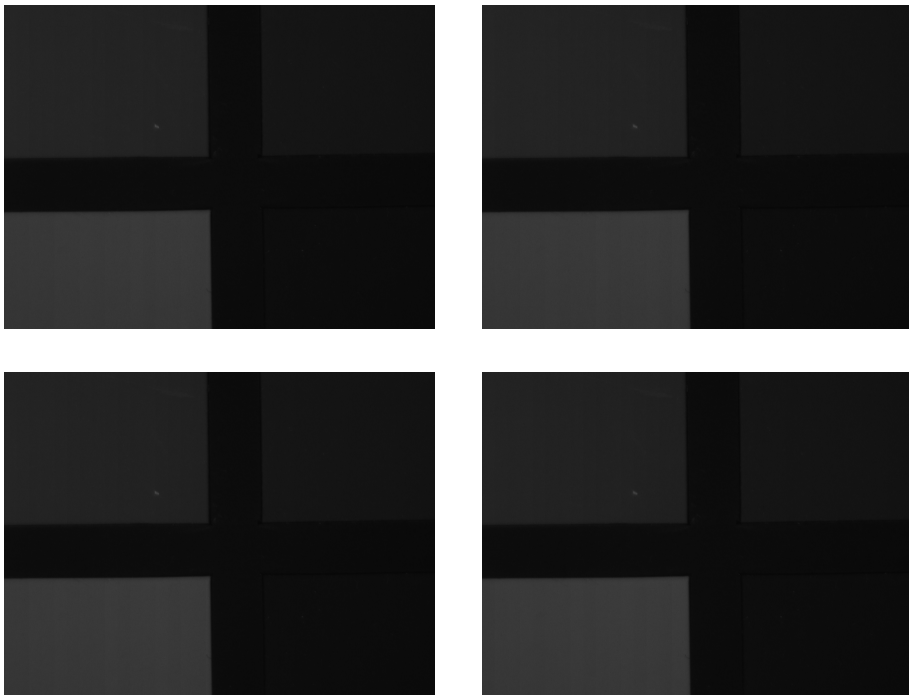
Figure 6.4: *Green Region*
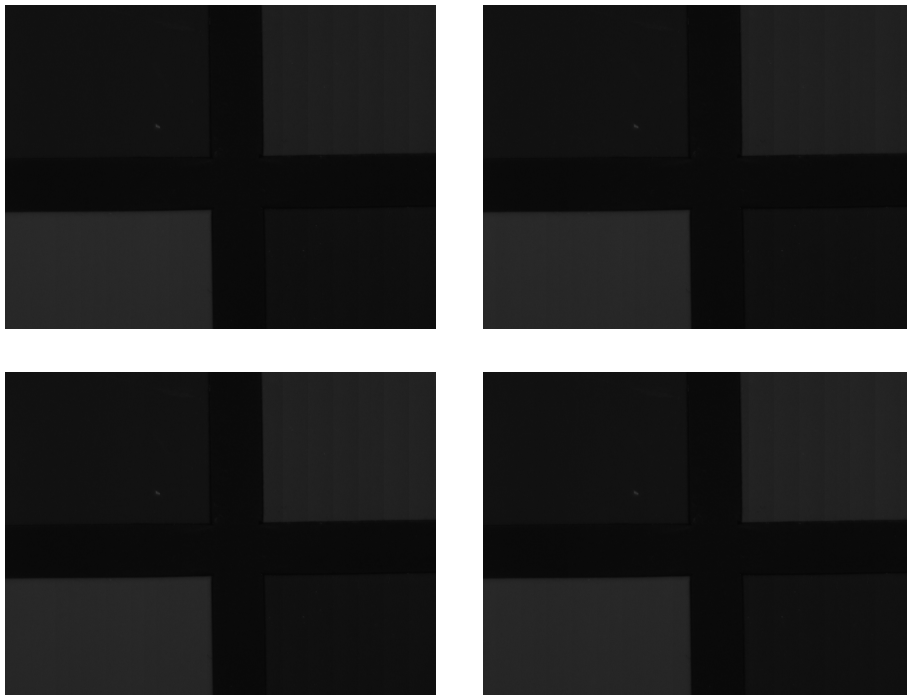
Figure 6.5: *Yellow Region*
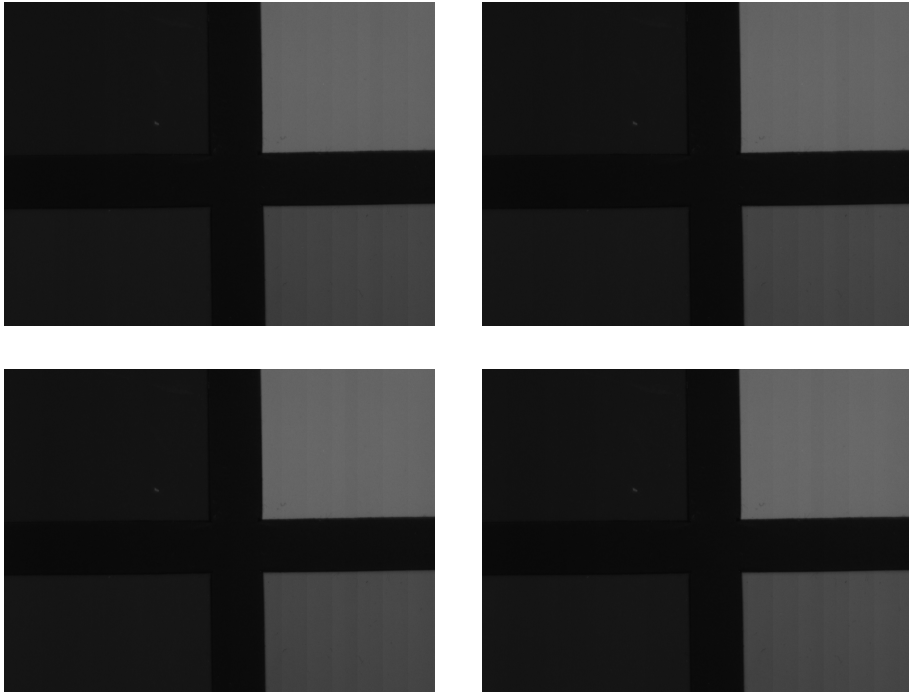
Figure 6.6: *NIR Region*
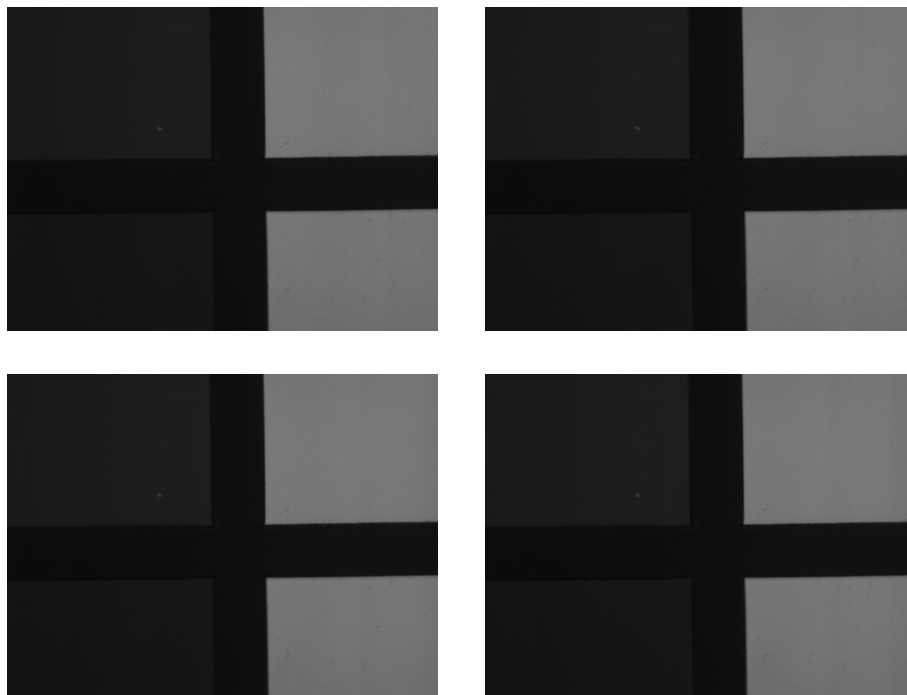
Figure 6.7: *IR Region*

Looking carefully at figures listed right above, it is demonstrated that we have come up with a remarkably improved cube reconstruction at odds with all the previous implementations. However, some bands of the filter and precisely the yellow and NIR region (figures 6.5 and 6.6 respectively) are still problematic. This misalignment will be the incentive for an intrusion to the hardware of the set up. Being more specific, attempts to reduce the distance between the filter and CCD camera will be conducted. In this way, physical phenomena like consecutive reflections and alternations in direction of light, which enhance the vulnerability of the set up during scanning, are likely to be eliminated.

It is necessary to mention that the reconstructed images regarding this implementation are not accompanied with their exact wavelength, because different movement of the motor step does require different correspondence. What is more, it is important to evaluate whether the too small movements we have provoked, such as 30 or 60 columns, truly indicate different spectral bands or not. Results of larger movements of the motor step have not been cited, since the reconstruction they perform is much more distorted.

Chapter 7

Modulation Transfer Function

7.1 Introduction

Most optical systems are expected to perform to a predetermined level of image integrity. Photographic optics, photolithographic optics, contact lenses, video systems, fax and copy optics are included in the list of such optical systems. A convenient and reliable measure of this quality level is the ability of the optical system to transfer various levels of detail from object to image. Imaging performance is measured in terms of **contrast** (degrees of gray) or **modulation**, and is related to the degradation of the image of a perfect source produced by the lens.

Modulation Transfer Function (MTF) [1], is one of the most important and fundamental parameters by which image quality is measured. Optical designers and engineers frequently refer to MTF data, especially in applications where success or failure is contingent on how accurately a particular object is imaged. To truly grasp MTF, it is necessary to first understand the ideas of resolution and contrast, as well as how an object's image is transferred from object to image plane. *While initially daunting, understanding and eventually interpreting MTF data is a very powerful tool for any optical designer.* With knowledge and experience, MTF can make selecting the appropriate lens a far easier endeavor, despite the multitude of offerings.

The Modulation Transfer Function (MTF) constitutes, as the name suggests, a measure of the transfer of modulation (or contrast/sharpness) from the subject to the image. In other words, it measures how faithfully the system reproduces (or transfers) detail from the object to the image produced by the lens. It is generally expressed as the ratio of the relative image contrast divided by the relative object contrast:

$$\boxed{Modulation\ Transfer\ Function = \frac{Relative\ Image\ Contrast}{Relative\ Object\ Contrast}}$$

$$(7.1.0.1)$$

---

[1] http://www.trioptics.com/knowledgebase/mtf.php

So, the sharpness of an imaging system or of a component of the system (lens, film, image sensor, scanner, enlarging lens, etc.) is characterized by the MTF, which is also known as **Spatial Frequency Response (SFR)** [2]. It is the contrast at a given spatial frequency relative to low frequencies. High spatial frequencies correspond to fine image detail. The more extended the response, the finer the detail, the sharper the image produced by the system. [20]

7.2   The Components Of MTF

As it has been previously mentioned, it is necessary to first define two terms regarding MTF, which are required in order to truly characterize image performance:

  i. *resolution*

 ii. *contrast*

7.2.1   Resolution

Resolution [3] is an imaging system's ability to distinguish object detail. It is often expressed in terms of line-pairs per millimeter (where a line-pair is a sequence of one black line and one white line). This measure of line-pairs per millimeter (lp/mm) is also known as frequency. The inverse of the frequency yields the spacing in millimeters between two resolved lines. Bar targets with a series of equally spaced, alternating white and black bars are ideal for testing system performance . For all imaging optics, when imaging such a pattern, perfect line edges become blurred to a degree, like in figure 7.1. High-resolution images are those which exhibit a large amount of detail as a result of minimal blurring. Conversely, low-resolution images lack fine detail.

---

[2]http://en.wikipedia.org/wiki/Spatial_frequency
[3]http://en.wikipedia.org/wiki/Optical_resolution
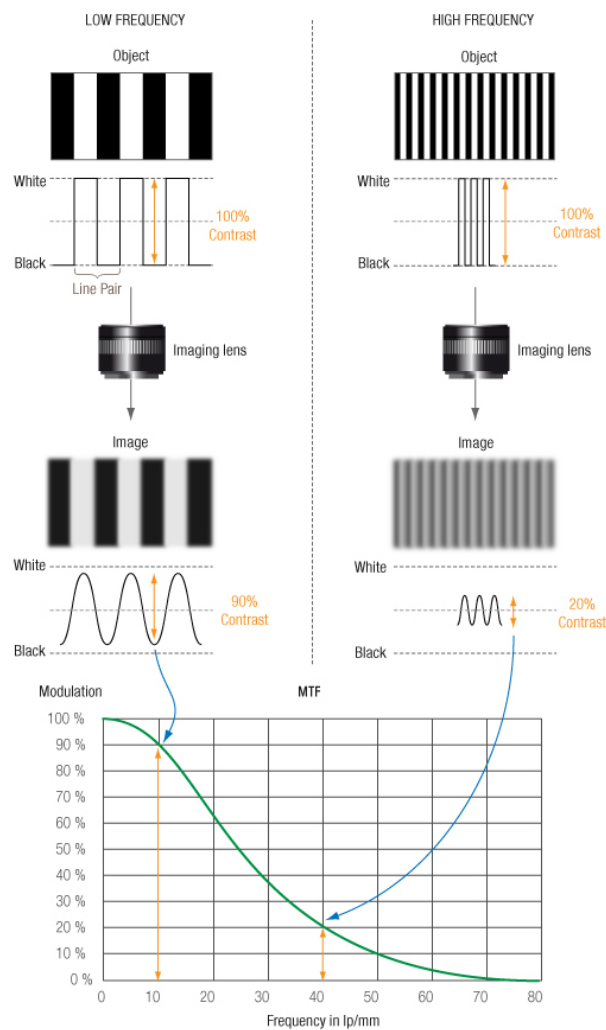
Figure 7.1: *Perfect Line Edges before and after passing through a low-frequency pattern (left), high-frequency pattern (right), their corresponding MTF value (bottom).*

A MTF curve is represented above. The x-axis represents the spatial frequency in line pairs per mm (here on the image sensor). The maximum attainable frequency on the sensor is called the Nyquist frequency and corresponds to alternating dark and bright lines one pixel wide. The y-axis (MTF value) represents the contrast restitution for the corresponding spatial frequency. This value is between 0 and 100%, meaning complete obliteration or perfect restitution of the frequency, respectively. The value of the MTF at frequency 0 is always 100% since a flat field is considered to have been reproduced perfectly, with no intensity loss. Attenuation due to lens

transmission is measured separately.

A practical way of understanding line-pairs is to think of them as pixels on a camera sensor, where a single line-pair corresponds to two pixels (see figure 7.2). Two camera sensor pixels are needed for each line-pair of resolution: one pixel is dedicated to the red line and the other to the blank space between pixels. Using the aforementioned metaphor, image resolution of the camera can now be specified as equal to twice its pixel size.
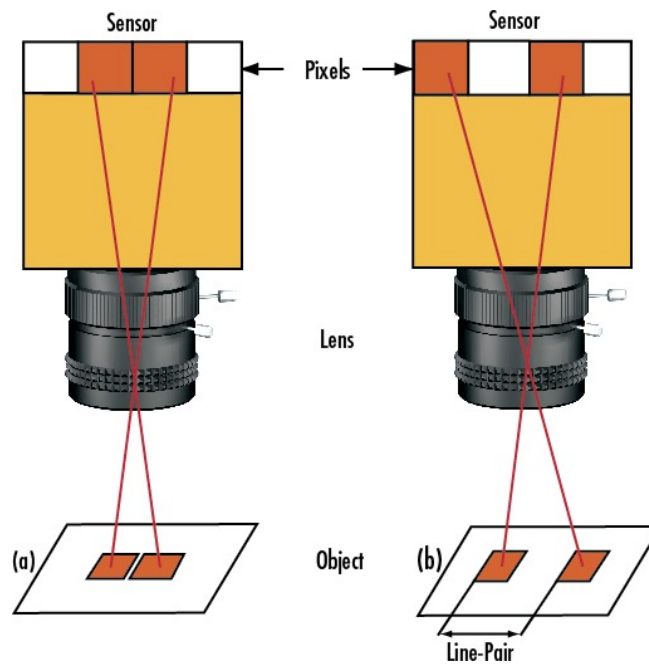
Figure 7.2: Imaging Resolution Scenarios where (a) the line-pair is not resolved and (b) the line-pair is resolved.

7.2.2 Contrast/Modulation

Consider normalizing the intensity of a bar target by assigning a maximum value to the white bars and zero value to the black bars. Plotting these values results in a square wave, from which the notion of contrast can be more easily seen in figure 7.3. Mathematically, contrast is calculated with equation (7.2.2.1), which is known as **Michelson contrast equation**:

$$Contrast/Modulation = \frac{I_{max} - I_{min}}{I_{max} + I_{min}} \qquad (7.2.2.1)$$
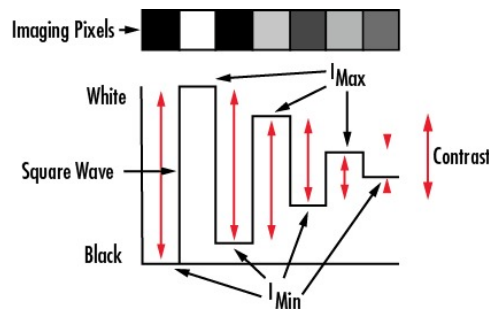
Figure 7.3: *Contrast expressed as a square wave at different levels of resolution.*

Based on equation (7.2.2.1), MTF is defined as:

$$MTF(f) = \frac{M_{captured}(f)}{M_{original}(f)} \qquad (7.2.2.2)$$

where $M_{captured}$ and $M_{original}$ are the modulations of the captured and the original image target respectively. The original target modulations are accompanied with the manufacturer.

When this same principle is applied to the imaging example in figure 7.1, the intensity pattern before and after imaging can be seen in figure 7.4. *Contrast or Modulation can then be defined as how faithfully the minimum and maximum intensity values are transferred from object plane to image plane.*

To understand the relation between contrast [4] and image quality, consider an imaging lens with the same resolution as the one in figure 7.1 and figure 7.4 , but used to image an object with a greater line-pair frequency. Figure 7.5 illustrates that as the spatial frequency of the lines increases, the contrast of the image decreases. This effect is always present when working with imaging lenses of the same resolution. For the image to appear defined, black must be truly black and white truly white, with a minimal amount of grayscale between.

---

[4]http://en.wikipedia.org/wiki/Contrast_(vision)
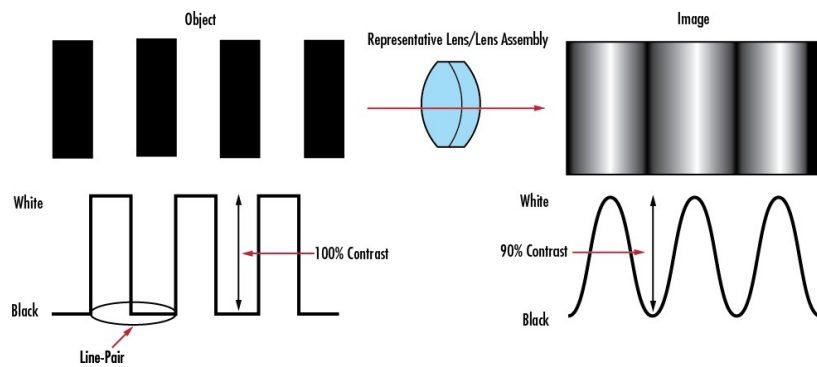
Figure 7.4: *Contrast of a low-frequency bar target.*
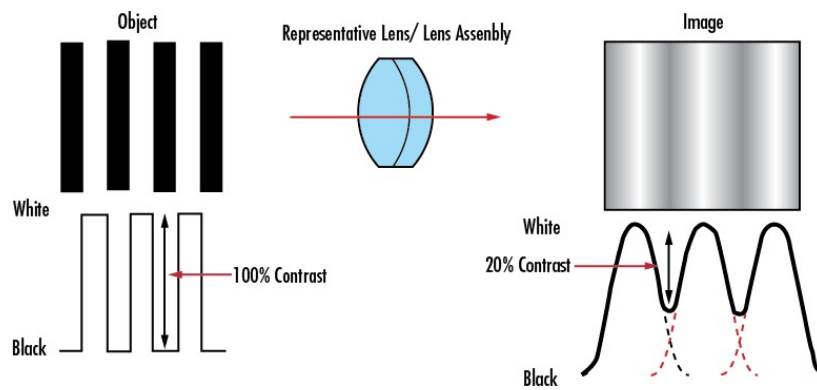
Figure 7.5: *Contrast of a high-frequency bar target.*

The point at which we can no longer see any variation in the image, as in the end of figure 7.6 (defined as straight line at a middle intensity value), is the point at which MTF is zero and that is the definition of the "resolution" of the lens. In this case, the final pattern set with an MTF value a little bit larger than zero, is classified as **"just resolved"** [5] by the lens.

---

[5] http://www.photo.net/learn/optics/mtf/
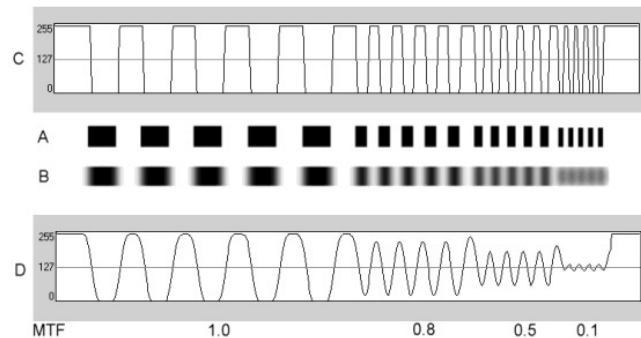
Figure 7.6: *A → original test pattern, B → image of the test pattern produced by the lens, C → spatial-line profile of the original test pattern (white → 255, black → 0), D → spatial-line profile of the image of the test pattern produced by lens (white → 255, black → 0).The fluctuations of MTF values are depicted in diagram D, where the value of 0.1 responds to the state of "just being resolved".*

7.3   What Do the Numbers Really Mean?

Now that the components of the Modulation Transfer Function (MTF), **resolution** and **contrast/modulation**, are defined, consider MTF itself. The MTF of a lens, as the name implies, is a measurement of its ability to transfer contrast at a particular resolution from the object to the image. In other words, *MTF consists a way to incorporate resolution and contrast into a single specification.* As line spacing decreases and thus frequency increases on the test target, it becomes increasingly difficult for the lens to efficiently transfer this decrease in contrast and as a result, MTF decreases.

Line pairs [6] are often described in terms of their frequency; the number of lines which fit within a given unit. This frequency is usually expressed in terms of **lp/mm**, indicating the number of line pairs that are concentrated into a millimeter(mm). Alternatively, sometimes this frequency is instead expressed in terms of **cycles/mm** or **line widths (LW)**, where two LW's equals to one lp.

MTF is a function of spatial resolution f, which refers to the smallest frequency, depending on the test method, the system can resolve. The cut-off frequency f_c is the frequency that MTF reaches zero and is given by equation (7.3.0.3):

---

[6]http://en.wikipedia.org/wiki/Line_pair

$$\boxed{f_c = \frac{1}{\lambda \times F\#}} \tag{7.3.0.3}$$

F# [7] is the f-stop number, which is defined as the focal length divided by the diameter of the lens :

$$\boxed{F\# = \frac{focal\ \ length}{diameter}} \tag{7.3.0.4}$$

As we deal with the mathematical and physical background of the Modulation Transfer Function [21], spread and transfer functions that contribute to the calculation of the aforementioned quantity are introduced. In the optical-image capture system lies the formula:

$$\boxed{g(x,y) = h(x,y) * *f(x,y)} \tag{7.3.0.5}$$

It should be mentioned that (x,y) are the spatial co-ordinates; $f(x,y)$ is the original input image; $g(x,y)$ is the captured image; $h(x,y)$ is considered as the system's impulse response; $**$ denotes 2d-convolution. When equation (7.3.0.5) is converted into the frequency domain, equation (7.3.0.6) is derived:

$$\boxed{G(u,v) = H(u,v) \times F(u,v)} \tag{7.3.0.6}$$

In equation (7.3.0.6), (u,v) are the co-ordinates in frequency domain; $G(u,v)$, $F(u,v)$, $H(u,v)$ are the fourier transform of the captured image, original input image and impulse response function, respectively. $H(u,v)$ is also defined as the *transfer function*. When $H(u,v)$ is normalized to have the unit value at zero spatial frequency, if applicable, $H(u,v)$ is referred to as the **Optical Transfer Function (OTF)** [8].

OTF is a complex function, having both the **magnitude** [9] and **phase** [10] portion. The magnitude portion is referred to as the **Modulation Transfer Function (MTF)** and the phase portion as the **Phase Transfer Function (PTF)**:

---

[7] https://en.wikipedia.org/wiki/F-number
[8] http://en.wikipedia.org/wiki/Optical_transfer_function
[9] http://en.wikipedia.org/wiki/Magnitude_(mathematics)
[10] http://en.wikipedia.org/wiki/Phase_factor

$$\boxed{OTF = H(u,v) = \quad \mid H(u,v) \mid e^{-j\theta(u,v)}}$$
(7.3.0.7)

$$\boxed{MTF \equiv \quad \mid H(u,v) \mid}$$
(7.3.0.8)

$$\boxed{PTF \equiv \theta(u,v)}$$
(7.3.0.9)

When the input image is a delta function $\delta(x,y)$, we will have the captured output image as a **Point Spread Function (PSF)** [11]:

$$
\begin{aligned}
PSF(x,y) &\equiv g(x,y) = h(x,y) * *\delta(x,y) \\
&= h(x,y)
\end{aligned}
$$
(7.3.0.10)

When the input image is a line like:

$$\boxed{f(x,y) = \delta(x)1(y)}$$
(7.3.0.11)

Then the output image $g(x,y)$ is a **Line Spread Function (LSF)**:

$$
\begin{aligned}
LSF(x) &\equiv g(x,y) = h(x,y) * *f(x,y) \\
&= h(x,y) * *[\delta(x)1(y)] \\
&= PSF(x,y) * *[\delta(x)1(y)]
\end{aligned}
$$
(7.3.0.12)

The y direction convolution with a constant is equivalent to an integration over the y direction, so:

$$\boxed{LSF(x) = \int_{-\infty}^{+\infty} h(x,y')\,dy'}$$
(7.3.0.13)

---

[11] http://en.wikipedia.org/wiki/Point_spread_function

Therefore, we can tell that the MTF of the x direction is the magnitude of the one-dimensional Fourier transform of the line spread function (LSF):

$$\boxed{MTF(u) = MTF(u,0) = \ | \mathcal{F}\{LSF(x)\} |} \tag{7.3.0.14}$$

When the input image $f(x,y)$ is a step function:

$$\boxed{f(x,y) = u(x)1(y)} \tag{7.3.0.15}$$

Then the output image $g(x,y)$ is an **Edge Spread Function (ESF)**:

$$
\begin{aligned}
ESF(x) &\equiv g(x,y) = h(x,y) ** f(x,y) \\
&= h(x,y) ** [u(x)1(y)] \\
&= PSF(x,y) ** [u(x)1(y)]
\end{aligned}
\tag{7.3.0.16}
$$

The convolution between the PSF and a constant produces an LSF in the y direction; the convolution between the PSF and a unit-step function is an integration:

$$\boxed{ESF(x) = \int_{-\infty}^{x} LSF(x')\,dx'} \tag{7.3.0.17}$$

Therefore, the derivative of the ESF generates the LSF in the x direction:

$$\boxed{\frac{d}{dx}ESF(x) = \frac{d}{dx}\int_{-\infty}^{x} LSF(x')\,dx' = LSF(x)} \tag{7.3.0.18}$$

Thus, MTF of the x direction can also be calculated from the ESF:

$$
\begin{aligned}
MTF(u) &= MTF(u,0) \\
&= | \mathcal{F}\{LSF(x)\} | \\
&= | \mathcal{F}\{\frac{d}{dx}ESF(x)\} |
\end{aligned}
\tag{7.3.0.19}
$$

7.3.1 Overall Imaging MTF Perfomance

In traditional system integration (and less crucial applications), the system's performance is roughly estimated using the principle of the *weakest link*. The principle of the weakest link proposes that a system's resolution is solely limited by the component with the lowest resolution. Although this approach is very useful for quick estimations, it is actually flawed because every component within the system inserts error to the image, yielding poorer image quality than the weakest link alone.

Every component within a system has an associated modulation transfer function (MTF) and, as a result, contributes to the overall MTF of the system. This includes the *imaging lens, camera sensor, image capture boards, and video cables*, for instance. The resulting MTF of the system is the product of all the MTF curves of its components, as it is depicted in figure 7.7.
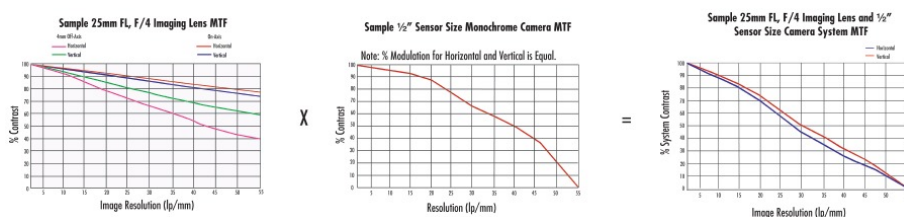
Figure 7.7: *System-MTF is the Product of the MTF of Individual Components: Lens MTF × Sensor MTF = Overall System MTF.*

MTF is one of the best tools available to quantify the overall imaging performance of a system in terms of resolution and contrast. As a result, knowing the MTF curves of each imaging lens and camera sensor within a system allows a designer to make the appropriate selection when optimizing for a particular resolution.

7.4 Methods and Test Targets

Three different kinds of resolution targets are usually used in order to measure MTF:

   i. *slanted-edge or knife-edge target*

  ii. *sine-wave target*

iii. *grill or bar pattern target*

Further analysis and elaboration concerning individually each one of the aforementioned cases are following.

7.4.1   Slanted-Edge/Knife-Edge Analysis

Slanted-edge target is a square target that contains four slanted edges. These are contrast edges compared with the background. The method used to measure MTF by slanted-edge target is called *slanted-edge method* or *slanted-edge analysis*. Figure 7.8 illustrates a widespread preferred target for this type of MTF analysis.
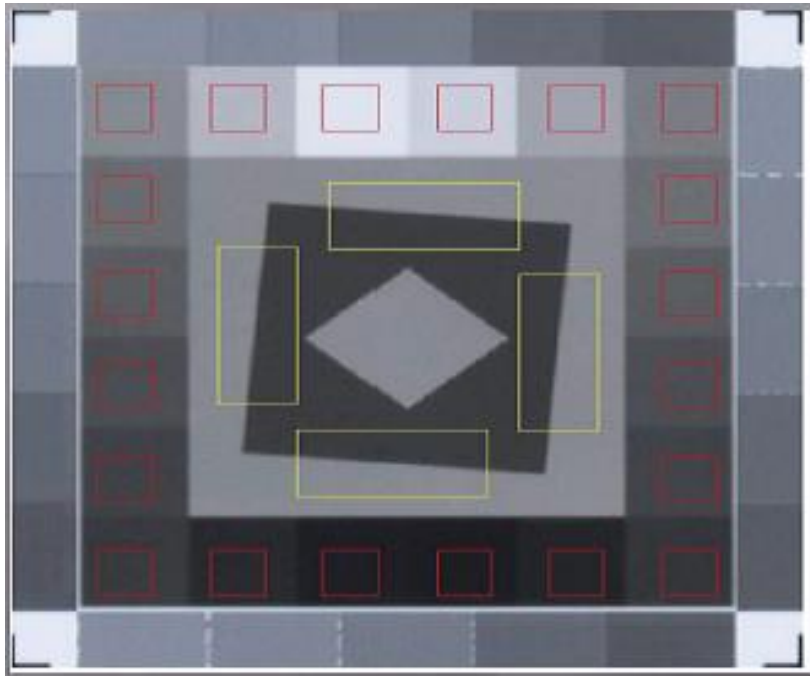
Figure 7.8: *QA-62 target for slanted-edge MTF analysis.*

The basic idea for this method is that after having the ESF, we get the LSF by estimating the first derivative of ESF, and then the prime type of MTF by computing the Fourier transform of the LSF. The normalized aforementioned Fourier transform constitutes the *Spatial Frequency Response (SFR)*, denoted as the MTF. The flowchart depicted in figure 7.9 provides a thorough inspection of this concept.
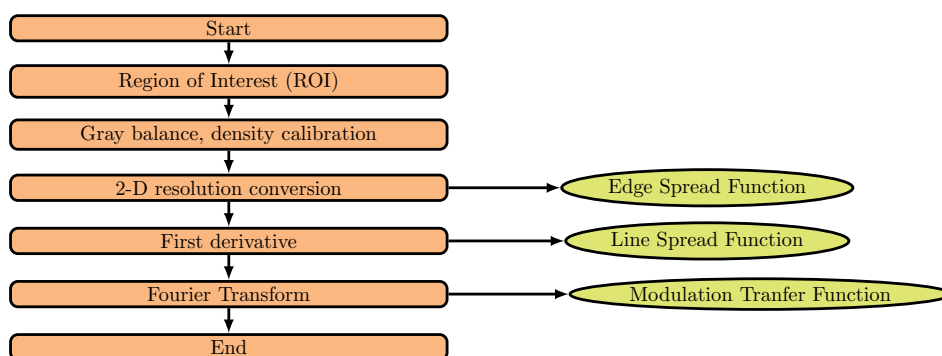
Figure 7.9: *Flow-chart of the slanted-edge method.*

7.4.2   Sine-Wave Target Analysis

Sine-wave analysis is performed by the contribution of the appropriate sine-wave targets, like this one depicted in figure 7.10. Each of the sinewave patterns has a different frequency. There exist two different ways to estimate Modulation Transfer Function using this kind of analysis:

Figure 7.10: *Sine Wave Target M-13-60-1x*

  i. *Direct method*

  ii. *Fourier method*

The modulation of captured images in such cases is calculated using equation (7.4.2.1).

$$Modulation(f) = \frac{Fundamental\ Frequency\ Component}{DC\ Component} \qquad (7.4.2.1)$$

Direct Sine-Wave Method

The flowchart of the direct method is shown in figure 7.11. When getting the captured image, the averaged peak value along with the mean value(direct component) of the sinewave are calculated. Two auxiliary steps have to be completed before the modulation is computed: gray balance and density

calibration of the reflective target. The modulation is based on the optical density, using equation (7.4.2.2):

$$Modulation = \frac{A - B}{B} \qquad (7.4.2.2)$$
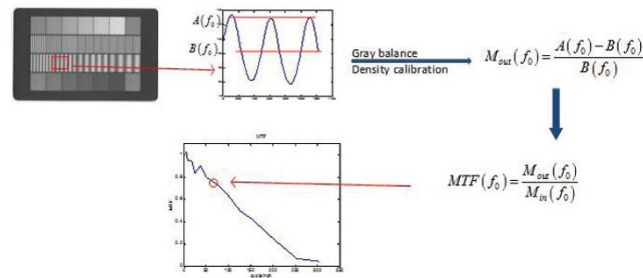
Figure 7.11: *Flow chart of the direct method using sine-wave target.*

Fourier Sine-Wave Method

The flowchart of the Fourier analysis method is shown in figure 7.12.The difference between the Fourier and the aforementioned Direct method is that after doing the Fourier analysis, equation (7.4.2.3) is utilized to compute the modulation.

$$Modulation = \frac{2 \times F(N)}{F(0)} \qquad (7.4.2.3)$$
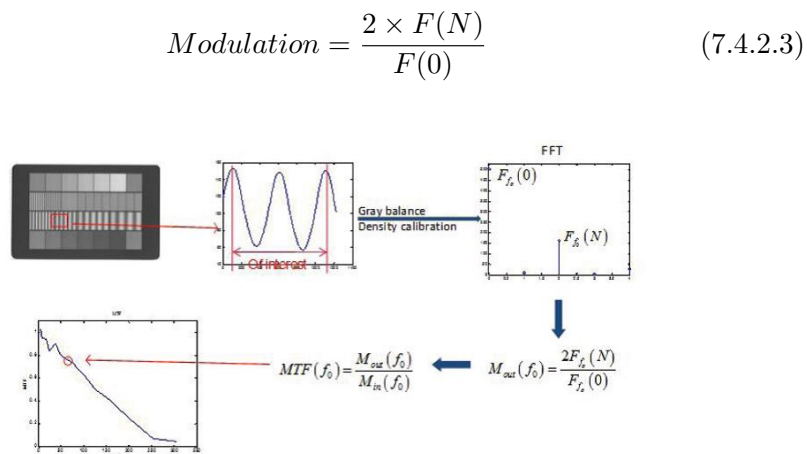
Figure 7.12: *Flow chart of the fourier analysis method using sine-wave target.*

It is necessary to clarify that $F(0)$ is the DC component energy and $F(N)$ is the energy at N, where N is the number of sinusoidal cycles in the selected

Region of Interest. Fourier analysis has its advantage over the direct method because by Fourier transformation, we can effectively suppress the random white noise.

7.4.3 Grill/Square-Wave Analysis Pattern

An accurate sinewave target is very dificult to fabricate if we want only the single frequency in the sinusoidal function. Therefore, sometimes we use the grill/bar/square wave target, as the one depicted in figure 7.13, which is much easier to produce. The depicted numbers indicate the line pairs per millimeter (lp/mm).
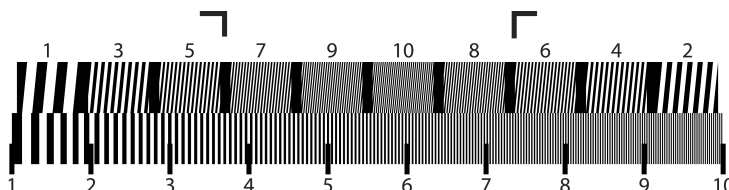
Figure 7.13: *Grill Pattern Target*

However, we similarly use the direct method for sinewave target, the ratio of the captured and the original modulation is larger than the MTF due to the fact that the bar pattern has lots of frequencies except for thr fundamental frequency. As a result, unnecessary energy will be included. **Contrast Transfer Function (CTF)** [12] is defined, for an infinite square wave, as the ratio of the captured and original modulations, which is similar to the MTF defined for the sinewave target. *Coltman formulas* yield the following equations between MTF and CTF:

$$MTF(f) = \frac{\pi}{4}\left(CTF(f) + \frac{1}{3}CTF(3f) - \frac{1}{5}CTF(5f) + \frac{1}{7}CTF(7f) + \frac{1}{11}CTF(11f) - \frac{1}{13}CTF(13f) + \cdots\right)$$

(7.4.3.1)

$$CTF(f) = \frac{4}{\pi}\left(MTF(f) - \frac{1}{3}MTF(3f) + \frac{1}{5}MTF(5f) - \frac{1}{7}MTF(7f) + \frac{1}{9}MTF(9f) - \frac{1}{11}MTF(11f) + \cdots\right)$$

(7.4.3.2)

Considering the Coltman formulas in order to calculate the MTF, a set of higher harmonically related frequencies for CTF measurement. Neverthe-

---

[12]http://en.wikipedia.org/wiki/Contrast_transfer_function

less, it is impractical to have many harmonic frequencies. Therefore, the first term of equation (7.4.3.1) stands as the *approximate* MTF.

$$MTF(f) \simeq \frac{\pi}{4}CTF(f) \qquad (7.4.3.3)$$

As equation (7.4.3.3) indicates, CTF is usually higher than the according MTF. If the measured CTF is directly considered as the MTF, without multiplying the CTF quantity by $\frac{\pi}{4}$, a high-biased MTF is obtained. Like the sinewave pattern, grill pattern also is characterized by two different methods:

   i. *Direct method*

  ii. *Fourier method*

Direct Grill Pattern Analysis

The direct method of the grill pattern requires one more step than the sinewave target, as the ratio of the modulations is the CTF. So, it is essential to multiply CTF by the factor of $\frac{\pi}{4}$, in order to acquire MTF.

Fourier Grill Pattern Analysis

The Fourier method of the grill pattern analysis has **two** differences compared to the respective method of the sinewave target. The first one is the multiplication of CTF by $\frac{\pi}{4}$, so as to get MTF. The second and the last one is that the modulation of the Fourier method needs to be normalized by $\frac{4}{\pi}$:

$$Modulation = \frac{\frac{2F(N)}{F(0)}}{\left(\frac{4}{\pi}\right)} \qquad (7.4.3.4)$$

7.4.4   Comparison of Methods

The aforementioned MTF analysis methods along with their test targets are useful when evaluating or calibrating an imaging system's perfomance or image quality. This could include troubleshooting the system, certifying or evaluating measurements, as well as establishing a foundation to ensure the system works well with another. Image quality can be defined by different

components, particularly resolution, contrast, modulation transfer function (MTF), depth of field (DOF) [13], and distortion; therefore, one or more types of test targets may be necessary or helpful depending upon the type of system being constructed or what does it need to be measured. Fortunately, an array of targets exists that cater towards specific systems including cameras, visual displays, or even a single, thin lens. Table 7.1 summarizes the potential of each method [22], whose selection would lead to the appropriate test target.

ANALYSIS	PROS	CONS
Slanted-Edge	single measurement, simpler and more popular method, edges are easy to generate, super-sampling to improve spatial resolution of analysis	further computational, long post-processing of the measurement(e.g subpixel localization, robust model fitting, Hough transform), limited variety of test targets
Sine-Wave	direct way to measure the signal constrast as a function of frequency, pattern where the optical density varies between black and white smoothly, line profile looks like a sine-wave, image quality information over a full range of frequencies instead of only the maximum obtainable resolution, suppress random white noise	measurement not in the same form as the image information is encoded, difficult to produce, lots of measurements, the image of such patterns is hard to measure by eye
Square-Wave	easy generation of such patterns, direct use of Michelson equation either in spatial(direct method) or frequency domain(fourier method), measurement in the same form as the image information is encoded	small distortion (not important) in the MTF, because transferring CTF to MTF is not a simple linear transformation and yields a slightly higher MTF, lots of measurements

Table 7.1: *Comparison of available methods for MTF analysis*

---

[13] http://en.wikipedia.org/wiki/Depth_of_field

ANALYSIS	DIRECT	FOURIER
Sine-Wave	$MTF(f_0) = \frac{M_{f_0}out}{M_{f_0}in}$	$MTF(f_0) = \frac{2F_{f_0}(N)}{F_{f_0}(0)}$
Square-Wave	$MTF(f_0) = \frac{\pi}{4}CTF(f_0)$	$MTF(f_0) = \frac{2F_{f_0}(N)}{F_{f_0}(0)}/\frac{4}{\pi}$

Table 7.2: *Sine-Wave vs. Square-Wave analysis*

Despite the method that is adopted for measuring a system's performance, there exists a great number of other factors that influence MTF measurements. It is important to take into consideration each one of them, so as to minimize the inserted error in estimations, sparked by the environment or the equipment. The most important factors causing abberations are listed below:

i. *Field Position*

ii. *Spatial Orientation*

iii. *Focal Length*

iv. *Numerical Apperture (NA)*

v. *Light Wavelength*

vi. *Light used for Illumination* (blue light gives higher MTF than red light. Normally, white light is used)

vii. *Size of Sensor*

viii. *Type of Sensor* (if the sensor is more sensitive to blue than red light, the result will be a higher MTF than a detector more sensitive to red)

7.5 Characterization

7.5.1 Characterization of our HSI

Taking seriously into consideration the contents of table 7.1, we adopt the **square-wave pattern analysis**. Our first priority was to create the appropriate software for our HSI from scratch. So, this task would be suitably accompanied with the development of a method that has rarely been used so far. In this way, slanted-edge analysis is being excluded as there are a lot of developed software systems that perform this kind of MTF measurements. **SFRedge** is the most prominent of them, contributed by *Peter D.Burns.*

Among sine-wave and square-wave pattern analysis, we ended up to the latter, as it provides the eligibility through the *direct method* to process the signals in the spatial domain where the image information is encoded and should be handled. However, the same processing could be implemented in the frequency domain as well, providing us with the ability to compare the two different ways of the same method.

As it is widely known, there is always a **trade-off** for all engineering issues. In this case, we prefer a more direct method with lots of measurements and a little distortion rather than a pre-existed, further computational but single measurement method (slanted-edge analysis) or a direct but only performed in the frequency domain and eye-inconvenient method (sine-wave analysis).

7.5.2 Test-Target

Resolution and constrast test targets use a variety of patterns, depending on the adopted processing method, to measure an optical system's resolution. Test Targets often feature an array of lines, dots, or other patterns to which an imaging system focuses on, in order to determine its level of precision. They do allow imaging systems to maintain a high level of accuracy over time or multiple applications.

Being more specific, **square-wave analysis** is performed by test patterns of consecutive bar patterns with augmented frequency. Such targets feature series of lines of specific frequencies that measure resolution by determining how far an imaging system can distinguish individual lines. The more different groups of variable frequencies in the test-target, the wider range of tested resolution the system reaches.

Variable Frequency Target #43−488 from Edmund Optics, which is depicted in figure 7.14, meets the requirements for a successful MTF square-wave analysis. It is made from soda lime float glass, which is transparent in the visible region, with deposited chromium of optical density greater than 3.0. Further technical information is provided by table 7.3.

Figure 7.14: *The Target we use to evaluate resolution of the Spectral Imager:* **Edmund** *Variable Frequency Target #43 − 488*

Dimensions (inches)	2×2
Pattern Size (mm)	25.4×39.37
Resolution Range (lp/mm)	$5 - 200$
Wide Step Size (mm)	1
Step Increments (lp/mm)	5
Edges	beveled
Thickness (mm)	1.5
Flatness (mm)	0.00254
Surface Quality	$40 - 10$
Substrate	Soda Lime Float Glass
Optical Density (OD)	≥ 3.0
Coating	Vacuum deposited durable chromium

Table 7.3: *Technical information of resolution target #43 − 488.*

It is important to mention that this kind of target and analysis correspond to the evaluation of the **overall** MTF system performance, as it has been extensively discussed in section 7.3.1. Specialized methods that go far beyond our implementation along with necessary feedback from the constructors are required in order to be able to estimate MTF of the separate components of an imaging system, such as the lens and sensor alone.

7.5.3   Experimental Set-Ups For Measuring MTF

As it has already been stated, the Hyper Spectral Imager we introduce, consists of two different set-ups, the **manual-step**, which is the initial construction, and **auto-step**. The first one is accompanied with the manual

movement of the filter in front of the CCD sensor, while the second one has been advanced to an automatic stepper filter scanning. As a consequence, the auto-step set up enhance the precision of measurements since the exact movement of the filter is guaranteed across all steps and experimental conditions are more ideal due to the enclosed automatic set up. As a result, noise and light from the environment are eliminated. Moreover, calibration is provided. All these facts influence the overall performance of the spectral imager. So, a different and specifically a better MTF behavior is expected by the automatic one. We are going to examine the MTF performance of each set-up separately. However, the measurements are going to be taken in the same wavelengths, so as to provide comparable results.

7.5.4 MTF of Hyper Spectral Scanning Procedure of HSI

MTF performance is being depicted in figures 7.16 for the manual and 7.18 for the automatic HSI. Each one of these figures shows the **raw** overall MTF for a specific wavelength of the imaging system in the frequency range between 0 lp/mm, where the system's efficiency to transfer contrast from object to the image captured by the system is **maximum** and 70 lp/mm, where we can no longer see any variation in the image, meaning that this is the point at which MTF reaches zero. This is also called **"cut-off frequency"**. 65 lp/mm and 50 lp/mm are the points at which MTF is a little bit larger than zero in the auto-step and manual-step HSI, respectively. In this case, the final pattern set is classified as **"just being resolved"**.

In this point, we should concentrate on estimating the maximum resolution reached by the specifications of the lens and properties of the CCD sensor being used, in order to verify the results, as far as the spatial frequencies are concerned. The maximum resolution can be evaluated theoretically. The resolution of our CCD sensor is 1024×768, meaning that there are 1024 pixels in width. In order to detect line pairs, one pixel for the white space and an other one for the black space are needed. So, one line pair corresponds to 2 pixels. In our case, a maximum of $1024/2 = 512$ lp can be recorded. Furthermore, the sensor measures 7 mm across, which indicates a maximum resolution of $512/7 \approx 73$ lp/mm, which is close to 50 lp/mm and even closer to 65 lp/mm, where our HSIs, not alone the lens, just resolve the pattern.

MTF perfomance of manual-step HSI

(a) 400 nm   (b) 555 nm   (c) 730 nm
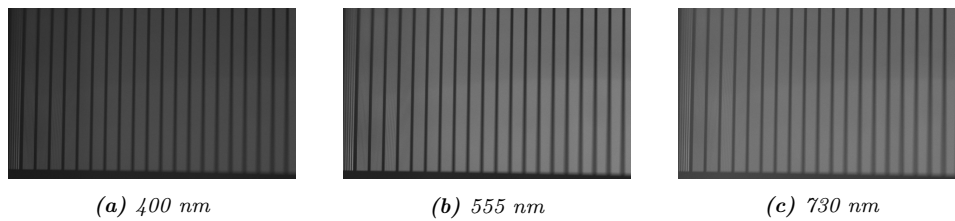
Figure 7.15: captured MTF target of Manual HSI

(a) 400 nm   (b) 555 nm   (c) 730 nm
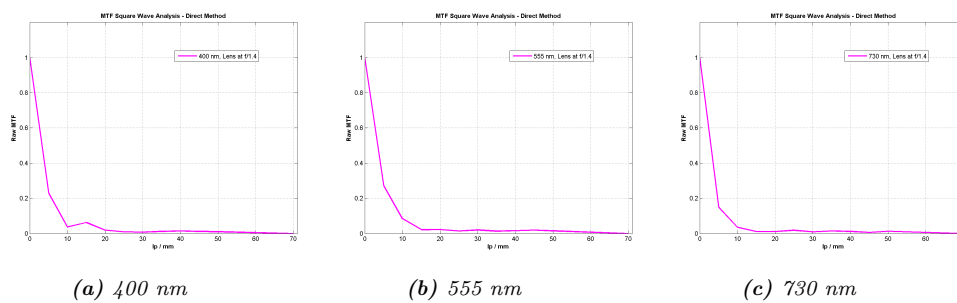
Figure 7.16: Raw MTF of Manual Set Up

MTF perfomance of auto-step HSI

(a) 400 nm   (b) 555 nm   (c) 730 nm
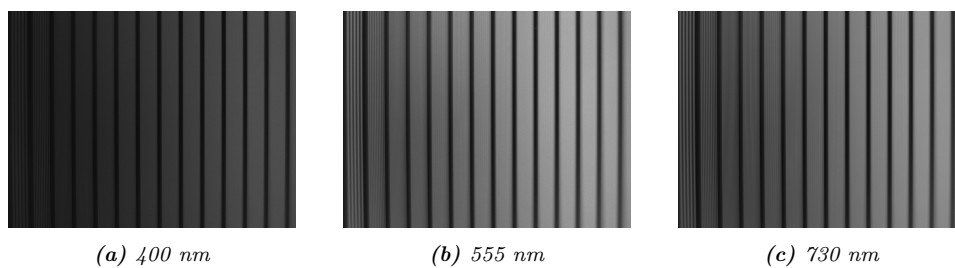
Figure 7.17: captured MTF target of auto-step HSI

(a) 400 nm   (b) 555 nm   (c) 730 nm
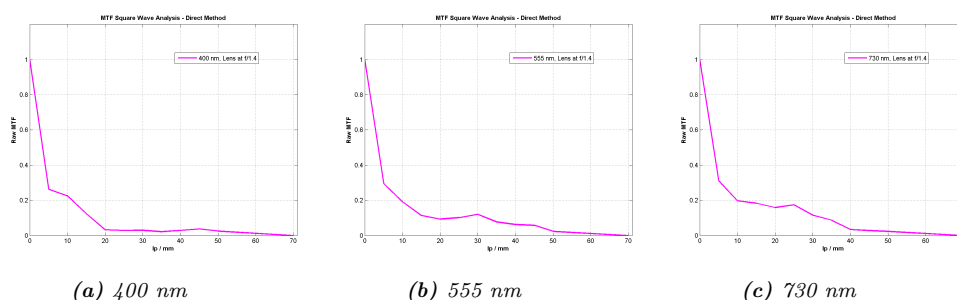
Figure 7.18: *Raw MTF*

Comparisons

Plotting all MTF curves of the three different chosen wavelengths in a common diagram gives us the opportunity to compare the performance in different spectral bands of the filter. Based on the properties (see table 2.2) of the variable filter being used, it is expected that the bands in the range of 400-745 nm would have the best response due to the specification of 97% transmission. On the other hand, spectral bandwidth in the range of 330-400 nm are expected to join a worse response, as the transmission in this area is fluctuated between 50% and 97%. However, judging by the figure 7.19, we realize that the two different HSIs correspond to different performances in the same wavelengths.

Being more specific, only the auto-step HSI abides by the expected performance mentioned above. This includes better performance in 730 and 555 nm, and worse in 400 nm. This behavior is verified by looking at figure 7.19b. However, the manual HSI does not follow the expected behavior. Figure 7.19a shows better MTF performance in 400, 555nm and worse performance in 730 nm. In this point, it should be stated that we have introduced and implemented a method for measuring the **net total MTF** of an imaging system and not the MTF of separate components **alone**. This net MTF represents the combined result from lens, camera sensor, filter, raw conversion, in addition to any sharpening and other post-processing. The construction of the manual HSI was the initial set up, so there were a lot of leaks that justify the respective MTF performance, which is boosted by upgrading the set up to the auto-step.

Furthermore, the specifications of the HSI, we introduce, hold a fundamental role. It is far from the "slit-scan" technique. This factor indicates possible deviation in the outgoing wavelengths of the scanning procedure due to consecutive reflections and alternations in the direction of light. The use of the slit guarantees limitation and accuracy, as far as the movements of the filter across the spectral range, are concerned. It is also important the fact that

the tasks of lens' focusing and camera's calibration take place once, before the beginning of the hyper spectral scanning procedure. As a consequence, although each spectral band of the filter may require extra intervention for capturing a perfect image, this is not possible in one scanning for our HSI. For instance, an image that is not so well focused or illuminated gives a poor MTF estimation. This is the reason why the captured images of the MTF target(7.15 and 7.17) are cited, apart from their MTF curves.

Considering all these parameters provides justification of the unexpected MTF performance in the three tested wavelengths.

(a) *manual HSI*   **(b)** *auto HSI*
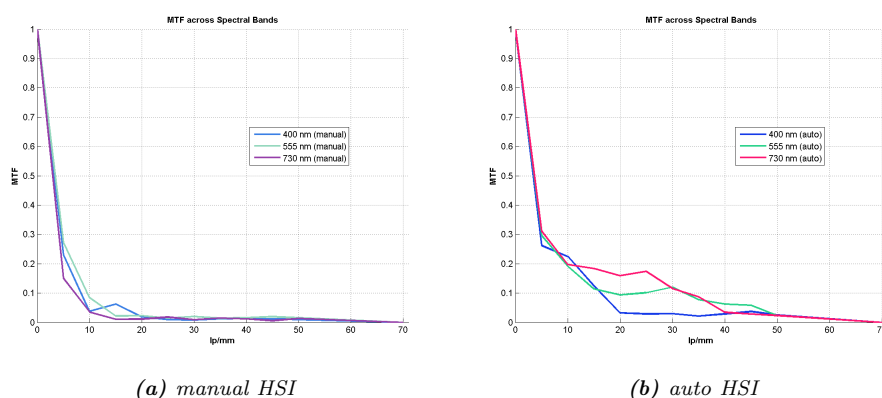
Figure 7.19: *MTF performances of Hyper Spectral Scanning procedure in the three different chosen wavelengths*

Looking at figures 7.19a and 7.19b more closely, we get a first, superficial impression of low MTF performance and extensively, low imaging efficiency of both systems, especially of the manual-step one. Conspicuous low MTF values are observed even in low spatial frequencies of 5 and 10 lp/mm. In addition, both systems after reaching a specific spatial frequency, tend to decrease slowly with increasing spatial frequency. In this range till the cut-off frequency is touched, MTF values with some oscillations, are observed. These oscillations indicate very small increments and decrements between increasing frequencies. This situation is known as **"spurious-resolution"** and is of practical importance with respect to focus-errors and motion-induced blurring. Undesirable reflections between the optical surfaces, light scattering at the interior barrel components and noise may affect a lot the total net MTF of our imaging system. Although all these erroneous factors cannot be seen with naked eye, they distort the final results, even if the quality of captured images is not as bad as the MTF values indicate.

As a result, resolving power and contrast rendition of a total imaging system are two characteristics too close and too far at the same time. We should be very careful with such MTF characterizations and remember that good MTF

values are no guarantee for brilliant images and vice versa. The overall MTF performance is strictly associated with all possible technical and physical misalignments, which sometimes may be inevitable.

Manual vs. Auto-Step HSI
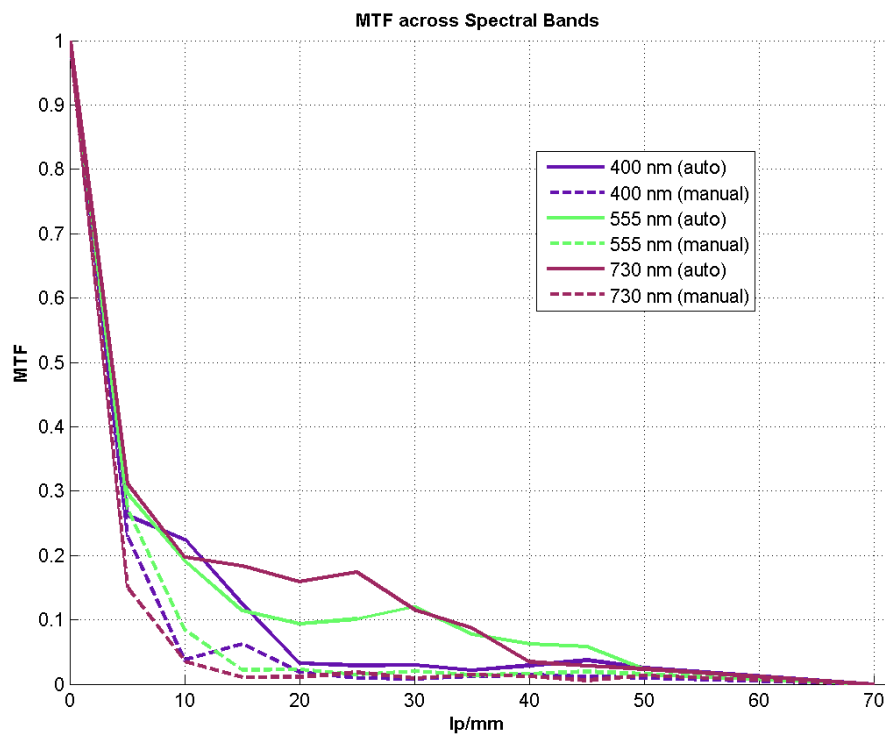
Figure 7.20: *Manual vs. Auto-Step HSI MTF performance of Hyper Spectral Scanning.*

As expected, auto-step HSI yields a better MTF performance than the manual-step HSI. It is important that the resolution of the automatic imaging system has been augmented by at least 20% in each measured frequency compared to the prime, manual set up. The imaging efficiency has been markedly improved and provides us with a final, balanced and quite satisfactory appraisal over a continuum of spatial frequencies, keeping in mind all physical problems and motion artifacts that such an imaging device may encounter, especially without a slit.

Auto-Step HSI with slit vs. without slit
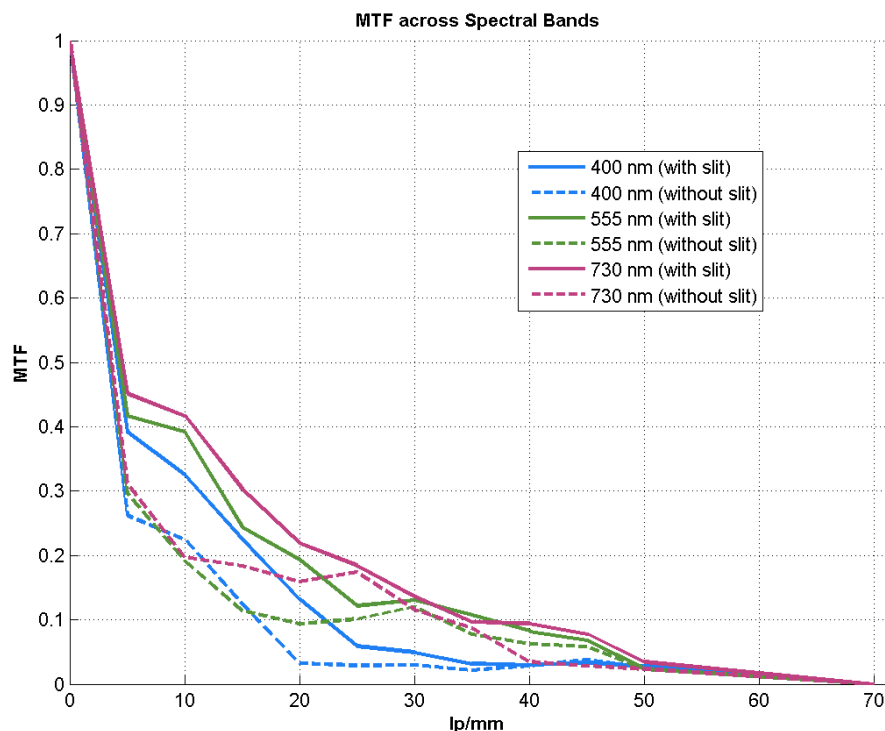
Figure 7.21: *Auto-Step HSI "with slit" vs. "without slit" MTF performance of Hyper Spectral Scanning.*

The last task was to evaluate the MTF perfomance of the HSI we introduce, *by adopting the slit-scan technique.* In this way, we have been able to ensure less quantity of incoming light and thus, minimize spectral contamination during the hyper spectral scanning procedure. Phenomena such as light scattering, consecutive reflections and possible alternations in the light direction are eliminated, as well. As a result, the spatial and spectral resolution are boosted, which means that the MTF performance is improved, as we can realize by looking at figure 7.21. This figure depicts the comparison between the HSI **with** and **without** a slit entrance, and the supremacy of the first on the second one. It is essential to mention that the set up we have constructed, can be easily modified in order to hold or not a slit, based on the type of application being developed. Our priority for this project, was to perform the reconstruction of the hyper spectral scanning without a slit, but it was also important to see the difference in resolving power of the same set up **equipped with** the slit entrance.

7.5.5 MTF of Reconstruction Procedure
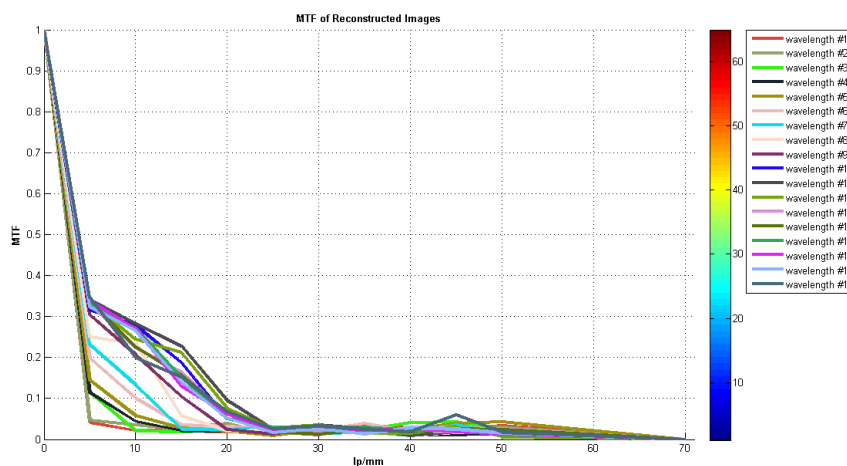
Figure 7.22: *MTF Performance along Reconstructed Images #1 − 18. All of them contain stripes. However, the greater the wavelength, the lighter the intensity of stripes.*

As far as the caption of figure 7.22 indicates, the MTF performance of the reconstructed spectral cube in bands distorted by stripes, is quite satisfactory. The colorbar shows the direction of the filter's hyper spectral scanning. Looking at MTF curves more closely, we realize that the MTF of reconstruction follows the same pattern as that one of the scanning procedure, which was analytically presented in section 7.5.4. Being more specific, this pattern refers to the augmentation of MTF values as the wavelength is increasing. Conspicuous low values are observed in UV and Violet region. However, greater values up to 25% are depicted in frequencies between 0 and 25 lp/mm. Larger values of frequency are accompanied with low values of resolution, exactly as it was captured in the hyper spectral scanning MTF performance. It is important that the different functions of our HSI pertain to similar MTF evaluations. The thinking goes that this fact indicates a **verified overall appraisal**.
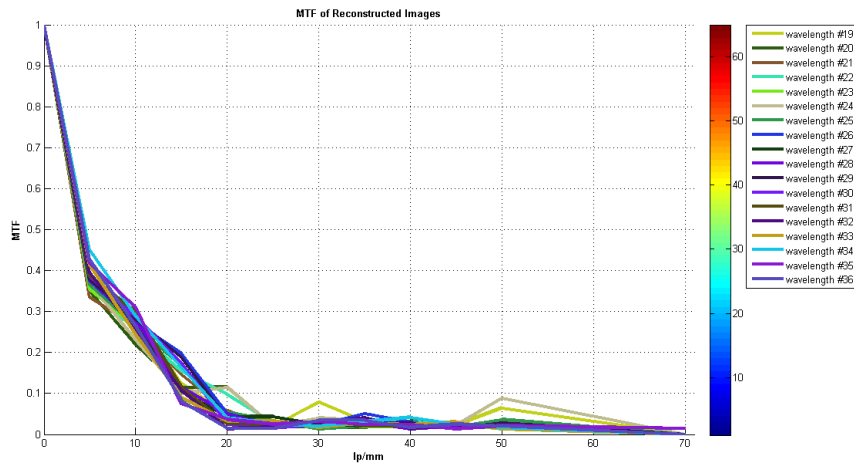
Figure 7.23: *MTF Performance along Reconstructed Images* #19 − 36. *None of them does contain stripes.*
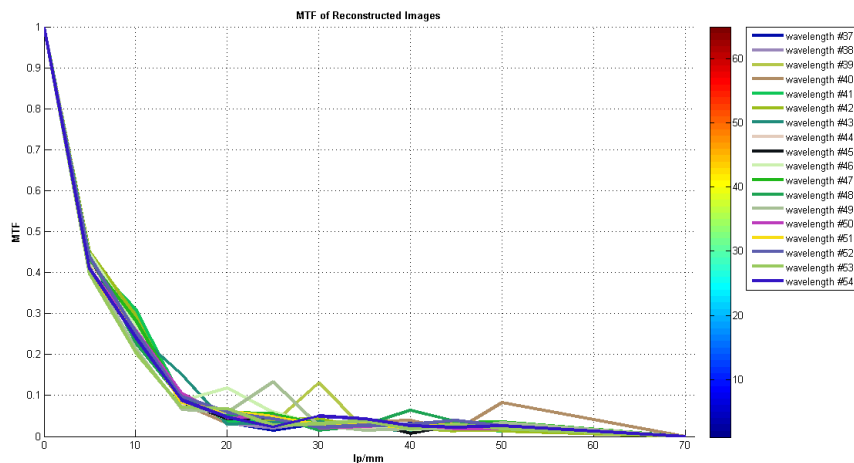
Figure 7.24: *MTF Performance along Reconstructed Images* #37 − 54. *None of them does contain stripes.*

Figures 7.23 and 7.24 depict the MTF performance of reconstruction of larger wavelength bands, green and red, respectively. It is deduced that increased values are obtained, especially in the first three variable frequencies, 5, 10 and 15 lp/mm. In general, the MTF performance is enhanced compared to that one of smaller wavelengths. However, it is of great importance that there are no stripes in these reconstructed images. Some signs of spurious resolution at values equal or greater than 20 lp/mm are pinpointed, as well. Meanwhile, keeping in mind that a group of spectral bands are

not perfectly reconstructed, we hold evidence that the performance of the reconstruction is as satisfactory as this one of the hyper spectral scanning function.

7.6   Developed Software For MTF Estimation

As it has been analytically presented in section 7.5.1, we choose to develop a software that performs the **direct square-wave MTF analysis**, whose implementation dates back to section 7.4.3.

A Graphical User Interface (GUI) for **direct square-wave MTF analysis** has been developed due to the multiple needs of our laboratory to characterize the performance of a great number of optoelectronic imaging systems. The concept of implementation was conformed to the chosen $\#43 - 488$ Edmund test target and respective mathematical background that square-wave analysis requires.

The user of the aforementioned GUI will be asked to deal with the environment that is shown in figure 7.25.
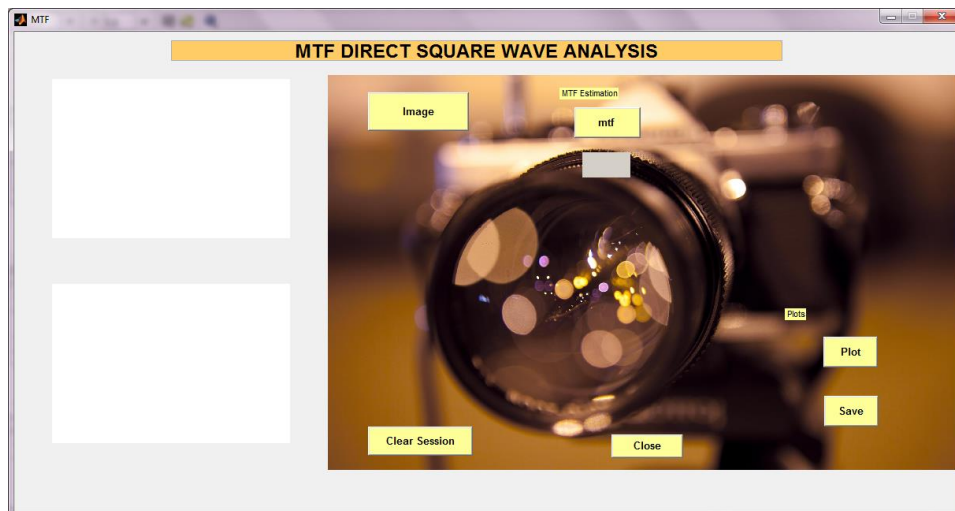
Figure 7.25: *Snapshot of MTF-GUI environment.*

Firstly, user has to choose the image of test target that is captured by the imaging system, whose performance is being tested through the **"image-button"**. The wavelength at which the image is being shot as well as the lens aperture, are being asked as an input before moving on. Secondly,

pressing the **"mtf-button"** opens the previously selected image and gives user the opportunity to select a region of interest (ROI) in a specific frequency, or otherwise a specific group of lp/mm. The Modulation Transfer Function is being estimating in this area and the result along with the spatial profile are depicted. This process can be repeated for as many variable frequencies as the user wants. After having evaluated the mtf-value at the desirable frequencies, there is a **"plot-button"**, whose clicking offers the mtf-curve across the frequencies that user has inserted before. Data, including mtf values and respective frequencies, are saved into text(.txt) and excel(.xls) files for further possible post processing. Furthermore, diagrams can also be saved by pressing the **"save-button"**. There are two more buttons left. The **"clear session-button"**, which clears the existent measurements and prepares the system for a new mtf evaluation session. Last but yet important, the **"close-button"** is responsible for closing the GUI application.

A flow chart of the described procedure that user should follow in order to come up with the desirable mtf results of the tested system, is illustrated in figure 7.26 for better understanding.
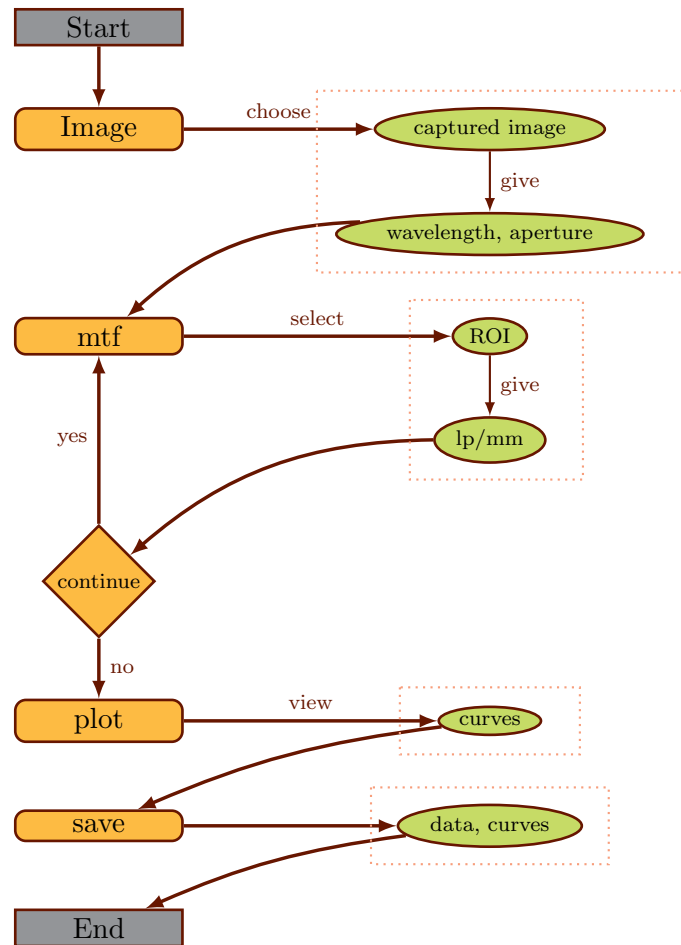
Figure 7.26: *Flow-chart for the MTF evaluation of a specific spectral band.*

The function of GUI while performing the flow of chart 7.26 is depicted in figure 7.27:
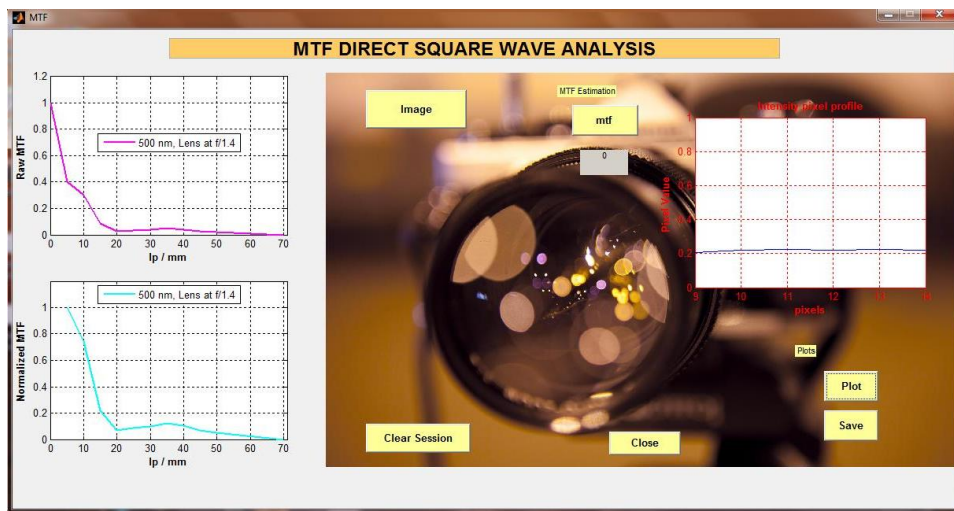
Figure 7.27: *MTF-GUI performing evaluations.*

Chapter 8

Conclusion and Future Work

The HSI that has been presented so far is fully equipped with the functions of hyper spectral scanning and reconstruction of spectral cubes. Calibration and configuration settings consist fundamental parts of this imaging system, which could find prospective application on medicine, agriculture, surveillance, mineralogy, astronomy and environment. The principal conclusion is that this type of imaging system is able to provide functional hyper spectral and single-spectral images across the electromagnetic spectrum divided into many more close bands, beyond the scope of human eye. The spectral response of the depicted visual material/sample conveys useful information as far as its composition and behavior are concerned in multidimensional spaces, which is strictly associated with non-invasive and non-destructive analysis.

Despite the fact that the HSI is provided with live display of the hyper spectral scanning procedure, the *reconstruction* procedure is *not real-time*. It requires the completion of the hyper spectral acquisition first. Curse of dimensionality is a fact for these structures of data. Furthermore, time complexity for acquiring the reconstructed spectral cube is O(n^3), where n represents the number of scanned images. The light throughput is extremely high due to the non slit-scan technique and photobleaching phenomena are kept away giving HSI a promising perspective for the protection of the tested samples. The system's MTF performance is satisfactory, which means that the HSI is endowed with a good level of resolution and contrast.

The fact that the development of the HSI is completed within the requirements of this thesis does not indicate that there is not any potential of further improvement and perfection. Being more specific, we have extensively coped with the problem of distorted and low-quality reconstructions. Although there has been important improvement throughout the implementation of this project, the procedure of reconstruction has not been perfected due to physical and constructive misalignments that may require long time of research and experimental trials. As a consequence, there exists strong evidence that the hyper spectral camera we introduce is efficient and it can be even more in terms of the reconstruction procedure and thus, light throughput.

Appendices

Algorithm 1 Algorithmic Diagonal Reconstruction of Spectral Cube

---

Require: *images* respond to the raw images of the hyper spectral scanning procedure, *step* to the fixed number of columns for each step of the filter, *reverse* to the direction of scanning which can be either *rightwise*($reverse = 0$) or *leftwise*($reverse = 1$).

1: **function** CREATESPECTALCUBE($images, step, reverse$)
2:     $[a, b, c, z] \leftarrow size(images);$ ▷ c responds to the dimensionality of color coordinates, z to the total number of raw images
3:     $cubeImage \leftarrow zeros(a, b, c, z);$
4:     **if** ($reverse == 0$) **then**
5:         **for** $i \leftarrow 1$ **to** z **do**
6:             $axis \leftarrow [0 : step : b, b];$
7:             $x \leftarrow 1;$
8:             $pic \leftarrow i;$
9:             **for** $j \leftarrow 1$ **to** $(length(axis) - 1)$ **do**
10:                 **if** $pic \leq z$ **then**
11:                     $cubeImage(:, ((axis(x) + 1) : axis(x + 1)), :, i) \leftarrow$
12:                     $images(:, ((axis(x) + 1) : axis(x + 1)), :, pic);$
13:                     $x \leftarrow x + 1;$
14:                     $pic \leftarrow pic + 1;$
15:                 **end if**
16:             **end for**
17:         **end for**
18:     **else**
19:         **for** $i \leftarrow 1$ **to** z **do**
20:             $num \leftarrow ceil(b/step) + 1;$
21:             $axis \leftarrow zeros(1, num);$
22:             $h \leftarrow b;$
23:             **for** $k \leftarrow 1$ **to** num **do**
24:                 **if** $k == 1$ **then**
25:                     $axis(1, k) \leftarrow h;$
26:                 **else**
27:                     $h \leftarrow h - step;$
28:                     **if** ($h == 0$) **then**
29:                         $h \leftarrow 0;$
30:                     **end if**
31:                     $axis(1, k) \leftarrow h;$
32:                 **end if**
33:             **end for**
34:             $x \leftarrow 1;$
35:             $pic \leftarrow i;$
36:             **for** $l \leftarrow 1$ **to** $(num - 1)$ **do**
37:                 **if** $pic \leq z$ **then**
38:                     $cubeImage(:, ((axis(1, x + 1) + 1) : axis(1, x)), :, i) \leftarrow$
39:                     $images(:, ((axis(1, x + 1) + 1) : axis(1, x)), :, pic);$
40:                     $x \leftarrow x + 1;$
41:                     $pic \leftarrow pic + 1;$
42:                 **end if**
43:             **end for**
44:         **end for**
45:     **end if**
46:     **return** $cubeImage;$ ▷ 3-D matrix of the reconstructed cube
47: **end function**

Algorithm 2 Estimating Spectrum of a pixel-neighborhood

Require: $r1$, $r2$, $c1$, $c2$ demonstrate the bounds of a subelement inside a patch. Specifically, $r1$ and $r2$ respond to the lower and upper bound of rows, whereas $c1$ and $c2$ to the lower and upper bound of columns respectively.

1: **function** ESTIMATESPECTRUM($image$, $r1$, $r2$, $c1$, $c2$)

2:     $spectrum \leftarrow median(median((image((r1:r2),(c1:c2)))));$

3:     **return** $spectrum$; $\triangleright$ spectrum of a $(r2 - r1) \times (c2 - c1)$ pixel-neighborhood

4: **end function**

Algorithm 3 Step of columns of a single patch

Require: $r1$ and $r2$ respond to the lower and upper bound of rows, whereas $c1$ and $c2$ to the lower and upper bound of columns respectively, len is the number of columns that a subelement has, $colSub$ is the number of first column of the patch's subelement, $previousSpec$ consists the spectrum of the subelement of the previous image, $threshold$ is used to minimize the difference of spectrums.

1: **function** PREDICTEDSTEPFOREACHPATCH($image$, len, $c1$, $c2$, $r1$, $r2$, $colSub$, $previousSpec$, $threshold$)

2:     $addTo \leftarrow (len - 1)$;
3:     $iterTill \leftarrow (c2 - addTo)$;
4:     $axisOfPatch \leftarrow [c1 : iterTill]$;
5:     $metric \leftarrow zeros(length(axisOfPatch), 1)$;

6:     **for** $i \leftarrow 1$ **to** $length(axisOfPatch)$ **do**

7:         $metric(i) \leftarrow abs(estimateSpectrum(image, r1, r2, axisOfPatch(i),$
8:         $(axisOfPatch(i) + addTo)) - previousSpec)$;

9:     **end for**

10:     $minimumMetric \leftarrow min(metric)$;

11:     **if** $(minimumMetric \leq threshold)$ **then**

12:         $[row, column] \leftarrow find(metric == minimumMetric)$;

13:         **if** $(length(row) == 1)$ **then**

14:             $position \leftarrow axisOfPatch(row)$;

15:         **else**

16:             $positionPro \leftarrow axisOfPatch(row)$;
17:             $stepPro \leftarrow abs(positionPro - colSub)$;
18:             $[r, c] \leftarrow find(stepPro == max(stepPro))$;
19:             **if** $(length(c) == 1)$ **then**

20:                 $position \leftarrow positionPro(c)$;

21:             **else**

22:                 $position \leftarrow stepPro(c(end))$;

23:             **end if**

24:         **end if**

25:         $step \leftarrow abs(position - colSub)$;
26:         $verify \leftarrow abs(estimateSpectrum(image, ri, r2, position, (position + addTo))$
27:         $-previousSpec)$;

28:         **if** $((verify - minimumMetric) == 0)$ **then**

29:             $fprintf(''Criterion\ Satisfied.'')$;

30:         **else**

31:             $fprintf(''Criterion\ Not\ Satisfied.'')$;

32:         **end if**

33:         $newPosCol \leftarrow position$;
34:         $newPosColEnd \leftarrow (newPosCol + addTo)$;

35:     **else**

36:         $step \leftarrow 0$;
37:         $newPosCol \leftarrow 0$;
38:         $newPosColEnd \leftarrow 0$;
39:         $fprintf(''None\ Satisfactory\ Citerion.'')$;

40:     **end if**

41:     **return** $step$, $newPosCol$, $newPosColEnd$;   ▷ step, first and last column of new position.

42: **end function**

Algorithm 4 Choice Of The Appropriate Step Between Two Consecutive Scans

---

Require: $stepsArray$ demonstrate the steps and $specArray$ the spectral differences of the four patches. For instance, if we consider the first row of table 3.1 , $stepsArray$ responds to columns 1-4, whereas $specArray$ to columns 5-8, $columns$ to the number of columns of images.

1: **function** CHOOSESTEPSFROM4PATCHES($stepsArray$, $specArray$, $columns$)

2:    $[r, c] \leftarrow find(stepsArray(1, :) == max(stepsArray(1, :)));$

3:    **if** $(length(c) == 1)$ **then**

4:        **if** $(specArray(1, c) == min(specArray(1, :)))$ **then**

5:            $stepToChoose \leftarrow stepsArray(1, c);$

6:        **else**

7:            $[r, c] \leftarrow find(specArray(1, :) == min(specArray(1, :)));$

8:            **if** $(length(c) == 1)$ **then**

9:                $stepToChoose \leftarrow stepsArray(1, c);$

10:            **else**

11:                $temp \leftarrow stepsArray(1, c);$
12:                $stepToChoose \leftarrow max(temp);$

13:            **end if**

14:        **end if**

15:    **else**

16:        **if** $(stepsArray(1, c(1)) == columns)$ **then**

17:            $len \leftarrow length(c);$
18:            $sortedStepsArray \leftarrow sort(stepsArray(1, :), ascend);$
19:            **if** $(length(sortedStepsArray) == len)$ **then**

20:                $stepToChoose \leftarrow stepsArray(1, c(1));$

21:            **else**

22:                $sortedMinus \leftarrow sortedStepsArray(1 : (end - len));$
23:                $len \leftarrow length(sortedMinus);$
24:                $array \leftarrow zeros(1, len);$
25:                **for** $i \leftarrow 1$ **to** len **do**

26:                    $[r\_temp, c\_temp] \leftarrow find(stepsArray(1, :) == sortedMinus(i));$
27:                    $array(1, i) = c_temp;$

28:                **end for**

29:                **if** $((len > 1) \ \&\& \ (len < 4))$ **then**

30:                    **if** $(specArray(1, array(1)) == specArray(1, array(2))) \ || \ (specArray(1, array(1)) >$
31:                    $specArray(1, array(2))))$ **then**

32:                        $stepToChoose \leftarrow sortedMinus(end);$

33:                    **else**

34:                        $stepToChoose \leftarrow sortedMinus(1);$

35:                    **end if**

36:                **else**

37:                    $stepToChoose \leftarrow sortedMinus;$

38:                **end if**

39:            **end if**

40:        **else**

41:            $[r1, c1] \leftarrow find(specArray(1, c) == min(specArray(1, c)));$
42:            **if** $(length(c1) == 1)$ **then**

43:                $stepToChoose \leftarrow stepsArray(1, c(c1));$

44:            **else**

45:                $stepToChoose \leftarrow stepsArray(1, c(c1(1)));$

46:            **end if**

47:        **end if**

48:    **end if**

49:    **return** $stepToChoose;$ ▷ step between two consecutive images

50: **end function**

Algorithm 5 Choice Of The Appropriate Step Between All Consecutive Scans

---

Require: $steps4Patches$ demonstrate the table 3.1 .

1: **function** CHOOSINGFORALLPATCHES($steps4Patches$, $columns$)

2:      $[a, b] \leftarrow size(steps4Patches)$;
3:      $steps \leftarrow zeros(1, a)$;

4:      **for** $i \leftarrow 1$ **to** a **do**

5:          $steps(1, i) \leftarrow chooseFromSteps4Patches(steps4Patches(i, (1 : 4))$,
6:          $steps4Patches(i, (5 : 8)), columns)$;

7:      **end for**

8:      **return** $steps$;   ▷ matrix with the steps for all the hyper spectral images

9: **end function**

Algorithm 6 Produce Axis Of Steps

Require: $shiftMatrix$ responds to the axis obtained by algorithm 5, $limit$ to the second dimension of scanned images(number of columns).

1: **function** PRODUCEAXIS($shiftMatrix$, $limit$)

2:     $b \leftarrow length(shiftMatrix)$;

3:     **for** $i \leftarrow 1$ **to** $(b - 1)$ **do**

4:        $check \leftarrow 1$;
5:        $counter \leftarrow 0$;
6:        $index \leftarrow i + 1$;
7:        $pivot1 \leftarrow index$;

8:        **for** $k \leftarrow 1$ **to** $index$ **do**

9:           **if** $(check == 1)$ **then**

10:             **if** $(k == 1)$ **then**

11:               $axis(i, k) \leftarrow 1$;

12:             **else if** $(k == 2)$ **then**

13:               $axis(i, k) \leftarrow shiftMatrix(1, index)$;

14:             **else**

15:               $previous \leftarrow k - 1$;
16:               $pivot1 \leftarrow pivot1 - 1$;
17:               $axis(i, k) \leftarrow axis(i, previous) + shiftMatrix(1, pivot1)$;

18:             **end if**

19:             **if** $(axis(i, k) \geq limit)$ **then**

20:               $counter \leftarrow counter + 1$;

21:               **if** $(counter == 1)$ **then**

22:                 $axis(i, k) \leftarrow limit$;
23:                 $check \leftarrow 2$;

24:               **end if**

25:             **end if**

26:           **end if**

27:        **end for**

28:     **end for**

29:     **return** $axis$;   ▷ pre completed total axis

30: **end function**

Algorithm 7 Pre-Complete The Total Axis Of Steps

Require: $oldAxis$ responds to the axis obtained by algorithm 6, $limit$ to the second dimension of scanned images(number of columns).

1: **function** PRECOMPLETEAXIS($oldAxis$, $limit$)

2:     $[rows, cols] \leftarrow size(oldAxis)$;

3:     **for** $i \leftarrow 1$ **to** $rows$ **do**

4:         $pic \leftarrow i$;
5:         $cleft \leftarrow 1$;
6:         $counter \leftarrow 1$;

7:         **for** $k \leftarrow pic$ **to** $rows$ **do**

8:             **if** $(oldAxis(k, cleft) > 0)$ && $(oldAxis(k, cleft) < limit)$ **then**

9:                 **if** $(oldAxis(k, (cleft + 1)) \leq limit)$ **then**

10:                     $axis(pic, counter) \leftarrow oldAxis(k, cleft)$;
11:                     $axis(pic, (counter + 1)) \leftarrow oldAxis(k, (cleft + 1))$;
12:                     **if** $(axis(pic, (counter + 1)) == limit)$ **then**

13:                         $break$;

14:                   **end if**
15:                   $cleft \leftarrow cleft + 1$;
16:                   $counter \leftarrow counter + 2$;

17:                 **end if**

18:             **end if**

19:         **end for**

20:     **end for**

21:     **return** $axis$;   ▷ pre completed total axis

22: **end function**

Algorithm 8 Complete The Total Axis Of Steps

Require: $precompletedAxis$ responds to the pre-completed axis obtained as output by the previously described algorithm 7, $limit$ to the second dimension of scanned images(number of columns).

1: **function** COMPLETEAXIS($precompletedAxis, limit$)

2:     $[rows, columns] \leftarrow size(precompletedAxis)$;

3:     **for** $i \leftarrow 1$ **to** $rows$ **do**

4:        **for** $j \leftarrow 2 : 2$ **to** $(columns - 2)$ **do**

5:           **if** $(precompletedAxis(i, j+1) \neq 0)$ **then**

6:              **if** $(precompletedAxis(i, (j+1)) == precompletedAxis(i, j))$ **then**   ▷ case i

7:                 $precompletedAxis(i, (j+1)) \leftarrow (precompletedAxis(i, (j+1)) + 1)$;

8:              **else if** $(precompletedAxis(i, (j+1)) < precompletedAxis(i, j))$ **then**   ▷ case ii

9:                 $precompletedAxis(i, (j+1)) \leftarrow (precompletedAxis(i, j) + 1)$;

10:              **else**   ▷ case iii

11:                 $precompletedAxis(i, (j+1)) \leftarrow precompletedAxis(i, (j+1))$;

12:              **end if**

13:           **end if**

14:        **end for**

15:        $[a, b] \leftarrow find(precompletedAxis(i, (1 : end)) == 0)$;

16:        **if** $(length(b) \geq 1)$ **then**

17:           **if** $(precompletedAxis(i, (b(1) - 1)) < limit)$ **then**

18:              $precompletedAxis(i, (b(1) - 1)) \leftarrow limit$;   ▷ if the second column of last pair is less than
19:   ▷ $limit$, it is then assigned to the value of $limit$
20:           **end if**

21:        **end if**

22:     **end for**

23:     **return** $finalAxis$;   ▷ completed, final axis for reconstruction

24: **end function**

Algorithm 9 Connect The Axis of Cube Images

Require: *axis* responds to the output-axis of algorithm 8, *images* to the whole set of images obtained by the hyper spectral scanning procedure, *upRow*, *downRow* to the first and last row of *axis*.

1: **function** CONNECTAXISCUBE(*axis*, *images*, *upRow*, *downRow*)

2: $[rows, columns] \leftarrow size(axis);$
3: $[a, b, c, z] \leftarrow size(images);$
4: $cubeImage \leftarrow zeros(a, b, c, rows);$

5: **for** $i \leftarrow upRow$ **to** $downRow$ **do**

6:   $pic \leftarrow i;$

7:   **for** $j \leftarrow 1 : 2$ **to** $(columns - 1)$ **do**

8:    **if** $(axis(i, j + 1) > 0)$ **then**

9:     $cubeImage(:, (axis(i, j) : axis(i, j + 1)), :, i) \leftarrow images(:, (axis(i, j) : axis(i, j + 1)), :, pic);$
10:     $pic \leftarrow pic + 1;$

11:    **end if**

12:   **end for**

13: **end for**

14: **return** $spectralCube;$ ▷ reconstructed spectral cube images

15: **end function**

Algorithm 10 Detects the first column that abides by the threshold

---

Require: $columnsOfMedian$ responds to the columns that are equal or smaller than the threshold, $subset$ to the continuous number of columns that we want the criterion to be valid, $threshold$ to the aforementioned threshold.

1: **function** DETECTFIRSTDATA($columnsOfMedian$, $subset$, $threshold$)

2:      $len \leftarrow length(columnsOfMedian)$;

3:      **for** $i \leftarrow 1$ **to** $(len - subset)$ **do**

4:          $counter \leftarrow 0$;

5:          **for** $j \leftarrow i$ **to** $(i + (subset - 2))$ **do**

6:              **if** $(abs(columnsOfMedian(j) - columnsOfMedian(j + 1)) <= threshold)$ **then**

7:                  $counter \leftarrow counter + 1$;

8:              **end if**

9:          **end for**

10:          **if** $(counter == (subset - 1))$ **then**

11:              $firstDataPoint \leftarrow columnsOfMedian(i)$;

12:              $break$;

13:          **end if**

14:      **end for**

15:      **return** $firstDataPoint$;   ▷ number of first column that responds to the criterion

16: **end function**

Algorithm 11 Detects the last column that abides by the threshold

---

Require: $columnsOfMedian$ responds to the columns that are equal or smaller than the threshold, $subset$ to the continuous number of columns that we want the criterion to be valid, $startSearch$ to the number of column before the last column that the search starts, $threshold$ to the threshold that derives from the criterion.

1: **function** DETECTLASTDATA($columnsOfMedian$, $subset$, $startSearch$, $threshold$)

2:     $len \leftarrow length(columnsOfMedian)$;

3:     **for** $i \leftarrow (len - startSearch)$ **to** $(len - subset)$ **do**

4:         $counter \leftarrow 0$;
5:         **for** $j \leftarrow i$ **to** $(i + (subset - 1))$ **do**

6:             $dif \leftarrow abs(columnsOfMedian(j) - columnsOfMedian(j + 1))$;
7:             **if** $(dif \geq threshold)$ **then**

8:                 $counter \leftarrow counter + 1$;

9:             **end if**

10:         **end for**

11:         **if** $(counter \geq 1)$ **then**

12:             $lastDataPoint \leftarrow columnsOfMedian(i)$;
13:             **if** $(lastDataPoint < 200)$ **then**

14:                 $lastDataPoint \leftarrow columnsOfMedian(end)$;

15:             **end if**
16:             $break$;

17:         **else**

18:             $lastDataPoint \leftarrow columnsOfMedian(end)$;

19:         **end if**

20:     **end for**

21:     **return** $lastDataPoint$;   ▷ number of last column that responds to the criterion

22: **end function**

Algorithm 12 Finds the columns-step between two consecutive scans

---

Require: $limit1$ and $limit2$ respond to allowed number of candidate first columns, $maxCol$ to the second dimension of images(number of columns), $firstDataPoint$ to the output of algorithm 10, $lastDataPoint$ to the output of algorithm 11.

1: **function** FINDSTEP($limit1$, $limit2$, $maxCol$, $firstDataPoint$, $lastDataPoint$)

2:      **if** (($firstDataPoint \leq limit1$) && ($lastDataPoint \leq maxCol$)) **then**

3:          $stepColumn \leftarrow (lastDataPoint + 1)$;
4:          **if** ($stepColumn > maxCol$) **then**

5:              $stepColumn \leftarrow maxCol$;

6:          **end if**

7:      **else if** (($firstDataPoint \geq limit2$) && ($lastDataPoint \leq maxCol$)) **then**

8:          $stepColumn \leftarrow (firstDataPoint - 1)$;

9:      **else**

10:          $stepColumn \leftarrow -10$;
11:          $fprintf(``Wrong \quad Prediction")$;

12:      **end if**

13:      **return** $stepColumn$;   ▷ step expressed in columns between two consecutive scans

14: **end function**

References

[1] D.A. Boas, C. Pitris, and N. Ramanujam. Multi/hyper-spectral imaging. In Balas Costas, Pappas Christos, Christos, and Epitropou George, editors, *Handbook of Biomedical Optics*, chapter 7, pages 131–164. Taylor & Francis, 2011. 1.3, 1.3.2, 1.5, 1.5.1, 1.5.1, 1.6

[2] T. Vo-Dinh. *Biomedical Photonics Handbook*. Taylor & Francis, 2010. 1.3, 1.6

[3] A. Tsapras, E. Terzakis, A. Makris, E. Papadakis, G. Papoutsoglou, E. Papagiannakis, C. Tsatsanis, E. Stathopoulos, and C Balas. *"Hyperspectral Imaging for Skin Cancer Diagnosis in Mice"*. *6th European Symposium on Biomedical Engineering*, June 2008. Available at: http://www.electronics.tuc.gr/Controller?event=SHOW_PUBLICATIONS&WHAT=BY_PERSON&PERSON=2&PAGE=1. 1.3.4

[4] Balas C Rapantzikos K. *"Hyperspectral imaging: potential in non-destructive analysis of palimpsests"*. *IEEE-International Conference on Image Processing (ICIP)*, page 11-14, September 2005. Available at: http://www.electronics.tuc.gr/Controller?event=SHOW_PUBLICATIONS&WHAT=BY_PERSON&PERSON=2&PAGE=1. 1.3.4

[5] H. Kalluri, S. Prasad, and L.M. Bruce. *"Fusion of Spectral Reflectance and Derivative Information for Robust Hyperspectral Land Cover Classification"*. *IEEE Workshop on Hyperspectral Image and Signal Processing: Evolution in Remote Sensing*, 2009. Available at: http://sun.library.msstate.edu/ETD-db/theses/available/etd-11062009-124333/. 1.3.4

[6] D. Manolakis, D. Marden, and G. Shaw. *"Hyperspectal Image Processing for Automatic Target Detection Applications"*. *Lincoln Laboratory Journal*, 14(1), 2009. Available at: http://www.ll.mit.edu/publications/journal/pdf/vol14_no1/14_1hyperspectralprocessing.pdf. 1.3.4

[7] W. Li, S. Prasad, J. E. Fowler, and L. M. Bruce. *"Locality Preserving Dimensionality Reduction and Classification for Hyperspectral Image Analysis"*. *Proceedings of the SPIE Defense and Security Symposium*, Orlando, Florida, USA, April 2007. Available at: http://hyperspectral.ee.uh.edu/?page_id=8. 1.3.4

[8] V.V. Tuchin. *Handbook of Coherent-Domain Optical Methods: Biomedical Diagnostics, Environmental Monitoring, and Materials Science*. Springer-Verlag GmbH, 2013. 1.6

[9] V.V. Tuchin, Society of Photo-optical Instrumentation Engineers, and Society of Photo-optical Instrumentation Engineers. Russian Chapter. *CIS selected papers: coherence-domain methods in biomedical optics.* Proceedings of SPIE–the International Society for Optical Engineering. SPIE, 1996. 1.6, 2.1

[10] Kurz, L., Benteftifa, and H. *Analysis of Variance in Statistical Image Processing.* Cambridge University Press, 2006. 1.7, 2.5.1

[11] Zheng, N., Xue, and J. *Statistical Learning and Pattern Analysis for Image and Video Processing.* Advances in pattern recognition. Springer London, Limited, 2009. 1.7, 3.1, 4, 5.1.1

[12] Chang and C.I. *Hyperspectral Data Processing: Algorithm Design and Analysis.* Wiley, 2013. 2.1

[13] Glasbey, C.A., Horgan, and G.W. *Image analysis for the biological sciences.* Statistics in practice. J. Wiley, 1995. 2.1, 2.5.1, 4, 5.1.1

[14] Poon, T.C., Banerjee, and P.P. *Contemporary Optical Image Processing with MATLAB.* Elsevier Science, 2001. 2.4

[15] Woods and J.W. *Multidimensional Signal, Image, and Video Processing and Coding.* Academic Press. Academic Press, 2011. 2.4, 5

[16] Parker and J.R. *Algorithms for Image Processing and Computer Vision.* Wiley, 2010. 2.4

[17] W. Li, S. Prasad, and J. E. Fowler. *"Classification and Reconstructions from Random Projections for Hyperspectral Image Analysis".* *IEEE Transactions on Geoscience and Remote Sensing*, 2012. Available at: http://hyperspectral.ee.uh.edu/?page_id=8. 2.4

[18] Parker and J.R. *Algorithms for Image Processing and Computer Vision.* Wiley, 2010. 3.1

[19] M. Petrou and C. Petrou. *Image Processing: The Fundamentals.* John Wiley & Sons, 2010. 4

[20] Boreman and G.D. *Modulation Transfer Function in Optical and Electro-optical Systems.* SPIE tutorial texts. Society of Photo-Optical Instrumentation Engi, 2001. 7.1

[21] Xujie Zhang, Tamar Kashti, Dror Kella, Tal Frank, Doron Shaked, Robert Ulichneyd, Mani Fischerc, and Jan P. Allebacha. *"Measuring the Modulation Transfer Function of Image Capture Devices: What Do the Numbers Really Mean?".* *Proceedings of SPIE-IS&T Electronic Imaging*, 8293 829307-1, 2012. Available at: http://www.hpl.hp.com/israel/documents/2012/ModulationTransferFunction_SPIE2012.pdf. 7.3

[22] Li Tiecheng, Feng Huajun, and Xu Zhihai. *"A new analytical edge spread function fitting model for modulation transfer function measurement"*, 2010. Availble at: http://col.org.cn/abstract.aspx?id=COL201109031101-04. 7.4.4